Motor unit recruitment in the tibialis anterior muscle during fatigue: electrophysiology and metabolism

Cover: Anke Kroon (advice) and Tom Boersma (realization)
Print: FEBO DRUK BV, Enschede
Paper: Epos, 100% recycled and Keaykolour Natural, 75% recycled (cover)
Ink: K+E ECO ink, vegetable

The studies presented in this thesis were performed at the Department of Clinical Neurophysiology and the Department of Radiodiagnostics of the University Medical Center Nijmegen (UMCN) St Radboud, The Netherlands. The work is part of the research program of the inter university graduate Institute of Fundamental and Clinical Human Movement Studies (IFKB).

The publication of this thesis was financially supported by the IFKB, the Institute of Neurology, UMCN St Radboud and Ipsen Farmaceutica.

Motor unit recruitment in the tibialis anterior muscle during fatigue: electrophysiology and metabolism

Een wetenschappelijke proeve op het gebied van
de Medische Wetenschappen

Proefschrift

ter verkrijging van de graad van doctor
aan de Katholieke Universiteit Nijmegen
op gezag van de Rector Magnificus Prof. Dr. C.W.P.M. Blom,
volgens besluit van het College van Decanen
in het openbaar te verdedigen op maandag 5 april 2004
des namiddags om 1.30 uur precies

door

Caroline Jantien Houtman
geboren op 16 september 1968
te Eindhoven

Promotores:	Prof. Dr. Ir. D. F. Stegeman
	Prof. Dr. A. Heerschap
	Prof. Dr. M. J. Zwarts
Manuscriptcommissie:	Prof. Dr. P. N. R. Dekhuijzen
	Prof. Dr. K. Nicolay
	Dr. I. Zijdewind

Readers guide

Chapter 1 is a general introduction, written for the interested outsider. Chapter 2 and 3 are introductions on human ^{31}P NMR spectroscopy and multi channel surface EMG, respectively. These chapters require more prior knowledge. Chapters 4 – 7 form the core of this thesis. Aimed readers are colleagues in this field of research. Chapter 8 gives a summary and some conclusions and is like chapter 1 written for a more generally interested readership.

Small pictures

The small pictures at bottom-right of odd pages represent successive ^{31}P NMR spectra of subject 6 (see chapter 4 and 5) from just before exercise at –45 s, page 123, until recovery at 732 s, page 25. The exercise performed at 30% of maximum force, started at 0 s and finished at 580 s. The spectra show the change in inorganic phosphate (small peak at left) and phosphocreatine.

Contents

Abbreviations and symbols

AMP	adenosine monophosphate
ADP	adenosine diphosphate
ATP	adenosine triphosphate
B_0	static magnetic field
B_1	oscillating magnetic field or radio frequency field
Ca^{2+}	calcium
CK-/-	creatine kinase-deficient
CR	Cramer-Rao
Cr	creatine
EDL	extensor digitorum longus muscle
EMG	electromyography
FID	free induction decay
Fmed	median frequency
GPC	phosphatidylcholine
GPE	phosphatidylethanolamine
^1H	proton
H_2O	water
I_i	injected current
I_l	longitudinal electric current
I_m	transmembrane ionic current
IAP	intracellular action potential
ISIS	image-selected in vivo spectroscopy
K^+	potassium
k	equilibrium constant
m.	musculus
MFCV	mean muscle fiber conduction velocity
Mg^{2+}	magnesium
MR	magnetische resonantie
MRI	magnetische resonantie 'imaging'
MVC	maximum voluntary contraction
n	number
Na^+	sodium
NMR	nuclear magnetic resonance
^{31}P	phosphor
P_i	inorganic phosphate

PCr	phosphocreatine
PDE	phosphodiesters
pH_{high}	pH level derived form the left (low-field) Pi peak
pH_{low}	pH level derived from the right (high-field) Pi peak
PME	phosphomonoesters
pK	dissociation constant
pK_a	dissociation constant for the acid
ppm	parts per million
PV	peak velocity
R	resistance
RMS	root mean square
SD	standard deviation
T	time delay
T_1	spin-lattice relaxation time
TA	tibialis anterior muscle
TR	repetition time
r_{ij}	distance between position i and j
t	time
U	velocity
V_j	potential on position j
WT	wild type
z	position along the muscle fiber direction
2D ^{31}P SI	two-dimensional phase encoded ^{31}P spectroscopic imaging
σ	electric conductivity
φ	phase difference
ω	angular frequency

1

General introduction

Introduction

The subject of muscle fatigue has attracted a lot of research in the past decades. Despite this fact, many questions still remain to be answered. Fatiguing processes during voluntary muscle contractions in humans are of particular interest. However, because of limited experimental access, these processes are difficult to disentangle. The purpose of this thesis is to contribute to the knowledge of muscle physiology during voluntary exercise. It is an elaborate investigation regarding the properties of one particular human muscle performing one type of exercise. Surface electromyography is used to measure details of motor units and their recruitment (see below). Phosphor nuclear magnetic resonance spectroscopy is used to acquire details of energy metabolism in the muscle.

Motor units

Motor nerve fibers make up the connection between the spinal cord and the muscles. The messengers are electrical signals called action potentials. They travel from the spinal cord to the muscle fibers. After the transition from the nerve fiber branch to the muscle fiber, the action potentials travel over the outer membrane of the muscle fibers towards the terminations (figure 1.1). The termination of a single motor nerve comprises numerous branches, each of which is connected to an individual muscle fibre. A set of one motor nerve fiber and all the connected muscle fibers is called motor unit. A muscle fiber is always active simultaneously with its ‘brothers and sisters’ belonging to the same motor nerve fiber. Therefore, motor units can be called the building blocks of the muscle.

How to measure the action of motor units

A muscle fiber contracts, as long as action potentials travel in both directions along its outer membrane from about the center to the terminations, where the muscle fiber connects to the tendon. These electrical signals can be measured on the skin with a surface electrode or

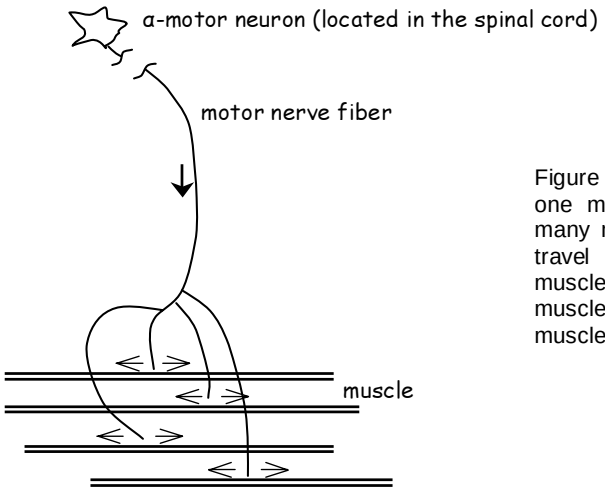

Figure 1.1: a motor unit consists of one motor nerve fiber connected to many muscle fibers. Action potentials travel along the nerve fiber to the muscle fibers and then along the muscle fibers in two directions to the muscle fiber terminations.

inside the muscle with a needle electrode. These techniques are called electromyography (myo = muscle). We used the surface electromyography (EMG) technique. The information content of a surface EMG recording increases (potentially) with the amount of electrodes. One pair of surface electrodes on the skin above the muscle tells us that the muscle is active or not. Many surface electrodes (and some signal processing) can give detailed information about the anatomy and electrical properties of the underlying motor units (Roeleveld & Stegeman, 2002). At low contraction levels, with only one or a few motor units active, the electrical signals measured at the skin surface are easy to understand (figure 1.2A). At a high contraction level many motor units are active, leading to noise-like signals that are difficult to disentangle (figure 1.2B). The mean amplitude of the surface EMG is therefore used as measure of muscle activity. The velocity of the action potential over the outer membrane of the muscle fiber is used as a measure of fatigue. The more the muscle fiber is fatigued, the more the propagation velocity slows down. With an array of electrodes

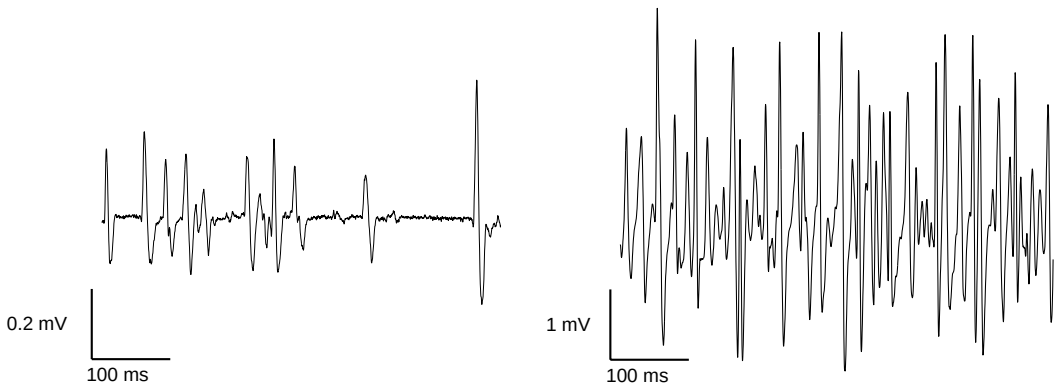

Figure 1.2A: single motor unit action potentials in a surface electromyography (EMG) signal measured at 5% of the maximum force level. B: intermingled and larger motor unit action potentials in a surface EMG signal measured at 80% of the maximum force level.

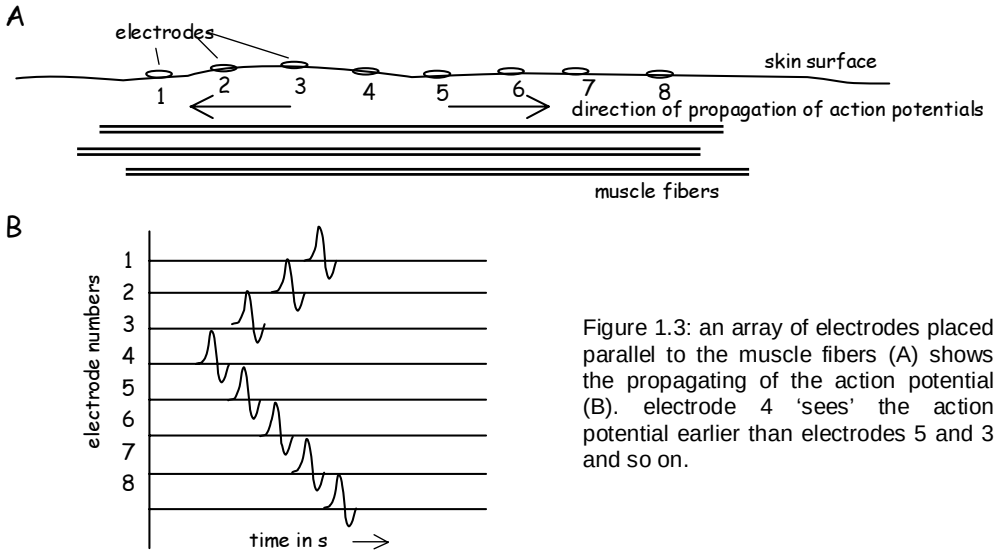

Figure 1.3: an array of electrodes placed parallel to the muscle fibers (A) shows the propagating of the action potential (B). electrode 4 'sees' the action potential earlier than electrodes 5 and 3 and so on.

placed parallel to the muscle fibers the propagation of (single) action potentials can be followed (figure 1.3A), as the action potential arrives earliest at the electrodes above the center of the muscle fiber (at the transition of the nerve branch to the muscle fiber) and latest at the electrodes at the muscle fiber ends (figure 1.3B). A review on the backgrounds and present status of (multichannel) surface EMG as applied to human skeletal muscle is presented in chapter 3.

Energy consumption of the muscle

Muscle fibers consume energy during effort. Their main energy source is glucose. Glucose can be consumed with (aerobic) or without (anaerobic) oxygen. The anaerobic consumption is quicker, but gives less energy than the aerobic consumption. Moreover, anaerobic glycolysis leads to the production of protons and thus to an acidification of the muscle as soon as the removal of protons is insufficient. Phosphocreatine (PCr) is an even quicker energy source for the muscle fibers than anaerobic glycolysis. Initially a muscle relies on PCr, then on the anaerobic and finally on the aerobic use of glucose. To maintain the effort, the muscle will use mainly glucose aerobically as long as the supply of oxygen is sufficient.

Nuclear magnetic resonance (NMR)

An atom is an ensemble of electrons, protons and neutrons. Protons and neutrons form the nucleus, while the electrons move in orbits around the nucleus, like planets around the sun. Additionally, electrons, protons and neutrons turn around their axes like a top (figure 1.4). This is called spin. A charged particle, such as a proton or an electron, that spins around causes a magnetic moment. The magnetic moments of an even amount of spinning protons

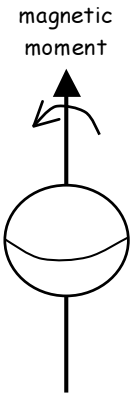

Figure 1.4: a proton turns around its own axes like a top. This property is called spin and is associated with a magnetic moment, drawn as an arrow.

in a nucleus cancel each other out. The phosphor atom contains an odd number of protons (15) and thus a very small magnetic moment, net one spin, is left.
The phosphor atoms in our body, including in our muscles, have these magnetic moments. Normally, the magnetic moments cancel out, because they are randomly directed (figure 1.5A). However, there is a way to rearrange them. If spins are placed in a strong magnetic field, they will arrange parallel to the magnetic field (figure 1.5B). The spins are orientated in the same or in the opposite direction to the magnetic field, according to quantum mechanical laws. Because the amount of spins orientated in the same direction as the magnetic field is slightly higher than the amount of spins orientated in the opposite direction, a net (still very small) magnetic moment, is left.

How can this small magnetic moment be measured? Disturb the arrangement of spins and wait until they return to their favorite (lowest energy) position. During this return, the spins transmit energy, which can be picked up. For the purposes of disturbing and measuring, an aerial is used as a transmitter (disturber) and receiver. For measurements on muscles so-

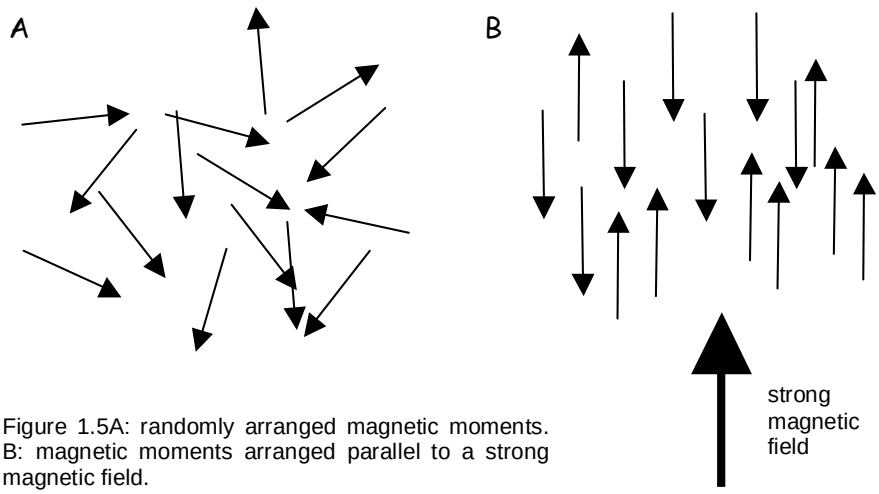

Figure 1.5A: randomly arranged magnetic moments. B: magnetic moments arranged parallel to a strong magnetic field.

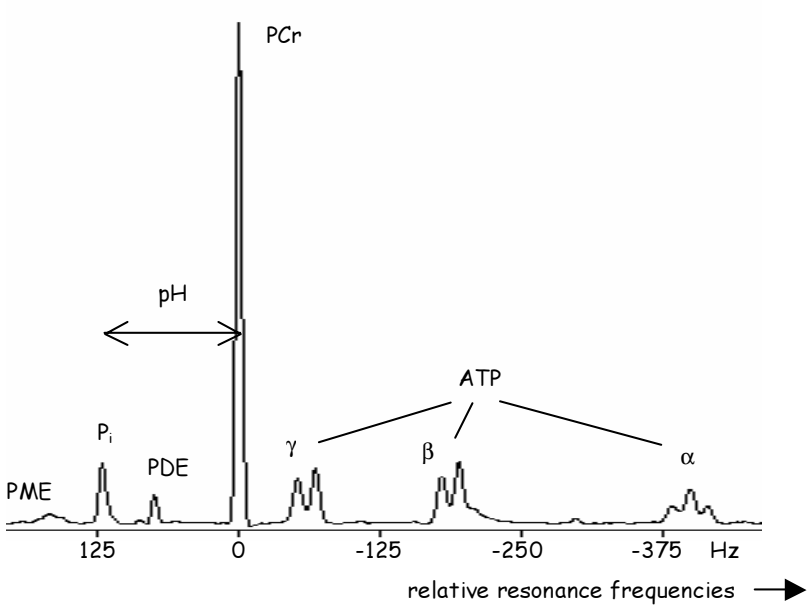

Figure 1.6: the received phosphor (^{31}P) frequencies, relative to the frequency of phosphocreatine (PCr), after disturbance of the arrangement of magnetic moments in muscle tissue, placed in a strong magnetic field. The frequency of PCr is about 25,7 MHz. PME, phosphomonoesters; P_i: inorganic phosphate; PDE phosphodiesters; ATP, adenosine triphosphate.

called surface coils are used as aerial. A surface coil is placed over the muscle to be studied. The subject is then moved into a large tube, the NMR magnet, which realizes the static magnetic field (as the large arrow indicated in figure 1.5B).

The received energy from the returning spins is an electromagnetic signal with a certain frequency. The frequency of phosphor in a magnetic field of 1.5 Tesla is 25,7 MHz (proton: 63,6 MHz), values that can be compared with the medium wave on the radio. A plot of the received energy as a function of frequency along an axis is called a spectrum (figure 1.6). In muscle tissue, phosphor is found in different molecules, like phosphocreatine (PCr), inorganic phosphate (P_i) and adenosine triphosphate (ATP). ATP is an important local energy supplier that remains almost stable during muscle fatigue, because other energy sources refill ATP continuously. A phosphate atom 'feels' the presence of the other atoms in the molecule. The strength of the main magnetic field and the (small) magnetic influence of the surrounding molecule determine the exact resonance frequency of a phosphor nuclear spin. So, for instance, the frequency of P_i is slightly lower (about 0.000125 MHz (=125 Hz), see the horizontal scaling in figure 1.6) than the frequency of PCr. As a consequence, instead of one, several phosphor resonance frequencies appear in the spectrum, all at about 25.7 MHz.

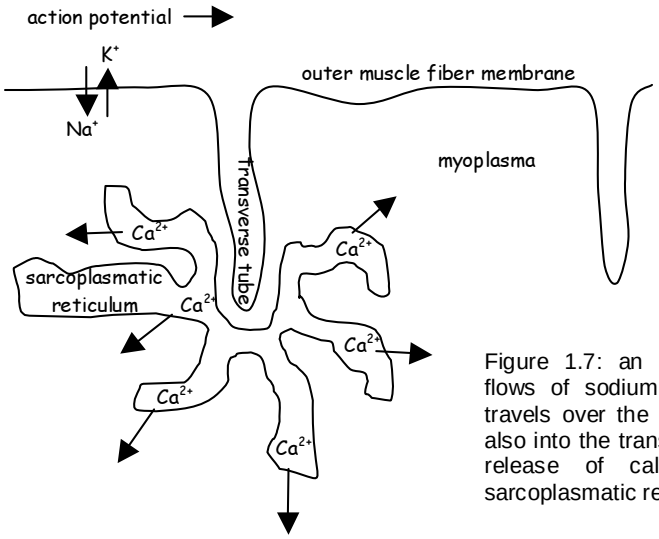

Figure 1.7: an action potential (formed by flows of sodium (Na^{+}) and potassium (K^{+})) travels over the muscle fiber membrane and also into the transverse tube. This causes the release of calcium (Ca^{2+}) out of the sarcoplasmatic reticulum into the myoplasma.

There is an influence of acid on the resonance frequency of P_i. At a higher pH level less protons (H^+) are associated with the P_i molecule than at a lower pH level. Therefore, the P_i resonance frequency changes with the pH level, whereas the PCr resonance frequency remains stable. This means that the frequency distance between PCr and P_i is a measure of pH. Moreover, as different acidification levels exist, more Pi resonance frequencies appear simultaneously. ATP contains three ^{31}P atoms. Each ^{31}P atom is located at another position in the molecule and has another resonance frequency in the spectrum. The interaction between the three ^{31}P atoms within the ATP molecule, also influences the resonance frequencies: they split in two or three. Looking at the ^{31}P NMR spectrum, two of the above mentioned energy sources of the muscle are present: PCr and indirectly (via the pH level) anaerobic glycolysis. The use of these energy sources and the (potential) occurrence of pH heterogeneity can thus be followed by ^{31}P NMR spectroscopy. A further review on the backgrounds and the present status of ^{31}P NMR spectroscopy applied to (human) skeletal muscle is given in chapter 2. See also Gadian, 1995.

Muscle fatigue

Many processes are involved in muscle activation. The action potential, which propagates along the muscle fibre membrane, results from the transmembrane flow of sodium (Na^+) and potassium (K^+) ions (figure 1.7). As the action potential reaches one of many transversal tubes, which connect the fiber inner structures, stored calcium (Ca^{2+}) is released within the muscle fibers (figure 1.7), and binds to the thin filaments of the force generating apparatus of the fiber (figure 1.8A). The overlapping thick filaments are then able to connect to the thin filaments, by small ‘headed’ branches . Next, ATP is necessary to move the filaments to each other: the muscle fiber contracts (figure 1.8B). ATP is also necessary to detach the

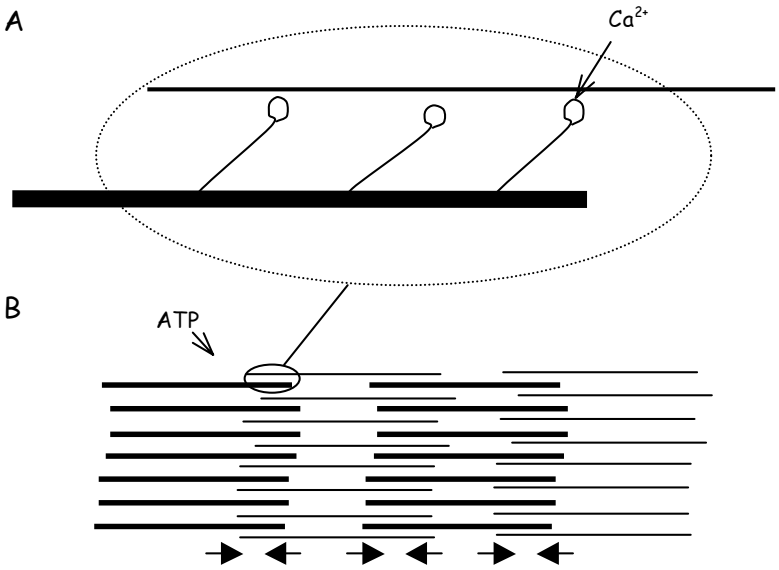

Figure 1.8A: calcium (Ca^{2+}) binds to the thin filament, by which the thick filaments are able to connect to the thin filaments, with small-headed branches. They form so-called cross-bridges. B: next, thin and thick filaments (situated within the myoplasma) slide along each other with the use of adenosine triphosphate (ATP): the muscle contracts.

filaments and to transport calcium back to where it comes from (the sarcoplasmatic reticulum): terminating the contractions and causing the muscle fiber to relax. In addition, ATP delivers the energy to recover the equilibrium of the ion concentrations, again and again, via the so-called ion pumps. Different energy sources are used to maintain ATP at an almost stable level. A muscle gets fatigued as for example Na^+ and K^+ levels get (too) far from equilibrium, or as a shortage of energy sources (PCr, glucose, glycogen, fatty acids) or oxygen arises.

Subject of investigation

The aim of this thesis is to obtain more insight into the processes underlying human muscle fatigue during voluntary contraction. With surface EMG, the drive to the muscle fibers is studied, namely the propagation of the action potentials and the total amplitude of their summed activity. Phosphor NMR spectroscopy enables the internal activity of the muscle fibers to be monitored, and gives information about the use of PCr and the anaerobic use of glucose, to maintain ATP at a stable level. The tibial anterior muscle was selected for this investigation, as it is large enough to enable phosphor NMR spectroscopy to be performed, in addition to having superficial muscle fibers parallel to the skin surface for the surface EMG experiment. The protocol consisted of sustained isometric exercise, in order to minimize movements of the leg, which could disturb the continuous measurements. Healthy

subjects, both male and female, participated in this study. All subjects had a relatively thin layer of fat above the tibialis anterior muscle enabling good signal quality. We instructed subjects to maintain the exercise as long as possible, as the latter part of the exercise, was expected to give the most interesting results. The results of these experiments are described separately in the chapters 4, 5 (both ^{31}P NMR spectroscopy) and 6 (surface EMG). Chapter 7 discusses the remaining questions when combining the results of these three preceding chapters.

References

Gadian DG. *NMR and its applications to living systems,* 2nd ed. Oxford: Oxford University Press, 1995.

Roeleveld K & Stegeman DF. What do we learn from motor unit action potentials in surface electromyography? *Muscle Nerve* 11: S92-87, 2002.

2

Introduction to in vivo ^{31}P NMR spectroscopy of (human) skeletal muscle*

Abstract

Phosphor nuclear magnetic resonance (^{31}P NMR) spectroscopy offers a unique non-invasive window on energy metabolism in skeletal muscle with possibilities for longitudinal studies and to obtain important bioenergetic data continuously and with sufficient time resolution during muscle exercise. The present paper provides an introductory overview of the current status of in vivo ^{31}P NMR spectroscopy of skeletal muscle, focussing on human applications, but with some illustrative examples from studies on transgenic mice. Topics which are described in the present paper are the information content of the ^{31}P NMR spectrum of skeletal muscle, some practical issues in the performance of this methodology, related muscle biochemistry and the validity to interpret results in terms of biochemical processes, the possibility to investigate reaction kinetics in vivo, and some indications for fiber type heterogeneity in spectra obtained during exercise.

Introduction

Following initial experiments on animal tissue (Hoult et al. 1974; Ackerman et al. 1980), NMR spectroscopy was first applied to humans in the early 1980's using the ^{31}P nucleus to monitor the levels and fate of high energy phosphates in skeletal muscle (Chance et al. 1981; Cresshull et al. 1981; Ross et al. 1981). From these first experiments it was clear that ^{31}P NMR spectroscopy offers a unique non-invasive window on energy metabolism in skeletal muscle. Of particular interest is the possibility of obtaining important bioenergetic data continuously and with sufficient time resolution during muscle exercise. Another important aspect is that longitudinal monitoring is possible. Numerous studies applying this

*adapted from **Heerschap A, Houtman CJ, in 't Zandt HJA, van den Bergh AJ & Wieringa B**. *Proc Nutr Soc* 58, 861-870, 1999.

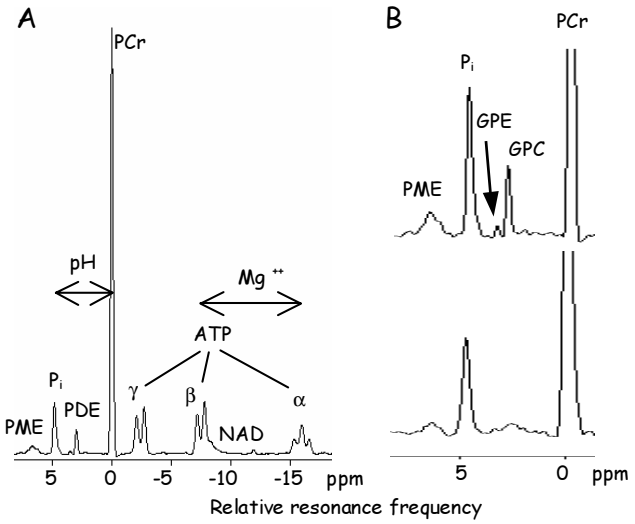

Figure 2.1A: phosphor nuclear magnetic resonance (^{31}P NMR) spectrum of human calf muscle at rest obtained at 1.5 T. A 45° adiabatic radio frequency pulse was used for excitation, and a repetition time of 1 second was applied. During the acquisition time broadband ^{1}H decoupling was applied. Resonances are visible for ATP, NAD, phosphocreatine (PCr), phosphodiesters (PDE), inorganic phosphate (P_i) and phosphomonoesters (PME). ↔, pH and magnesium (Mg^{2+}) sensitive resonance shifts of P_i and β-ATP. B: effect of broadband ^{1}H decoupling on the PDE region in the ^{31}P NMR spectrum of skeletal muscle at 1.5 T. The lower spectrum is obtained without ^{1}H decoupling, the upper spectrum with ^{1}H decoupling. At the PDE region two resonances resolve for phosphatidylcholine (GPC) and phosphatidylethanolamine (GPE). Ppm, part per 10^{6}.

technique to human subjects have been published and several reviews are available addressing specific results obtained in this way (e.g. Barbiroli, 1992; Cozzone & Bendahan, 1994; Kemp & Radda, 1994; McCully et al. 1994; Radda et al. 1995).

This paper provides an introduction to ^{31}P NMR spectroscopy as applied to skeletal muscle of human subjects, and also gives some illustrative examples from our recent studies on skeletal muscle of transgenic mouse models lacking creatine kinase.

Information content of the ^{31}P NMR spectrum of skeletal muscle

To appreciate the potential of the method, first, the information content of a spectrum obtained from human skeletal muscle at rest should be examined (see figure 2.1A). The most dominant signals in the spectrum are from phosphocreatine (PCr) and the three non-equivalent phosphate groups of ATP. Usually also a signal for inorganic phosphate (P_i) can be observed, and under favourable conditions signals for phosphomonoesters and phosphodiesters are observable as well.

What is the origin of the distinct resonance frequencies of the ^{31}P nuclei in these compounds? In a first approximation the resonance frequency of the signals is determined by the main magnetic field. In addition this main field interacts with the electronic environment of the nuclei, inducing small counter magnetic fields. The strength of the counter field at each nucleus depends on its chemical environment. This factor has an important consequence, i.e. nuclei within different chemical structures acquire different resonance frequencies. As a result of this chemically-related frequency separation of phosphate resonances, the spectrum provides a type of fingerprint of the phosphate

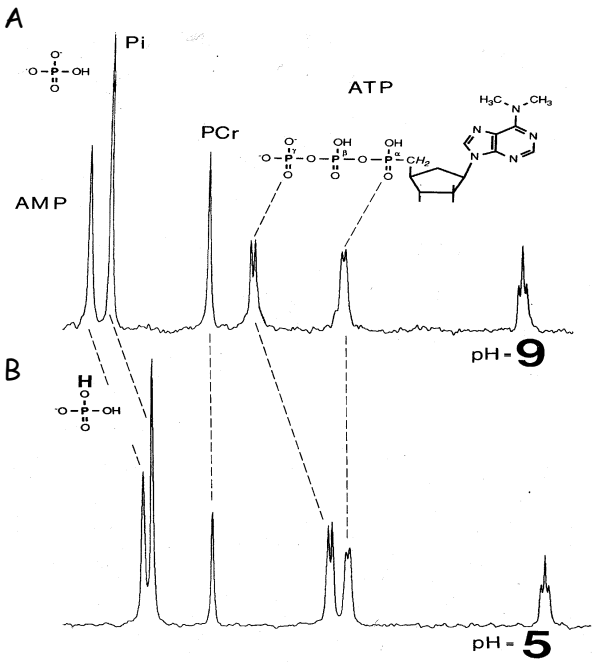

Figure 2.2: effect of pH change on resonance positions in ^{31}P NMR spectra. The spectra have been obtained from a solution containing ATP, phosphocreatine (PCr), inorganic phosphate (P_i) and AMP. The change from pH = 9 (A) to pH = 5 (B) affects the degree of protonation of some of the phosphate groups depending on the dissociation constant (pK) values of these groups. From a titration curve (pH as a function of resonance shift) obtained under the appropriate conditions the pH value of a sample can be obtained using the Henderson-Hasselbach equation, i.e.

$pH = pK_a + \log$ (base concentration/acid concentration), where pK_a is pK for the acid.

chemical content of the muscle. For convenience the relative resonance frequencies, or chemical shifts, are expressed with respect to the resonance frequency of the main field in parts per million (ppm). For in vivo ^{31}P NMR spectroscopy the position of the PCr resonance is usually selected as reference (0 ppm).

A closer inspection of some resonances in the ^{31}P NMR spectrum of skeletal muscle may reveal some fine structure, which is due to their phosphate nuclear spins being subject to an interaction with other nearby spins; the so-called spin-spin coupling. This coupling may be with either neighbouring phosphate spins or proton spins. Phosphate-phosphate spin coupling can be observed for the resonances of ATP as line splittings, i.e. the β-ATP signal becomes a triplet and the α- and γ-ATP signals become doublets (see figure 2.1A). Proton-phosphate spin couplings are effective for phosphomonoesters, phosphodiesterş, α-ATP and diphosphodiester resonances. In vivo these couplings are usually not resolved, but result in broadened lines.

As the chemical environment of the ^{31}P nuclei may change with changes in the physiological condition of the muscle, the phosphate resonance positions may change as well. Of particular importance is the effect of pH variation on spectral resonance positions (Moon & Richards, 1973). This is demonstrated in the spectra shown in figure 2.2, which were obtained from a solution containing various biochemical compounds such as ATP, PCr and P_i at two different pH values. The frequency shift observed for the peak of P_i with its pK of about 6.9 is physiologically most relevant. The position of the PCr peak remains constant. Therefore the P_i-PCr shift difference is used to derive pH values, applying the appropriate

titration curves. Because the signal for P_i in spectra for skeletal muscle arises from the sarcoplasm, under normal conditions, it is the intracellular pH that is determined in this way (see Gadian, 1995).

Another physiological condition that may affect resonance positions is the cellular magnesium (Mg^{2+}) content. In particular, the β-ATP resonance frequency is sensitive to Mg^{2+} binding (Gupta & Moore, 1980). Recent studies based on calculations of the free cytosolic Mg^{2+} concentration in skeletal muscle from shifts in ATP resonances have revealed changes in this concentration as a result of exercise (Iotti et al. 1999) and pathology (Park et al. 1999).

^{31}P NMR spectra of individual skeletal muscles in normal adult humans obtained at rest are fairly reproducible, although some conditions may cause variations, e.g. training and oral supplementation with creatine may increase the NMR visible phosphate content (Park et al. 1988; Kreis et al. 1996), strenuous exercise may increase the P_i to PCr ratio for some days (McCully et al. 1994) and the phosphodiester signal may be increased in older subjects (Sastrustegui et al. 1988). Significant changes are observed during postnatal development (Heerschap et al. 1988; McCully et al. 1994). A higher P_i to PCr ratio and tendency to alkaline tissue pH is a common finding in the diseased state (Heerschap et al. 1993, Cozzone & Bendahan, 1994). In mitochondrial dysfunction this change may be associated with increased ADP levels in the muscle at rest; however, metabolic abnormalities are better characterized in dynamic experiments performing ^{31}P NMR spectroscopy during exercise and recovery (see later).

Some practical issues in the performance of ^{31}P NMR spectroscopy

Hardware

Current clinical NMR machine's, mostly operating at 1.5 T, are focussed on the use of the ^{1}H nucleus for imaging of H_2O in the body. To perform ^{31}P NMR spectroscopy on these systems additional hard- and software is required such as dedicated radio frequency coils and for optimal performance a so-called second radio-frequency channel. ^{31}P NMR spectroscopy of human skeletal muscle is also performed on experimental NMR systems up to field strengths of 4.7 T with limited space in the magnet bores, so that usually only the distal half of arms or legs can be studied. On most of these magnets a fixed horizontal position for the limb is required, while the clinical systems with larger magnet bores allow for more positional freedom. The major advantages of higher field strengths are the improvement in sensitivity and spectral resolution. This is one of the driving forces to install higher-field magnets, and it can be expected that the application of in vivo ^{31}P NMR spectroscopy to human muscle at still higher field strengths (7 or 8 T) will allow the study of

more subtle and ill-understood features of phosphate metabolism in the future. Since dynamic experiments including muscle exercise are most informative, some effort has been put into the development of in-magnet exercise devices (ergometers), which obviously should be constructed without magnetic materials.

^{1}H decoupling

As described earlier, the spins of some ^{31}P nuclei experience an interaction with nearby ^{1}H spins causing line broadening. Using a so-called second radio frequency channel, it is possible to decouple this interaction by irradiation at the ^{1}H frequency (Luyten et al. 1989). The line splittings collapse and gives narrower and higher spectral lines, which improves spectral resolution and sensitivity. Additional peaks become resolved, such as for phosphatidylcholine and phosphatidylethanolamine at the phosphodiester position (see figure 2.1B). On increasing the field strength the line widths of ^{31}P resonances obtained in vivo become broader, and this effect starts to dominate the spin-spin coupling, which is independent of field strength. In practice decoupling above field strengths of about 4 T has little effect, but as the improvement in chemical shift separation brings more gain than the resolution loss caused by line broadening, such a higher field can compete favorably with a lower field combined with ^{1}H decoupling.

Another useful effect is the so-called nuclear Overhauser effect, by which it is possible to "pump" magnetization from the ^{1}H nuclei to the ^{31}P nuclei. Also, for this effect a second radio frequency channel may be useful. In this way the sensitivity of detecting ^{31}P resonances at 1.5 T can be improved up to about 70% (Bachert & Belleman, 1992; Brown et al. 1995).

Localization, spatial and temporal resolution

The possibility of obtaining ^{31}P NMR spectra from selected tissue areas and the spatial and temporal resolution of ^{31}P NMR spectroscopy are important issues to take into consideration in the design of experimental protocols. For ^{31}P NMR spectroscopy of human muscle it is very common to employ a circular (or ellipsoid) radio frequency surface coil for signal excitation and reception. The dimensions of the coil are adapted to the muscle or muscle part of interest. Signals from the tissue adjacent to the coil are selectively sampled in this way from a hemisphere with a radius approximately equal to the radius of the coil. Although this is a convenient and sensitive approach to perform ^{31}P NMR spectroscopy it sometimes is necessary to apply more precise localization of the tissue region from which the signal has to be sampled. Several methods have been developed for this purpose over the years. Currently, gradient-based methods for the selection of tissue volumes are used in which voxel location and dimensions can be set arbitrarily. This technique enables researchers and clinicians to zoom in on different subtypes of muscles if required. A popular single voxel

technique for ^{31}P NMR spectroscopy is a multi-acquisition-shot method called image-selected in vivo spectroscopy (ISIS; Ordidge et al. 1986). The minimum volume that can be selected with a sufficient signal to noise ratio depends on a number of factors, but as a 'rule of the thumb' it needs to be at least about 15 ml for ^{31}P NMR spectroscopy at the field strength of 1.5 T. Multi-voxel localization may be provided by so-called spectroscopic imaging or chemical shift imaging methods (Brown, 1992). This can also be applied to human skeletal muscle as illustrated by the example shown in figure 4.5 (page 70, 71 & 73).
In dynamic studies it is often important to optimize the time resolution of an experiment. As larger volumes of detection produce a better signal to noise ratio in the same measurement time, generally the largest possible volume that is assumed to be sufficiently homogeneous is selected in time-critical experiments. In dynamic ^{31}P NMR spectroscopy of human skeletal muscle time resolution is usually between 1 second and 1 minute.

Sensitivity and NMR visibility in the detection of phosphorus metabolites.

As ^{31}P nuclei are present at 100% natural abundance in body compounds the question may arise why not all phosphate compounds present in skeletal muscle are visible in the NMR spectrum. This is related to the sensitivity of the NMR spectroscopy method. At the presently-employed clinical field strengths and experimental conditions the phosphate concentration of a compound has to be more then 0.1 mM/kg wet weight and in most experiments a threshold concentration of 0.5 mM/kg wet weight is required. Furthermore, only small mobile compounds generate resonances with sufficiently small line widths to make them visible. These restrictions limit the number of visible phosphate compounds in skeletal muscle to about eight. The determination of differences in glucose-6-phosphate levels in human muscle of less than 0.1 mM/kg (Rothman et al. 1992) illustrate the current lower limits of in vivo ^{31}P NMR spectroscopy measurements under optimal conditions.
Binding of small phosphate compounds to large subcellular structures or macromolecules limits their rotational freedom and renders them NMR invisible. This limitation implies that with ^{31}P NMR spectroscopy only the tissue contents of free phosphate compounds are monitored, which is of interest as this measurement provides the relevant parameters in the evaluation of biochemical processes in the cell. Invasive methods involving biopsies or freeze clamping of muscle tissue usually only can provide the total cellular level of a compound. Since quantitative analyses by both invasive methods and ^{31}P NMR spectroscopy result in similar skeletal muscle contents for ATP, it is assumed that this compound is fully NMR spectroscopy visible in this tissue (Gadian, 1995). However, ^{31}P NMR spectroscopy often gives a relatively higher level for PCr, and the difference has been attributed to the rapid breakdown mediated by the creatine kinase reaction during the freeze

clamping procedure (Meyer et al. 1982); therefore, the PCr level is also considered to be fully NMR spectroscopy visible. On the other hand, ^{31}P NMR spectroscopy often gives lower levels for P_i than invasive methods, and therefore it is assumed that a significant proportion of this compound is immobilized in subcellular structures or bound to macromolecules (Gadian, 1995). More detailed studies suggest that immobilization in the mitochondrial matrix is the causative element underlying this difference (Hutson et al. 1992). Based on this knowledge, changes in the intensity of the P_i signal have been used to quantify the mitochondrial uptake of P_i (Iotti et al. 1996).

Data processing

Finally, appropriate quantitative evaluation of resonance integrals and chemical shifts in ^{31}P NMR spectra is of importance. This evaluation is most easily performed using special software developed for this purpose, such as the time domain analysis software developed by de Beer & van Ormondt (1992) and van den Boogaart (1997), which allows the incorporation of previous knowledge for improved spectral fitting. In spectroscopic imaging experiments or in dynamic experiments with repetitive measurements, large data sets may be produced which need some type of automatic processing for which methods such as proposed by Stoyanova et al. (1995) and VanHamme et al. (1999) may be appropriate. Resonance integrals may be further evaluated as ratios. However, absolute quantities in terms of tissue or cellular contents of compounds can also be derived, provided that a proper reference is available and other variables such as signal saturation are known. Often ATP is taken as a reference, assuming a certain cellular ATP concentration at rest. This assumption seems legitimate, as tissue ATP appears relatively constant under most conditions. Also, tissue water has been introduced as an internal reference (Thulborn & Ackerman, 1983).

Cellular and molecular conclusions from macroscopic measures by ^{31}P NMR spectroscopy

It should be clear that in vivo ^{31}P NMR spectroscopy essentially provides information on phosphate compounds at the tissue level. Individual muscle cells and intracellular micro-compartments with different metabolite levels are not directly accessible by in vivo ^{31}P NMR spectroscopy. However, evaluations and interpretations at a cellular or sub-cellular level are possible when certain assumptions can be made about the origin of the signals under observation. For instance, as the sarcoplasm in muscle is the cellular compartment which contains the bulk of the ^{31}P NMR spectroscopy visible compounds, it is the phosphate metabolism of this compartment that is principally observed, although metabolic processes in cell-organelle compartments, such as the mitochondria, may have profound effects on

metabolism in the sarcoplasm. One complicating factor in data interpretation could be the presence of cellular heterogeneity. However, some compelling arguments have been put forward by Kushmerick (1995) in favor of the view that any human skeletal muscle can be considered as a unimodal continuum of properties of a relatively small range of cell types, from which it is concluded that, overall, bioenergetic variables measured by ^{31}P NMR spectroscopy of a given skeletal muscle can be interpreted in terms of biochemical and molecular mechanisms. A further complicating factor in interpretations could be metabolic compartmentalization within the cytoplasmic domain of the muscle cell. Specifically designed experiments by Wiseman & Kushmerick (1995) appear to indicate that in skeletal muscle the physicochemical properties of bulk cytoplasm is not influenced by possible sub-compartments with different ATP or ADP contents, and that the creatine kinase reaction observed by ^{31}P NMR spectroscopy can be most easily understood in terms of solution thermodynamics, with all subtrates of creatine kinase being freely available to the enzyme. However, this viewpoint, in which cellular interpretation of muscle ^{31}P NMR spectroscopy data for muscle does not consider the existence of metabolic micro-environments and subcellular structures, has been criticised (Walliman, 1996).

Muscle bioenergetics as observable by dynamic ^{31}P NMR spectroscopy

The immediate source of free energy for energy-consuming processes in the muscle comes from the reaction:

$$ATP + H_2O \rightarrow ADP + P_i + H^+ \quad (1)$$

During a contractile event this reaction is catalysed by the enzyme myosin ATPase and by ATPases involved in Ca homeostasis, as the major players. The ATP pool in the muscle is only sufficient for very brief periods of contractile activity, and therefore energy has to be provided by other pathways. A readily-available back-up reserve is present in the form of the high-energy phosphate compound PCr. The enzyme creatine kinase catalyses the reversible reaction:

$$PCr + ADP + H^+ \leftrightarrow ATP + Cr \quad (2)$$

and thereby enables the pool of high energy phosphate groups present in ATP to be replenished by that in PCr. This reaction occurs in different cellular locations, both in the cytosol and in the mitochondria, where it is mediated by different members of the creatine kinase family.

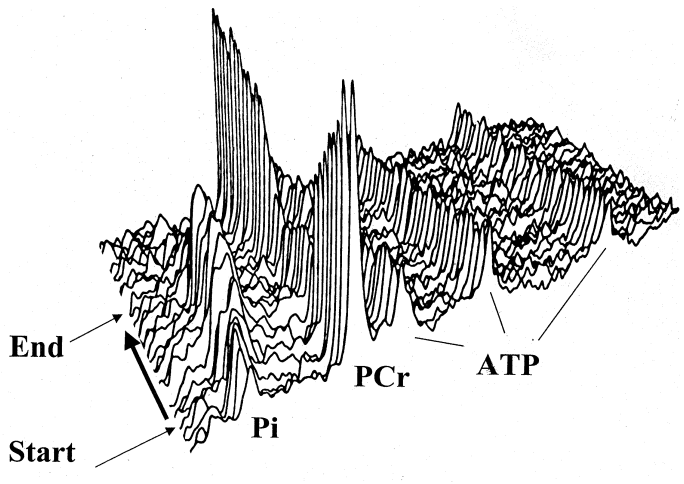

Figure 2.3: effect of exercise on ^{31}P NMR spectrum of skeletal muscle. Stacked plot of spectra obtained from thumb muscle for a period of 16 second each. The first two spectra in the stack were obtained from the thumb muscle at rest and show resonances for ATP, phosphocreatine (PCr) and inorganic phosphate (P_i). → the start and end of a period of exercise (squeezing a rubber bulb). Clearly PCr is declining and P_i increasing while ATP levels remain constant. It should be noted that the P_i peak shifts towards the PCr peak, reflecting acidification of muscle tissue. After exercise PCr rapidly increases to its original level and P_i decreases.

Combination of equations 1 and 2 gives :

$$PCr + H_2O \longrightarrow Cr + P_i \qquad (3)$$

When ATP levels are maintained at a constant level during energy consumption, a decrease in PCr levels should be accompanied by a stoichiometric increase of P_i levels. ^{31}P NMR spectroscopy provides the most direct evidence that this is indeed what happens, as illustrated in a stack plot of spectra obtained sequentially during exercise (see figure 2.3). A more detailed analyses of such experiments often shows some subtle differences from this simple viewpoint: e.g. some breakdown of ATP and some uncompensated loss of P_i signal intensity may occur.

Furthermore, PCr levels are only sufficient for a limited period of muscle activity, and would rapidly be depleted in the absence of further energy sources and/or mechanisms for vectorial transport of high-energy phosphate groups. Under aerobic conditions mitochondrial respiration serves as the major source of high-energy phosphate groups, such as ATP and PCr. In addition to having a role in balancing ATP levels, the PCr-creatine kinase system is considered to be an efficient intermediate in the transfer of high-energy phosphates from the sites of energy production (mitochondria, glycolytic loci) to the energy-consuming locations in the muscle cell, a potential function which has attracted considerable attention (Bessman & Geiger, 1981; Meyer et al. 1984; Walliman et al. 1992; Saks & Ventura-Clapier, 1994). Under anaerobic conditions, when glycogenolysis is left as the main energy-generating process, the role of the PCr circuit as back-up system for preserving the integrity of energy homeostasis becomes clearly evident. Some direct evidence for this role came from experiments with skeletal muscle of transgenic mice that were genetically depleted of the

enzyme creatine kinase (In 't Zandt et al. 1999a). During an ischemic period the ATP levels decrease in these mice, while they are maintained in control mice (see figure 2.4A).
The reaction scheme shown in equation 2 suggests that the creatine kinase reaction may also function in stabilizing pH during contraction or hypoxia-ischemia. This function was indeed apparent in the ischemia experiments with the creatine kinase-deficient mice described earlier. In the deficient mice the pH decreased to much lower values than those in control mice. Also, the pH undershoot observed in the first part of the recovery phase of normal muscle, which is due to PCr resynthesis, was absent (see figure 2.4B).
These experiments illustrate the type of information that can be obtained directly from the ^{31}P NMR spectra of skeletal muscle. From this information further quantitative biochemical data can be derived, provided the assumptions made hold true. For instance from the ATP to PCr ratio and the pH values the global free muscular ADP content can be calculated from the equilibrium equation derived from reaction 2:

$$ADP = (Cr \times ATP) / (k \times PCr \times H^{+}),$$

where Cr is the creatine concentration and k is the equilibrium constant.
Free ADP is at too low a level in the muscle cell to be assessed experimentally by direct measurements using ^{31}P NMR spectra. Thus, the calculation gives a valid indirect assessment, but the method requires that the creatine kinase reaction is in equilibrium, that the equilibrium constant k is known, and that the total creatine concentration available in muscle is known and constant. There is good evidence that in skeletal muscle the creatine kinase reaction is in equilibrium (Rees et al. 1989). The extent to which cellular creatine is completely free in solution and available to the enzyme is currently a subject of combined ^{31}P and ^{1}H NMR spectroscopy studies (for example, see In 't Zandt et al. 1999b; Kreis et al. 1999; Kruiskamp & Nicolay, 1999). ADP concentrations calculated in this way resulted in much lower values than derived by chemical methods after freeze clamping, which makes sense as in the latter methods total ADP levels (free and bound) are obtained. In a similar way global free AMP concentrations may be estimated from the equation:

$$AMP = (ADP)^{2} / (k \times ATP).$$

Thus, a number of essential parameters obtained either directly or indirectly from dynamic ^{31}P NMR spectroscopy can be used for quantitative studies of the kinetics of energy metabolism in vivo. In this manner it is possible to obtain reliable estimates of the rates of aerobic and anaerobic ATP synthesis, and the influence of metabolic control. This information is the major contribution that ^{31}P NMR spectroscopy can offer to the field of

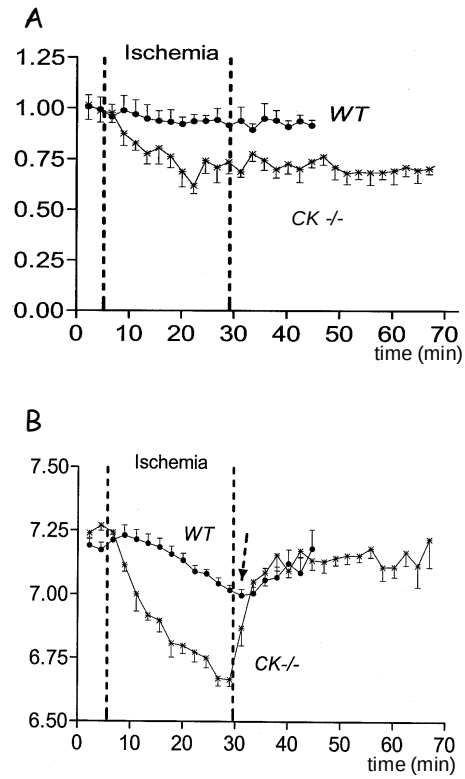

Figure 2.4: effect of ischaemia on ATP levels and pH in wild type (WT: •–•) and creatine kinase-deficient mice (CK-/-: ∗–∗). The period of ischemia was 25 min. A: Time course of ATP levels relative to the starting ATP level (ATP(0)). It should be noted that recovery of ATP in the CK-/- mice is slow. B: time-course of skeletal muscle pH. → further decrease in pH during the first minutes of recovery because of phosphocreatine synthesis. This effect is not seen for the CK-/- mice. Values are means with their standard errors for six mice.

physiology and metabolism of human skeletal muscle. At present no other technique can match this potential for longitudinal non-invasive metabolic investigations of the intact living muscle.

As an example, a central issue in ^{31}P NMR spectroscopy of skeletal muscle has been the metabolic control of mitochondrial function. Several approaches have been followed; for instance Chance et al. (1986) have used a graded steady-state non-exhaustive exercise protocol to identify ADP as a principal control element of oxidative metabolism in human skeletal muscle under these conditions. In this study a Michaelis-Menton type of equation yielded an apparent maximum velocity as a measure of oxidative capacity. Others (for example, see Taylor et al. 1983, 1986; Bendahan et al. 1990; Barbiroli, 1992; Radda et al. 1995) have measured the rate of oxidative metabolism under non-steady-state exercise conditions. In particular the recovery rate of PCr immediately after submaximal exercise appears to reflect mitochondrial capacity (Lodi et al. 1997). No recovery of the PCr content occurs during ischemia after exercise (Taylor et al. 1983; Quistorff et al. 1993).

Thus, to confirm qualitative information, quantitative assessment is becoming increasingly important. A comprehensive method for the quantitative interpretation of ^{31}P NMR spectroscopy measurements of muscle before, during and after several types of muscle exercise has been presented by Kemp & Radda (1994). With this method it is possible to estimate rates of glycogenolytic and aerobic ATP synthesis during exercise, as well as the

magnitude of oxidative ATP synthesis and proton efflux during recovery from exercise. The oxidative capacity associated with steady-state exercise can be assessed quantitatively. An improved method of assessing ADP recovery after exercise has recently been reported (Chen et al. 1999). Results from NMR spectroscopy studies of human skeletal muscle have also been interpreted in terms of metabolic control analysis (Shulman et al. 1995) or metabolic control theory (Jeneson et al. 1999).

Importantly, in either a more qualitative or a quantitative sense, ^{31}P NMR spectroscopy approaches have also been used to characterize various conditions of human muscle energy metabolism, e.g. in diseased muscle, injured muscle, fatigued muscle, muscle adapted to increased (dis)use, etc. (for example, see Ross et al. 1981; Duboc et al. 1987; deGroot et al. 1993; Cozzone & Bendahan, 1994; McCully et al. 1994; Radda et al. 1995).

Combinations of ^{31}P NMR measurements with other NMR measurements (e.g. ^{1}H , 13C) in the same measurement session or experimental setting may offer a powerful extended view on metabolic and physiological processes in skeletal muscle, for example as demonstrated in studies of diabetes mellitus (Shulman et al. 1996).

Chemical reaction kinetics in vivo by ^{31}P magnetization transfer

^{31}P NMR spectroscopy offers an unique possibility to determine flux rates in biochemical pathways in vivo by the magnetization transfer method (Brindle, 1988; Rudin & Sauter, 1992). The technique involves perturbation of the magnetization of a nuclear spin system in a particular compound, and monitoring how this perturbation influences the nuclear magnetization of this spin system present in another compound with which it is in chemical exchange. This process is illustrated by the spectra in figure 2.5 (A-C) for wild type mouse skeletal muscle. Figure 2.5A is a control spectrum, while for the spectrum in figure 2.5B the γ-phosphate spin of ATP is selectively irradiated to make its signal disappear. Figure 2.5C shows the difference spectrum, and it is immediately clear that part of the PCr signal is disappeared as well, which is because it is in rapid exchange with the γ-phosphate of ATP in the creatine kinase reaction. Magnetization transfer in this type of experiment is commonly called saturation transfer. From a series of such experiments it is possible to estimate the rate-constants of the creatine kinase reaction, and thus the flux through this reaction. Reaction rates of between about 0.05 and 10 s^{-1} can be estimated by this method (Meyer, 1982; Rudin & Sauter, 1992). We have also performed a saturation transfer experiment on mouse skeletal muscle deficient in the creatine kinase (see figure 2.5 (D-F)). Irradiating the γ-phosphate peak had no effect on the PCr signal (figure 2.5F), a clear demonstration that the magnitude of exchange has decreased below NMR spectroscopy detection. In these mice PCr was found to be almost metabolically inactive (Steeghs et al.1997; In ‘t Zandt et al. 1999a).

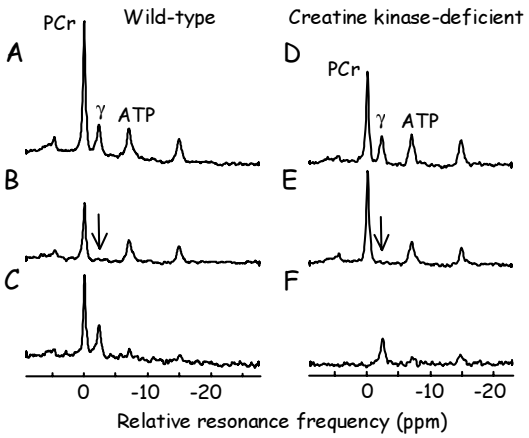

Figure 2.5: saturation transfer experiment using mouse skeletal muscle. A-C: spectra obtained from the hind limb of a wild-type mouse. D-F: spectra from a creatine kinase-deficient mouse. A&D: control spectra. B&E: spectra obtained with saturation of the γ-ATP (↓). C&F: the difference spectra showing an effect on phosphocreatine in the case of wild-type mice and the absence of an effect for creatine kinase-deficient muscle. Ppm, part per 10^6.

This technique has also been applied to human skeletal muscle (for example, see Rees et al. 1989). Both animal and human studies are in agreement with the notion that in skeletal muscle at rest the creatine kinase reaction is in equilibrium and that the flux through this reaction is faster than the net ATP turnover rates. Contrary to expectation, in two studies on human subjects the flux from PCr to ATP decreased during muscle exercise (Rees et al. 1989; Goudemant et al. 1997). However, a recent study showed that this flux was increased or at resting levels during exercise (Horska et al. 1999).

Heterogeneity in muscle pH during exercise

In general ^{31}P NMR spectra of resting human skeletal muscle appear to be rather uniform, in agreement with the viewpoint of Kushmerick (1995), although some studies indicate small variations in the P_i to PCr ratio possibly related to fast- and slow-twitch fiber composition of the muscle studied (VandenBorne et al. 1995). During exercise more than one P_i peak may appear in the spectra at different positions, and this pH heterogeneity has been taken as a reflection of different fiber types in the muscle under study (Park et al. 1987): i.e. the glycolytic fibers show faster acidification during exercise than the oxidative fibers. An alternative explanation for this observation was that the surface coil used in these experiments views more than one muscle type; for example two muscles of which one is more heavily involved in exercise than the other. However, further experiments indicated that these different P_i peaks indeed may arise from within a single muscle (vandenBorne et al. 1993; Mizuno et al. 1994). We have explored this phenomenon in the m. tibialis anterior, as described in chapter 4.

Acknowledgement

We thank Mark Rijpkema for obtaining the ^{31}P NMR spectrum of human skeletal muscle at rest. We also thank Erik van den Boogert for excellent technical assistance.

References

Achten E, van Cauteren M, Willem R, Luypaert R, Malaisse W, van Bosch G, Delanghe G, de Meirleir K & Osteaux M. ^{31}P-NMR spectroscopy and the metabolic properties of different muscle fibers. *J Appl Physiol* 68: 644-649, 1990.

Ackerman J, Grove T, Wong G, Gadian D & Radda G. Mapping of metabolites in whole animals by 31P NMR using surface coils. *Nature* 283: 167-170, 1980.

Bachert P & Belleman M. Kinetics of the in vivo 31P-^{1}H Nuclear Overhauser effect of the human-calf-muscle phosphocreatine resonance. *J Magn Reson* 100: 146-156, 1992.

Barbiroli B. 31P MRS of human skeletal muscle. In: *Magnetic Resonance Spectroscopy in Biology and Medicine*, edited by De Certaines JD, Bovee WMMJ & Podo F. Oxford: Pergamon Press, 1992, p. 369-386.

Bendahan D, Confort-Gouny S, Kozak-Reiss G & Cozzone P. Heterogeity of metabolic reponse to muscular exercise in humans. New criteria of invariance defined by in vivo phosphorus-31 NMR spectroscopy. *FEBS Letters* 269: 155-158, 1990.

Bessman S & Geiger P. Transport of energy in muscle. The phosphoryl-creatine shuttle. *Science* 211: 448-452, 1981.

Brindle K. NMR methods for measuring enzyme kinetics in vivo. *Prog NMR Spec* 20: 257-293, 1988.

Brown T. Practical applications of chemical shift imaging. *NMR Biomed* 5: 238-243, 1992.

Brown TR, Stoyanova R, Greenberg T, Srinivasan R & Murphy-Boesch J. NOE enhancements and T_1 relaxation times of phosphorylated metabolites in human calf muscle at 1.5 Tesla. *Magn Reson Med* 33: 417-421, 1995.

Chance B, Eleff S, Leigh J, Sokolow D & Sapega A. Mitochondrial regulation of phosphocreatine / inorganic phosphate ratios in excersizing human muscle: gated 31P NMR study. *Proc Natl Acad Sci USA* 78: 6714-6719, 1981.

Chance, B, Leigh J, Kent J, McCully K, Nioka S, Clark B & Maris Graham T. Multiple controls of oxidative metabolism in living tissues as studied by magnetic resonance. *Proc Natl Acad Sci USA* 83: 9458-9462, 1986.

Chen J, Argov Z, Kearney R & Arnold D. Fitting cytosolic ADP recovery after exercise with a step response function. *Magn Reson Med* 41: 926-932, 1999.

Cozzone P & Bendahan D. 31P NMR spectroscopy of metabolic changes associated with muscle exercise: physiopathological applications. In: *NMR in Physiology and Biomedicine,* edited by Gillies RJ. New York: Academic Press, 1994, p. 389-402.

Cresshull, I, Dawson M, Edwards R, Gadian D, Gordon R, Radda G, Shaw D & Wilkie D. Human muscle analysed by 31P nuclear magnetic resonance in intact subjects. *J Physiol* 317: 18P, 1981.

de Beer R & van Ormondt D. Analysis of NMR data using time domain fitting procedures. *NMR: basic principles and progress* 26: 201-248, 1992.

DeGroot M, Massie B, Boska M, Gober J, Miller R & Weiner M. Dissociation of [H^+] from fatigue in human muscle detected by high time resolution ^{31}P-NMR. *Muscle Nerve* 16: 91-98, 1993.

Duboc D, Jehenson P, Tran Dinh S, Marsac C, Syrota A & Fardeau M. Phosphorus NMR spectroscopy study of muscular enzyme deficiencies involving glycogenolysis and glycolysis. *Neurology* 37: 663-671, 1987.

Gadian D. *NMR and its applications to living systems,* 2nd ed. Oxford: Oxford University Press, 1995.

Goudemant J, Francaux M, Mottet I, Demeure R, Sibomana M & Sturbois X. 31P NMR saturation transfer study of the creatine kinase reaction in human skeletal muscle at rest and during exercise. *Magn Res Med* 37: 744-753, 1997.

Gupta R & Moore R. 31P NMR studies of intracellular free Mg2+ in intact frog skeletal muscle. *J Biol Chem* 255: 3987-3993, 1980.

Heerschap A, Bergman A, van Vaals J, Wirtz P, Loermans H & Veerkamp J. Alterations in relative phosphocreatine concentrations in preclinical mouse muscular dystrophy revealed by in vivo NMR. *NMR in Biomed* 1: 27-31, 1988.

Heerschap A, den Hollander J, Reynen H & Goris R. Metabolic changes in reflex sympathetic dystrophy : a 31P NMR spectroscopy study. *Muscle Nerve* 16: 367-373, 1993.

Horska A, Fishbein K, Fleg J & Spencer R. The relationship between creatine kinase reaction kinetics and exercise intensity in human forearm is unchanged by age. *Proc Internat Soc Magn Reson Med* 7: 1537, 1999.

Hoult D, Bushy S, Gadian D, Radda G, Richards R & Seeley P. Observation of tissue metabolites using 31P nuclear magnetic resonance. *Nature* 252: 285-287, 1974.

Hutson S, Williams G, Berkich D, LaNoue K & Briggs, R. A 31P NMR study of mitochondrial inorganic phosphate visibility : effects of Ca2+, Mn2+ and the pH gradient. *Biochem* 31: 1322-1330, 1992.

In 't Zandt H, Klomp D, Oerlemans F, Wieringa B & Heerschap A. Dipolar coupling of creatine and taurine in proton MRS of mouse skeletal muscle. *Proc Internat Soc Magn Reson Med* 7: 193, 1999a.

In 't Zandt H, Oerlemans F, Wieringa B & Heerschap A. Effects of ischemia on skeletal muscle energy metabolism in mice lacking creatine kinase monitored by in vivo ^{31}P nuclear magnetic resonance spectroscopy. *NMR Biomed* 12: 327-334 1999b.

Iotti S, Lodi R, Gottardi G, Zaniol P & Barbiroli B. Inorganic phosphate is transported into mitochondria in the absence of ATP biosynthesis: an in vivo ^{31}P NMR study in the human skeletal muscle. *Biochem Bioph Res Co* 225: 191-194, 1996.

Iotti S, Tarduci R, Gottardi G & Barbiroli B. Cytosolic free Mg2+ in the human calf muscle in different metabolic conditions: in vivo 31P MRS and computer simulation. *Proc Internat Soc Magn Reson Med* 7: 1540, 1999.

Jeneson J, Westerhoff H & Kushmerick M. Kinetic control in homeostasis of ATP free energy potential in skeletal muscle. *Proc Internat Soc Magn Reson Med* 7: 197, 1999.

Kemp G & Radda G. Quantitative interpretation of bioenergetic data from ^{31}P and ^{1}H magnetic resonance spectroscopic studies of skeletal muscle: an analytical review. *Magn Reson Quart* 10(1): 43-63, 1994.

Kreis R, Jung B, Felblinger J & Boesch C. Effect of exercise on the creatine resonance in ^{1}H MR spectra of human skeletal muscle. *J Magn Reson* 137: 350–357, 1999.

Kreis R, Koster M, Kambler M, Felblinger J, Slotboom J, Walker G, Hoppeler H & Boesch C. Effect of creatine supplementation upon muscle metabolism studied by ^{1}H and 31P MRS, MRI, excersize performance testing and clinical chemistry. *Proc Internat Soc Magn Reson Med* 4: 25, 1996.

Kruiskamp M & Nicolay K. Unraveling the magnetization transfer effect on the ^{1}H signal of creatine in rat skeletal muscle. *Proc Internat Soc Magn Reson Med* 7: 196, 1999.

Kushmerick M. Bioenergetics and muscular cell types. *Adv Exp Med Biol* 384: 175-184, 1995.

Lodi R, Kemp G, Iotti S, Radda G & Barbiroli B. Influence of cytosolic pH in vivo assessment of human muscle mitochondrial respiration by phosphorus magnetic resonance spectroscopy. **MAGMA** 5: 165-171, 1997.

Luyten P, Bruntink G, Sloff F, Vermeulen J, van der Heijden J, den Hollander J & Heerschap A. Broadband proton decoupling in human ^{31}P NMR spectroscopy. *NMR Biomed* 1: 177-183, 1989.

McCully K, VandenBorne K, Posner J & Chance B. Magnetic Resonance of muscle bioenergetics. In: *NMR in Physiology and Biomedicine*, edited by Gillies RJ. New York: Academic Press, 1994, p. 405-411.

Meyer R, Kushmerick M & Brown T. Application of 31P NMR spectroscopy to the study of striated muscle metabolism. *Am J Physiol* 242: C1-C11, 1982.

Meyer R, Sweeney L & Kushmerick M. A simple analysis of the "phosphocreatine shuttle" *Am J Physiol* 246: C365-C377, 1984.

Mizuno M, Secher N & Quistroff B. ^{31}P-NMR spectroscopy, rsEMG and histochemical fiber types of human wrist flexor muscles. *J Appl Physiol* 76: 531-538, 1994.

Moon R & Richards J. Determination of intracellular pH by 31P magnetic resonance. *J Biol Chem* 248: 7276–7278, 1973.

Ordidge J, Connelly A & Lohman J. Image selected in vivo spectroscopy (ISIS). A new technique for spatially selective NMR spectroscopy. *J Magn Reson* 66: 283–294, 1986.

Park J, Brown R, Park C, Cohn M & Chance B. Energy metabolism of the untrained muscle of elite runners as observed by 31P magnetic resonance spectroscopy: evidence suggesting a genetic endowment for endurance exercise. *Proc Natl Acad Sci USA* 85: 8780-8784, 1988.

Park J, Brown R, Park C, McCully K, Cohn M, Haselgrove J & Chance B. Functional pools of oxidative and glycolytic fibers in human muscle observed by ^{31}P magnetic resonance spectroscopy during exercise. *Proc Natl Acad Sci USA.* 84: 8976-8980, 1987.

Park J, Niermann K, Das A, Carr B & Olsen N. Abnormalities in Magnesium (Mg2+) and ATP levels in muscle disorders: dermatomyositis and fibromyalgia. *Proc Internat Soc Magn Reson Med* 7: 1536, 1999.

Quistorff B, Johansen L & Sahlin K. Absence of phosphocreatine resynthesis in human calf muscle during ischemic recovery. *Biochem J* 291: 681-686, 1993.

Radda G, Odoom J, Kemp G, Taylor D, Thompson C & Styles P. Assessment of mitochondrial function and control in normal and diseased state. *Biochim Biophys Acta* 1271: 15–19, 1995.

Rees D, Smith M, Harley J & Radda G. In vivo functioning of creatine phosphokinase in human forearm muscle, studied by 31P NMR saturation transfer. *Magn Reson Med* 9: 39–52, 1989.

Ross B, Radda G, Gadian D, Rocker G, Esiri M & Falconer-Smith J. Examination of a case of suspected McArdle's syndrome by 31P Nuclear magnetic resonance. *N Engl J Med* 304: 1338–1342, 1981.

Rothman D, Shulamn R & Shulman G. 31P nuclear magnetic resonance measurements of glucose-6-phosphate: evidence for reduced insulin-dependent muscle glucose transport or phosphorylation activity in non-insulin-dependent diabetes mellitus. *J Clin Invest* 89: 1069–1075, 1992.

Rudin M & Sauter A. Measurement of reaction rates in vivo using magnetization transfer techniques. *NMR: basic principles and progress* 27: 257–293, 1992.

Saks V & Ventura-Clapier R. (editors) *Cellular bioenergetics: role of coupled creatine kinase.* London: Kluwer Academic Publishers, 1994, p. 1–346.

Sastrustegui J, Berkowitz H, Boden B, Donlon E, McLaughlin A, Maris J, Warnell R & Chance B. An in vivo phosphorus nuclear magnetic resonance study of the variations with age in the phosphodiesters' content of human muscle. *Mech Age Dev* 42: 105-114, 1988.

Shulman R, Bloch G & Rothman D. In vivo regulation of muscle glycogen synthase and the control of glycogen synthesis. *Proc Natl Acad Sci USA* 92, 8535 – 8542, 1995.

Shulman R, Rothman D & Price T. Nuclear magnetic resonance studies of muscle and applications to exercise and diabetes. *Diabetes* 45: S93–S98, 1996.

Steeghs K, Benders A, Oerlemans F, de Haan A, Heerschap A, Ruitenbeek W, Jost C, van Deursen J, Perryman B, Pette D, Bruckwilder M, Koudijs J, Jap P, Veerkamp J & Wieringa B. Altered Ca2+ responses in muscles with combined mitochondrial and cytosolic creatine kinase deficiencies. *Cell* 89: 93–103, 1997.

Stoyanova R, Kuesel A & Brown T. Application of principal-component analysis for spectral quantitation. *J Magn Reson* 115: 265–269, 1995.

Taylor D, Bore P, Styles P, Gadian D & Radda G. Bioenergetics of intact human muscle. A 31P Nuclear Magnetic Resonance study. *Mol Biol Med* 1: 77–94, 1983.

Taylor D, Styles P, Matthews P, Arnold D, Gadian D, Bore P & Radda G. Energetics of human muscle: exercize induced ATP depletion. *Magn Reson Med* 3: 44–54, 1986.

Thulborn K & Ackerman J. Absolute molar concentrations by NMR in inhomogeneous B1. A scheme for analysis of in vivo metabolites. *J Magn Reson* 55, 357-371, 1983.

Van den Boogaart A. Quantitative data analysis of in vivo MRS data sets. *Magn Reson Chem* 35: S146-S152, 1997.

Vandenborne K, Walter G, Leigh J & Goelman G. pH heterogeneity during exercise in localized spectra from single human muscles. *Am J Physiol* 265: C1332-C1339, 1993.

Vandenborne K, Walter G, Ploutz-Snyder L, Staron R, Fry A, de Meirleir K, Dudley G & Leigh J. Energy-rich phosphate in slow and fast human skeletal muscle. *Am J Physiol* 268: C869-C876, 1995.

VanHamme L, van Huffel S & van Hecke P. Extension of AMARES to quantitate series of biomedical MRS signals. *Proc Internat Soc Magn Reson Med* 7, 1558, 1999.

Wallimann T. 31P NMR measured creatine kinase reaction flux in muscle: a caveat. J Muscle Res Cell Motil 17: 177-181, 1996.

Wallimann T, Wyss M, Brdiczka D, Nicolay K & Eppenberger H. Intracellular compartmentation, structure and function of creatine kinase isoenzymes in tissues with high and fluctuating energy demands: the 'phosphocreatine circuit' for cellular energy homeostasis. *Biochem J* 281: 31–40, 1992.

Wiseman R & Kushmerick M. Creatine kinase equilibrium follows solution thermodynamics in skeletal muscle. *J Biol Chem* 1270: 12428–12438, 1995.

3

Introduction to multichannel surface electromyography*

Introduction

In clinical neurophysiology, surface electromyography (EMG) is a well-known recording technique in the context of routine motor nerve conduction studies. However, the judgement of voluntary recruitment of motor units and muscle function is regarded to be best possible with intramuscular needle EMG. With a needle EMG electrode the electrical activity of a limited number of activated motor units is measured. However, the small measurement area causes the signal amplitude to be dependent on the position of a few muscle fibers near the needle tip, which impairs the reproducibility of needle EMG measurements. In fact, surface EMG recordings are superior in motor nerve conduction studies for just those reasons. The most rational approach in judging techniques, including the comparison of surface EMG and needle EMG, is to take the particular clinical question as starting point to determine the best method of recording. This approach was used historically, as the needle EMG recording technique evolved through single fiber electrodes, concentric and monopolar needles, macro EMG needle and adapted recording procedures such as scanning EMG (Stålberg, 1986; Stålberg & Falck, 1997). In each of these the recording area and type of needle electrode were adapted to the clinical and scientific questions at hand. More recently, surface EMG also has evolved in different directions, dependent on the type and character of the investigation (Stegeman et al. 2000b; Zwarts et al. 2000). Essential to the question of which electrode and technique has to be used, is what information and at what scale do we want to get information regarding the muscle, motor unit or muscle fiber. When a needle electrode is used, the investigator can observe spontaneous depolarization of single muscle fibers and the motor unit action potential as the electrical reflection of the motor units microarchitecture. In surface EMG, the investigator takes a more distant viewpoint and uses the EMG signal to

*adapted from **Stegeman DF, Houtman CJ, Lapatki BG & Zwarts MJ**. Multichannel surface EMG. In: *Clinical neurophysiology of disorders of muscle and neuromuscular junction, including fatigue*. Handbook of Clinical Neurophysiology, Vol. 2, 2003.

collect data regarding the integrated activity of a motor unit or of a whole muscle. An important limitation of needle recordings and in general of single channel EMG recordings is that electrical events originating in the motor unit are exclusively measured as a time-varying signal. This is so obvious that it usually does not receive much consideration. Although the motor unit action potential passes by from left to right on the oscilloscope screen, this passage has no relation with the physical propagation of the motor unit action potential along the muscle fibers. A change in time of a locally measured potential is observed, principally limiting what can be extracted or concluded from a signal. Nevertheless, some spatial properties of the motor unit, such as the mean fiber length are reflected in the temporal characteristics of the needle recorded motor unit action potential, in this case its duration (Dumitru et al. 1999). But most spatial motor unit characteristics (position, spatial extent, neuromuscular junction position, length of the muscle fibers and action potential propagation), that are essential for the motor unit's force generating capacity, are only marginally or indirectly accessible with a single channel electrode examination. Still it is so that changes in disease, such as sprouting following axonotmesis or myopathic processes, are predominantly reflected in spatial motor unit changes. This spatial, or topographical, aspect can be better visualized with multichannel EMG recordings than by a single channel (needle or surface) EMG recording. In this review, we will first introduce the biophysical basis of the EMG signal, which is a prerequisite for proper surface EMG data understanding and interpretation. Clinical applications of action potential propagation estimation by linear array electrodes are then discussed. It will be shown how needle EMG and surface EMG can be complementary in the diagnostic process. Next, we will show how spatial aspects of the motor unit change with pathology and how two-dimensional high-density surface EMG can deepen our knowledge. Present applications and future possibilities of multichannel surface EMG techniques will be discussed.

The muscle fiber as track for a propagating bioelectric source

The membranes of muscle and nerve fibers have the well-known property of actively keeping a potential difference of about 70 mV between the intra- and the extracellular environment. After a breach of the equilibrium by the opening of sodium channels in the membrane (excitation), the potential difference is cancelled out and even inverted within a fraction of a millisecond. In the remaining part of that millisecond, the steady state balance situation is almost re-established, mainly with the help of potassium ions. We will not discuss the final slow phase of the repolarization of the intracellular action potential, which was recently discussed (for example, see McGill & Lateva, 2001). Thus, a transient waveshape is generated. The well understood biophysical background of this process, that is

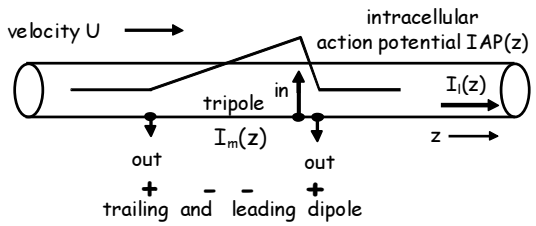

Figure 3.1: stylized presentation of an intracellular action potential as a function of position along a muscle fiber during steady propagation. Indications of propagation velocity U, the short depolarization and the (longer tail) repolarization phase are included, as well as the schematics (tripole) for the transmembrane ionic current I_m and its ultimate simplification in terms of a leading (- +) and trailing (+ -) dipole pair.

complicated in muscle fibers by the presence of the T-tubular system (Wallinga et al. 1999), neither will be discussed.

But action potential generation on the spot is not “all-there-is”. If it were, clinical neurophysiology would become very difficult. The EMG electrode would never be at the right place. Moreover, an essential “design driver” for membranes in neurological and neuromuscular structures is fast transport of information. An intracellular longitudinal electric current I_l (figure 3.1) produces a transmembrane potential also affecting adjacent sarcolemma segments. This transient potential change opens the sodium channels there and a new action potential arises. Effectively, it starts propagating and thus transporting information. In the case of a muscle fiber, the propagation along the sarcolemma happens with a speed of approximately 4 m/s (Arendt-Nielsen & Zwarts, 1989). This velocity depends on a number of factors that are discussed later. Although often taken for granted, the active propagation of the action potential and its start and termination have non-trivial consequences. We continue this review with some basic concepts to provide insight to the combined processes of action potential propagation and electric volume conduction.

Because of its propagation, an action potential does not merely exist as a function of time. It also spreads out along the fiber as a function of space. As long as the intracellular action potential (IAP) is propagating with constant velocity U in fiber direction z, the relation between the action potential as a function of time t and as a function of space z is simple:

$$IAP(z) = IAP(U.t) \qquad (1)$$

The intracellular action potential as a function of position z along a muscle fiber is depicted schematically in figure 3.1. A triangular wave shape in which the short de- and the longer re-polarization phase can be recognized. This way of presenting the intracellular action potential is reflected in the transmembrane ionic current ($I_m(z)$), that is restricted to three points along the fiber: the tripole concept (Rosenfalck, 1969). The muscle fiber source can be considered a leading and a trailing current dipole (Dumitru & King, 1992; Dumitru et al. 2002). The validity of this simplification depends on the type of recording. In general, for surface EMG the leading/trailing dipole description of the transmembrane source is sufficiently accurate.

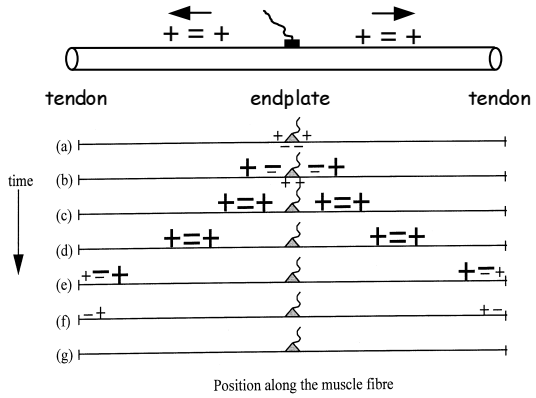

Figure 3.2: the spatio-temporal development of the transmembrane ionic current along a muscle fiber. The transmembrane ionic current starts as two dipoles at the endplate after excitation by a motoneuron action potential (a). After full development of these first (leading) dipoles, a second (trailing) pair emerges (b). The balanced, double pair then propagates as two tripoles in opposite directions (c, d). On arrival at the tendon, the leading dipoles decline in strength (e). Subsequently, also the trailing dipoles decline (f) and disappear (g). Adapted from Roeleveld et al. (1997a).

It is obvious that the propagation of action potentials is a process that has to start and terminate somewhere. In figure 3.2, the life cycle of an action potential propagating over the sarcolemma of an excited muscle fiber is schematically shown on the basis of the leading/trailing dipoles concept. It shows that even in the case of a single fiber, the source of the surface EMG signal is a complicated function of time and position.

Electric volume conduction

The knowledge on muscle fiber excitability and a propagating intracellular action potential would still be without clinical relevance if the clinical neurophysiologist had to penetrate muscle fibers to measure IAP(t), or to record in the immediate vicinity of the fibers to measure $I_m(t)$ (figure 3.1). The finite electric impedance of living tissue makes the transmembrane ionic current I_m (leaving and entering the fiber) visible "indirectly". According to Ohm's law, an electric current I [unit: Ampere, A], flowing between two locations that are connected through a resistance R [unit: Ohm, Ω], generates a potential difference V [unit: Volt, V] between these locations: V=I.R. Ohm's law is one dimensional, but a similar principle relates electric current and voltage in a three dimensional structure with a resistance, such as tissue. This resistance is reciprocally expressed as the electric conductivity σ [unit: 1/(Ω.m)]. The principle of volume conduction, as the three dimensional version of Ohm's law is often referred to, relates an injected current I_i at site i in the volume to a potential V_j at site j in that same volume. When the distance between sites i and j is r_{ij}, this principle states that for the simple case of a very large (until infinity) volume with conductivity σ everywhere

$$V_j = I_i/(4\pi\sigma r_{ij}) \qquad (2)$$

The potential V_j is then compared to a (zero) reference potential infinitely far from the sites i and j. It is important, first of all, to see confirmed that when the membrane source strength I_i

doubles, the potential V_j also becomes twice as large. That makes bioelectric potential measurements useful for diagnostic medicine. But also both the conductivity σ and the distance r_{ij} are in the denominator of the equation. So, assuming a constant source I_i, the potential decreases with increasing observation distance and with increasing conductivity σ (lowering resistance). Unfortunately, the values of σ and r_{ij} are hardly relevant for diagnostic conclusions. Interindividual changes in both, can be annoying or, even worse, mislead the experimenter. The simplicity of equation 2 is deceiving. Unfortunately, it can only be used qualitatively to explain surface EMG signals for a number of reasons. First, the electric source, even of a single muscle fiber, never can be described by one injected current I_i at a certain point i, but is a composite of multiple sources, brought about by the spatial extension of the IAP(z). Think of I_i as one of the poles of the tripole depicted in figure 3.1. Second, the tissue never has an infinitely large volume. It is always finite, a property that has substantial consequences with respect to volume conduction (Stegeman et al. 1997). Third, a single parameter σ would imply that the whole volume has the same uniform property as conductor of electric current. This also is a simplification. In surface EMG recordings, the tissue layers with different properties between the source and the recording electrodes (muscle, subcutaneous fat, skin) require special attention (Roeleveld et al. 1997a; Blok et al. 1998; Merletti et al. 1999a,b; Stegeman et al. 2000a; Farina & Merletti, 2001; Lowery et al. 2002). Despite these concerns, equation 2 can well be used for explaining the important effects of volume conduction.

Volume conduction and action potential propagation

Monopolar recorded potentials

The muscle as bioelectric source and the effect of volume conduction together determine the electrophysiological wave shapes recorded with a distant reference electrode (monopolar montage, see also note 1 below). Figure 3.3 shows model simulated single fiber action potentials of the same muscle fiber at a varying observation distance away from the fiber (Blok et al. 2002a). This distance increases from 0.5 mm, for example, from a needle electrode recording close to muscle fiber, to 25 mm for a monopolar surface EMG recording of a simulated action potential from a single muscle fiber in a deep motor unit. Since all the other characteristics remain unchanged, the differences between the waveforms are entirely due to volume conductor effects. Note that in figure 3.3 the horizontal axis denotes the variable time, rather than the observation position along the fiber as in figure 3.1 and 3.2.

Most apparent is the difference in duration and amplitude of the triphasic waveform. For the lowest trace, the single fiber action potential almost equals the (tripolar) waveform of the transmembrane current. For that trace, the influence of volume conduction on the potential wave shape is limited. Apart from a substantial broadening of the triphasic waveform in the

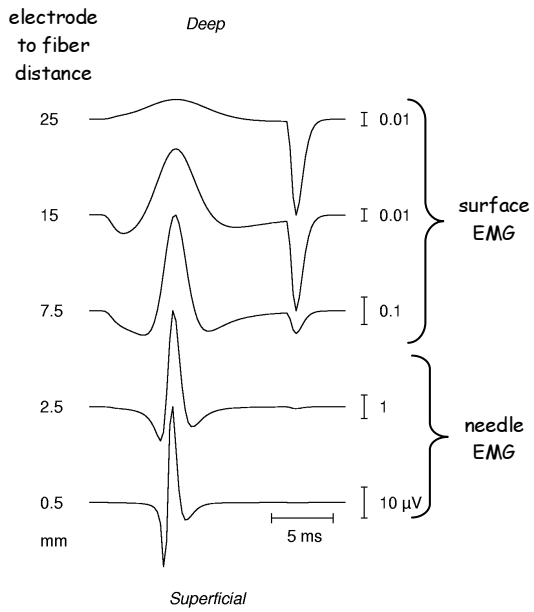

Figure 3.3: simulated single fiber action potentials from one muscle fiber. The observation distance to the muscle fiber decreases from 25 mm (upper trace, say a monopolar skin recording from a single fiber in a deep motor unit) to 0.5 mm (lowest trace, say a monopolar needle electrode recording near to the fiber). Note the large amplitude and waveform differences. Note the differences in vertical scaling. The propagation velocity is 4 m/s, half fiber length is 6 cm and the electrode is positioned at 2 cm from the endplate zone. Positive deflection downward. Adapted from Blok et al. (2002a).

higher traces, two other aspects can be seen. Most obvious is the change in the monophasic positive deflection (drawn downward) at the end of the single fiber action potential. This peak seems to increase with increasing observation distance. In fact, it only becomes more dominant in the upper waveforms because of the decreasing amplitude of the triphasic component (note scaling). This peak's almost constant waveform and amplitude is not predicted from the above simple equation on volume conduction. It has another peculiarity that cannot be observed in figure 3.3: it is not propagating along the muscle membrane as does the triphasic component. Additionally, a rather abrupt positive deflection evolves at the beginning of the traces, especially in the 2nd and 3rd trace. The positive deflections at the beginning and end of the single fiber action potential are related to the start and the extinction of the transmembrane current source, periods in time when the source is different from the (balanced) leading/trailing dipoles situation along the muscle fiber (figure 3.2).

It should be stressed that all aspects of the single fiber action potential are present in all traces of figure 3.3. The virtual invisibility of the positive deflections in the lowest traces (like in monopolar needle recordings) is due to amplification and amplitude ratios between the triphasic component and the other components (Dumitru, 2000). The amplitude preservation and waveform constancy of the termination peak have consequences for the frequency contents of the surface EMG signal (Dimitrov & Dimitrova, 1998a,b). In the context of terminology of volume conduction phenomena, it might be relevant to mention that the single fiber action potential origination and termination peaks can be explained as "classical" far field phenomena (Stegeman et al. 1997). The termination peak wave shape in the single

Figure 3.4: three examples of surface electromyography (EMG) array electrodes. The upper and middle one (interelectrode distances are 5 mm and 10 mm respectively) by courtesy of R. Merletti, Torino. The lower one is a double column version for specific purposes (interelectrode distance is 3 mm).

fiber recordings of figure 3.3 equals the intracellular action potential waveform as a function of time. As will be shown, the phenomena demonstrated for a simulated single fiber action potential, all have specific consequences for the waveform of a surface motor unit action potential as a summation of many single fiber action potentials, and for the characteristics of surface EMG interference patterns as a summation of many surface motor unit action potentials.

Multi-electrode montages

Common in all electric potential measurements is that voltage differences between two electrodes are measured. In case of a monopolar recording, as in the simulations of figure 3.3, one electrode is far away from the target muscle. Combining the activity of one electrode with that of one or several surrounding electrodes close to the muscle results in "higher order" derivations. Two nearby electrodes over the muscle result in a bipolar recording; this is a classic configuration. One step further in complexity leads to the so-called "double differential" recording (Broman et al. 1985; Van Vugt & Van Dijk, 2001). The effect always is a "spatial high pass filtering" which gives a narrowing of the spatial view. A Laplacian configuration is again more complex: the central electrode is connected with four surrounding electrodes (Disselhorst-Klug et al. 1997). The montage to be used depends on the clinical or research question. It should be realized that the recording area of the electrodes becomes progressively smaller with higher order derivations, and with shorter interelectrode distances (Roeleveld et al. 1997c). As a natural consequence, usually the amplitude of the signal decreases. An important and often intended consequence of bipolar and higher order montages and a short interelectrode distance is the suppression of cross-talk between muscles and of far-field activity originating from the start and extinction of the action potential (Broman et al. 1985).

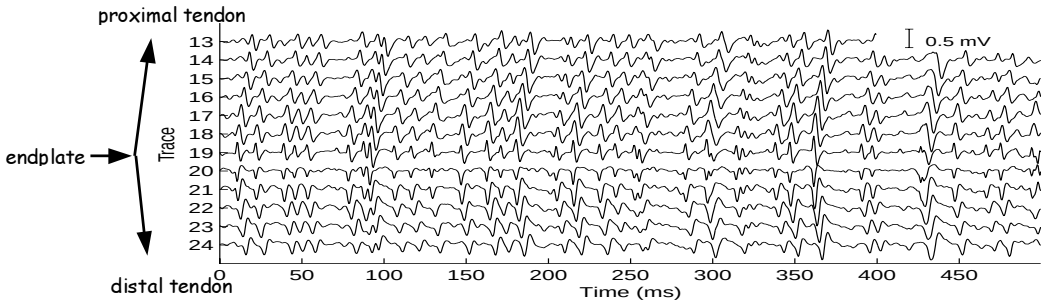

Figure 3.5: example of a surface EMG measurement, with a linear array of electrodes in bipolar montage, positioned in fiber direction, from isometric biceps brachii exercise at 20% MVC of a healthy subject. Interelectrode distance is 5 mm. Note that the position of the endplate zone is visible from the low amplitude trace (channel 20) and from the "phase reversal". Different motor unit action potentials are visible. The propagation over the sarcolemma is seen as the time delay between the consecutive channels.

Note 1: monopolar data storage

Since many electrode montages can be conceived, it is recommended that all surface EMG measurements, as in multichannel EEG, be recorded and stored as signals from individual electrodes referenced to a remote electrode, thus in a so-called monopolar fashion. This enables a versatile and purpose-dependent selection afterwards, with respect to the desired montages (bipolar, Laplacian etc.

Multichannel surface EMG and linear array electrodes

A second major reason for increasing the number of electrodes in surface EMG is to increase the number of recording positions. In this way, topographical information concerning the distribution of the EMG activity over a muscle or the timing relationships between different muscles becomes accessible. In principle, there is no limitation to increasing the number of surface electrodes over the muscle or arranging more or less complex montages from different electrodes. Moreover, multichannel surface EMG is accomplished more easily than most multichannel needle EMG techniques.

Connecting several bipolar recording electrodes placed in line results in a linear array (examples in figure 3.4) (Van der Hoeven et al. 1993; De Luca, 1997; Farina et al. 2000; Rongen et al. 2002). This enables the measurement of sarcolemmal propagation by comparing the time delay of the consecutive signals, provided the electrodes are aligned with the muscle fiber direction (figure 3.5). Here, we encounter the first spatial properties of the motor unit action potential: its origin at the neuromuscular junction or endplate zone and its propagation along the sarcolemma. In this bipolar recording, the neuromuscular junction is often characterized by a low amplitude (two electrodes symmetrically over the site of origination of the intracellular action potential record the same potential) and signal phase reversal (between traces 19, 20). Knowing the location of the neuromuscular junction might be useful in guiding placement of conventional electrode configurations (Falla et al. 2002). The propagation of the motor unit action potential is seen as the later arrival of the potentials

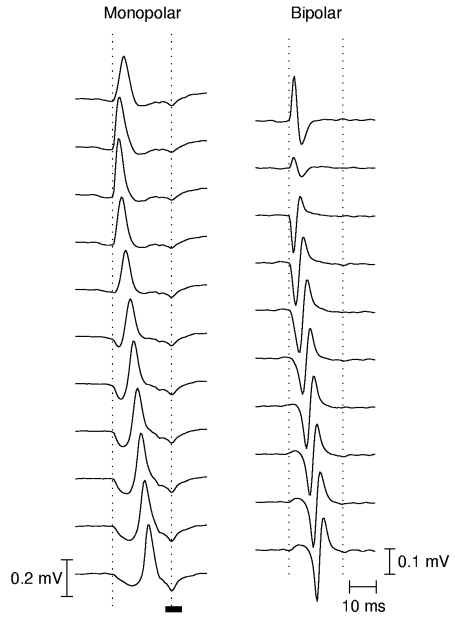

Figure 3.6: column selection (in fiber direction) of a distribution of motor unit action potentials in monopolar and bipolar montage from experimental data. These data are obtained after averaging decomposed single motor unit activity (as described later). The dashed lines indicate the initiation and the extinction of the action potentials. The small bar across the second vertical line in the left part indicates the positive termination peak. Adapted from Blok et al. (2002a).

at the consecutive electrode pairs. The skew arrows indicate the propagation of the motor unit action potentials along the muscle fibers away from the endplate. After recognition of single motor unit activity from such a surface EMG pattern (see below), the activity pattern of a single motor unit can be studied in detail (figure 3.6, Blok et al. 2002b). The right column of figure 3.6 shows a single motor unit action potential distribution, recorded in a bipolar montage along the fiber direction as in figure 3.5. The neuromuscular junction is now located below the second channel from above and propagation can clearly be observed in the direction to the lower channels. After motor unit decomposition (see sections 8.2 and 8.3), this activity as recorded in a monopolar montage is presented in the left column. Now the initiation and the extinction of the action potentials can also be observed as a simultaneous inflection and a non-propagating positive peak in all channels (vertical dashed lines). Note the shape similarity between the simulated middle trace of figure 3.3 and e.g. the 7th trace in the left column of figure 3.6.

The quantification of action potential propagation

The above paragraph elucidates how the propagation of the motor unit action potential along the sarcolemma, expressed as the mean muscle fiber conduction velocity (MFCV), can be followed in a recording over a linear array of surface EMG electrodes in a bipolar montage (Masuda & Sadoyama, 1987; Zwarts & Van Dijk 1998; Farina et al. 2000). For a short array of electrodes (3-5) this principle has been exploited over the last two decades (Broman et al. 1985). For a review of different techniques and normal values, see Arendt-Nielsen & Zwarts (1989). Important pre-requisites are that the electrode array lies parallel to the muscle fibers

that must be arranged in parallel to the surface of a superficial muscle. Muscles that can easily be measured are the biceps brachii, brachioradialis, the vasti medialis and lateralis and distal portion of the tibialis anterior muscle (Masuda & Sadoyama, 1987). Any departure from the parallel arrangement of the electrodes results in an overestimation of the MFCV. An important quality control can be derived from the fact that the signals from the consecutive channels should be almost identical (albeit displaced in time). From the examples in figure 3.5 and 3.6 it can be concluded that this requirement is not fulfilled in a region around the endplate region and at the muscle-tendon transition zone. If the shift in time is calculated by cross-correlating both signals (which is very common), this agreement in signal form is expressed by the maximal value of this cross-correlation function. MFCV estimations from signals with lower maximal cross-correlation values than about 0.8 are usually not reliable. It is important to note that the MFCV is dependent on the force level during the experiment. At low forces, mainly type I motor units are recruited at relatively low firing frequencies. With increasing force, larger (type II) motor units are recruited and the firing frequency of the already recruited motor units increases. Increasing motor unit firing rates do give rise to higher muscle fiber conduction velocities, as does -according to the Henneman's size principle (Henneman et al. 1965)- the recruitment of motor units with faster fibers (Andreassen & Arendt-Nielsen, 1987). The first phenomenon reflects the arrival of motor nerve impulses in the supernormal period of the sarcolemma just following the repolarization phase (Stålberg, 1966). The combined result is an increase of MFCV with force level (Sadoyama & Masuda, 1987). The conduction velocity of the muscle fiber action potential is -like the nerve action potential- dependent on the cable properties of the muscle fiber. Typically, the conduction velocity is around 4 m/s, in the same range as it is for (thick) unmyelinated axons. It should be realized that in surface recordings during voluntary activity, the MFCV is the weighted average of many motor units each containing a few hundred muscle fibers. The rather homogeneous composition of muscle fibers within one motor unit results in a -more or less- unchanged form of the motor unit action potential between endplate region and muscle-tendon transition zone when a bipolar montage is used (see figure 3.5 and 3.6, left column). Some decrease in amplitude and broadening of the potential is usually seen, mainly due to dispersion of the signal because of slightly different conduction velocities of the individual muscle fibers. Depending on the level of contraction, the number of motor units contributing to the MFCV estimation varies. The possibility of separating the contributions of different surface EMG peaks in the MFCV and thus to measure a distribution of conduction velocities has received attention in recent literature (Prutchi, 1995; Van Dijk et al. 1999; Farina et al. 2000; Lange et al. 2002). To do that, instead of cross-correlating long segments of surface EMG, time delays are measured in

different distinguishable peaks in the surface EMG. Such a method is described and applied in chapter 6.

Surface electromyography in exercise and fatigue

Surface EMG changes accompanying local muscle fatigue are well known (for a review see De Luca, 1984). These changes occur in signal amplitude, frequency content and MFCV and appear to be significantly dependent on age (Merletti et al. 2002). At low to moderate levels of contraction, the amplitude of surface EMG usually increases (Kleine et al. 2000b). This is mainly a consequence of recruitment of new motor units in the course of fatigue, but is in part also due to increasing firing frequencies. At maximal contractions, the surface EMG amplitude shows a more or less steady decline, despite the fact that an increased drive to motor units can be expected then as well. Possible mechanisms are lowering of the membrane potential, lowering MFCV (Stålberg, 1966; Stegeman & Linssen, 1992) and decreasing firing frequencies (Macefield et al. 2000). The MFCV almost invariably declines during fatigue if force levels are moderate to maximal. Since the first description of slowing of propagation velocity of single muscle fiber action potentials by Stålberg (1966) and later of MFCV by Lindstrøm & Peterson (1983), this has practically and theoretically been confirmed in numerous studies. A combination of high metabolic demand, fast firing rates, diminution of circulation and accumulation of metabolic byproducts gives rise to a progressive change in the membrane microenvironment (Miller et al. 1995). The accumulation of extracellular potassium, especially in the tubuli, and the accumulation of lactate, together with a lowering of the pH, seems to be the main determinants for the change in MFCV. At low force levels an increase of MFCV can be found during long lasting contractions, most likely due to recruitment of new fresh motor units (Zwarts & Arendt-Nielsen, 1988; Krogh-Lund & Jørgenson, 1991).

Note 2: surface EMG frequency

Concomitant with the fatigue induced decline in MFCV, the frequency content of the surface EMG signals shifts to lower frequencies. This is usually expressed as the change in the median frequency. The shift is mainly due to the lowering of the MFCV, although central factors (synchronization) also play a significant role (Zwarts et al. 1987; Hagg, 1992; Stegeman & Linssen, 1992). This can be deduced indirectly from the fact that the relative change in median frequency is always greater than that of the MFCV. Kleine et al. (2001b) obtained further evidence for the influence of central drive factors regarding the median frequency from topographical surface EMG differences. For muscles that do not permit MFCV estimation, measurement of the frequency content is often regarded as an alternative to estimate changes in the state of the sarcolemma or, more generally, of ongoing muscle fatigue. When interpreting the surface EMG signal frequency content, the intermingling influence of central factors should be taken into consideration.

Notes on clinical relevance of muscle fiber action potential propagation

Pathological conditions can result in lower, but also in higher muscle fiber conduction velocities. These MFCV changes can be fixed, intermittent or may depend on activity/fatigue, and can even be non-homogeneous along the muscle fiber. In the context of relating needle EMG and surface EMG, it is important to note that needle EMG findings can be normal, despite the fact that the abnormalities in MFCV were obvious (Zwarts et al. 1988; Van der Hoeven et al. 1994). Slowed muscle fiber conduction may not or hardly be reflected in a change of the action potential as measured by needle EMG. An elegant and convincing explanation for the difference between needle and surface EMG, which applies to this counterintuitive observation, has been presented by Lateva et al. (1990). They pointed to the fact that the needle motor unit action potential form and its duration are mainly determined by closely observed membrane current profiles of a few fibers. The influence of volume conduction on the potential wave shapes generated by those closely observed fibers is very limited. This, combined with the fact that MFCV mainly affects the influence of volume conduction phenomena (Lateva et al. 1990; Stegeman & Linssen, 1992), makes the invisibility of MFCV changes in needle EMG plausible.

Obviously, membrane function abnormalities as reflected in MFCV can be expected in channelopathies. Nonetheless, MFCV abnormalities, low surface EMG amplitudes and EMG pattern abnormalities are also found in patients suffering from a dystrophy. A reduced MFCV is then assumed to be the result of the presence of atrophic muscle fibers. In neurogenic conditions (ALS), it was found that the average MFCV as measured by surface EMG in voluntary contractions was increased (Van der Hoeven et al. 1993). Interestingly from a methodological point of view, using an invasive method of MFCV estimation with electrical stimulation of fibers, the latter authors found that MFCV was decreased in the same muscles. It was argued that the difference is caused by the fact that the surface method only measures the surviving (and adapting) motor units during voluntary contractions, while the invasive method of measuring MFCV also stimulates and measures the not innervated, and thus denervating muscle fibers. The difference between these findings thus elegantly reflects such adaptive processes in the motor unit.

Recent interest in the pathophysiology behind complaints of fatigue induced a revival of surface EMG in establishing pathological fatigue processes. In fact, few alternatives are available for objectively assessing fatigue. The absence of a decline of MFCV in the McArdle patients underscores the importance of lactate accumulation as a cause of the MFCV decline during normal fatigue (Linssen et al. 1990, 1991).

The potential relevance of the spatiotemporal aspect of surface EMG studies with linear arrays is illustrated in myotonia congenita by Drost et al. (2001). Membrane properties along

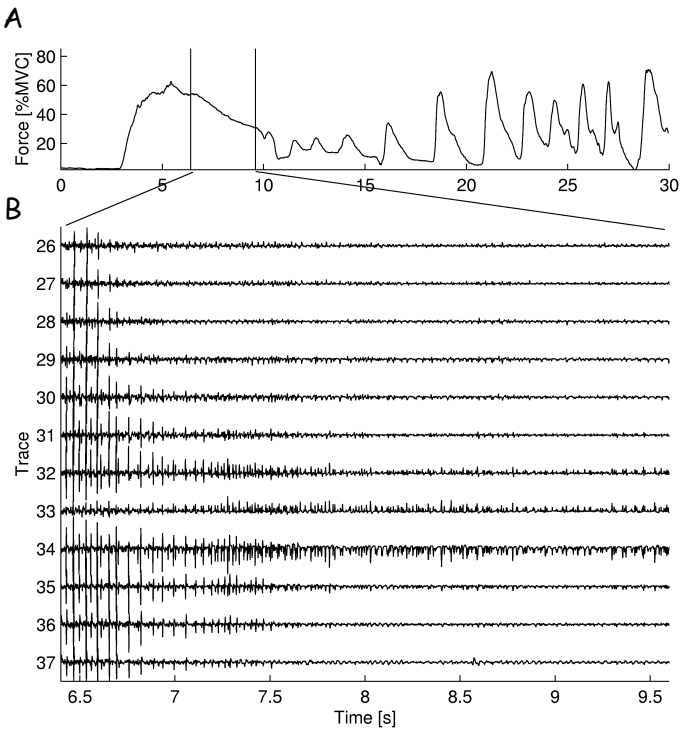

Figure 3.7 A: the force profile of a patient with myotonia congenita at 60% MVC with clear signs of transient paresis. The time period between the vertical lines corresponds to the surface EMG signals in B. B: the change of amplitude in time and along the course of muscle fibers from endplate to tendon during the phase of transient paresis in the patient. Bipolar data in fiber direction from one column of the 126-channel grid (Figure 3.8A). The position of the endplate is at channel 33. Adapted from Drost et al. (2001).

fiber direction showed a fascinating spatiotemporal process. The decline in amplitude of the surface EMG during transient paresis was found to be electrode position dependent: the further away from the endplate, the more progressive the deterioration of motor unit action potential amplitude. This deterioration eventually results in conduction block. This position and time dependent block has as a corollary a unique V-shaped surface EMG pattern (figure 3.7). It is argued that following a number of normal firings, the muscle membrane is incompletely repolarized, eventually resulting in conduction block. Needle EMG gives support for an explanation at a single fiber level (Trontelj & Stålberg, 1995). They report the decrease of single fiber action potentials in consecutive firings of a motor unit, which fits with impairment over time of action potential generation at a specific site along the fiber.

Proper positioning of the electrodes can be a problem when using a single linear array electrode configuration (figure 3.4). The above-cited finding of action potential propagation in myotonia congenita has actually been obtained with a two-dimensional grid electrode of the type that will further be introduced in the next sections. Among others, such a grid allows selection of the column of electrodes with the best and/or the most representative signals in muscle fiber direction. It also allows proper alignment of electrodes with muscle fiber direction.

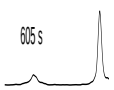

High-density surface EMG electrode arrays

Spatial spread of surface EMG signals

Apart from a limited number of reports on techniques like “scanning” needle EMG or multi-needle EMG (Buchthal et al. 1959; Stålberg, 1986; Gootzen et al. 1992) the spatial distribution of EMG signals is not widely used in clinical EMG practice. We will further elaborate on the use of spatial surface EMG information, whereby it will be shown that the information from two dimensional electrode arrangements, also those perpendicular to the fiber direction, may contribute substantially. In 1980, Monster & Chan published a basic study using the “perpendicular” surface EMG topographical distribution. Later, Masuda and co-workers (1985) introduced a two dimensional grid to study the spatial distribution of surface EMG over the skin surface above a single muscle. They showed the possibilities of such a system in the study of the already discussed propagation of the EMG patterns over the muscle fibers, and of the location of the neuromuscular junction. A technically advanced two-dimensional grid to analyze distributed motor unit action potential velocities was described by Prutchi (1995). In order to explore its practical possibilities, some years ago the principle of a two dimensional high-density grid electrode in an easy to use EMG system was adopted (Stegeman et al. 1996; Blok et al. 1998; Blok et al. 2002b). The system uses over 100 electrodes. In the grid presented in figure 3.8A, 126 electrodes are connected. This grid is used in the study of larger muscles (figure 3.8B). Figure 3.8C shows the use of flexible grids that can be adhered for instance to the skin of the face with special double sided adhesive tape (Lapatki et al. 2003; Lapatki et al. 2004). Facial muscle multichannel surface EMG is exemplified because of the advantages of the two dimensional technique considering the complex anatomy of the facial musculature and because of the advantages of its noninvasive character in that region.

Different from the earlier versions of multi-electrode systems, in our high-density surface EMG system signals are recorded in a monopolar montage (note 1). In case of the arm muscles, the reference electrode is placed at the elbow joint; for the measurements on leg muscles the patella is an appropriate reference; for the facial measurements the dorsum nasi has been chosen. Usually, the grid is positioned over a muscle with its long side (13 electrodes in the grid of figure 3.8A) parallel to the muscle fibers. In principle, this can be achieved in a number of superficial muscles (Masuda & Sadoyama, 1986, 1987). Two examples of an ensemble of signals from the m. biceps brachii in the direction perpendicular (figure 3.9A) and, as presented earlier, parallel (figure 3.9B) to the fiber direction in a healthy biceps brachii muscle are shown as they are recorded by the grid of figure 3.8A.

The 12 bipolar signals in figure 3.9B show the position of the neuromuscular junctions around the third signal from below and propagation of motor unit action potentials with approximately 4 m/s along the muscle fibers in two directions away from it. The 10 bipolar

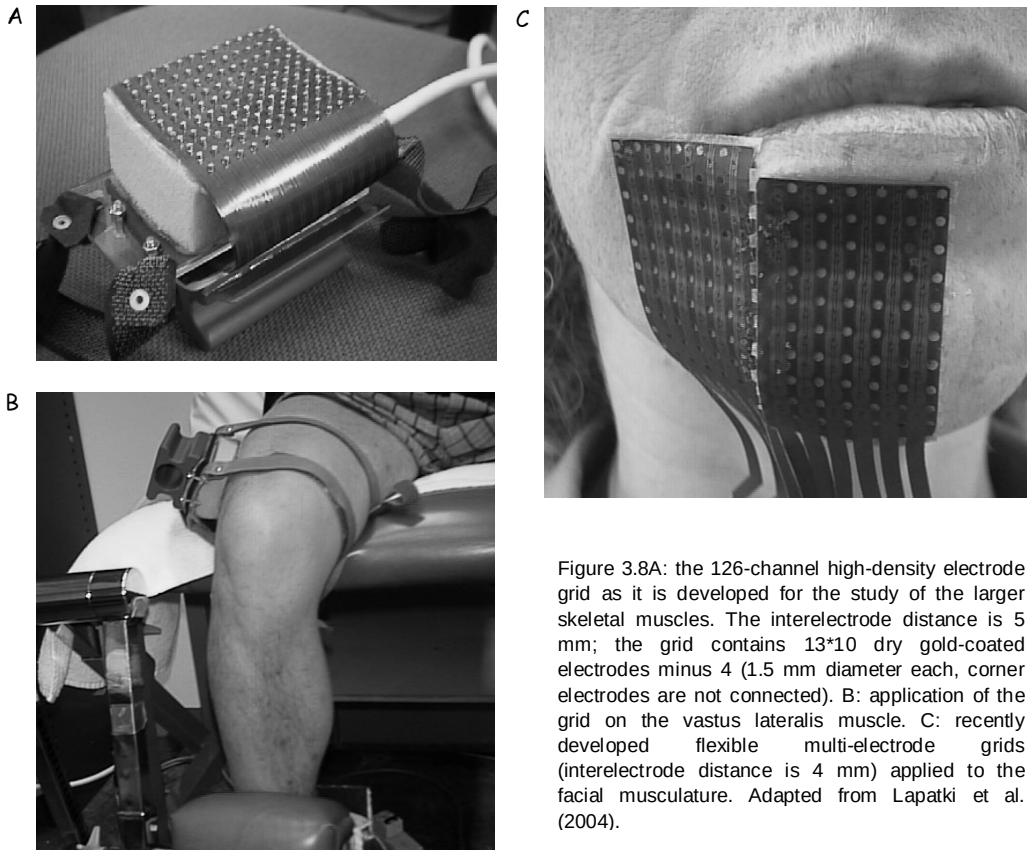

Figure 3.8A: the 126-channel high-density electrode grid as it is developed for the study of the larger skeletal muscles. The interelectrode distance is 5 mm; the grid contains 13*10 dry gold-coated electrodes minus 4 (1.5 mm diameter each, corner electrodes are not connected). B: application of the grid on the vastus lateralis muscle. C: recently developed flexible multi-electrode grids (interelectrode distance is 4 mm) applied to the facial musculature. Adapted from Lapatki et al. (2004).

signals in the direction perpendicular to the fibers (figure 3.9A, each bipolar signal calculated from one electrode minus the signal from the adjacent electrode in fiber direction) show a different pattern. The surface EMG amplitude changes in the muscle in medial – lateral direction and no propagation can be observed. Note that the surface motor unit action potential peaks from different motor units have their maximum at different medial – lateral positions, which indicates a spatial (transversal) spread of motor units. Equation 2 states that the potential decreases with increasing distance between the electrode and the bioelectric source. Hence, it can be concluded that the center of a motor unit is located where the highest amplitude of a surface motor unit action potential is detected. In fact, as can be seen in figure 3.5 and 3.6, the temporal dynamics of the surface EMG signal (the peak to peak amplitudes and the differences in waveform) are rather limited when compared to a needle EMG signal, especially in montages with a small interelectrode distance. This potentially poses a problem in separating firings of different motor units from the surface EMG signal. However, note from figure 3.9A, that the activity of six motor units (numbered 1-6) can already be separated visually, which is hardly possible from a single surface EMG trace, nor from figure 9B.

Table 3.1: Sequence of steps in obtaining motor unit templates from surface EMG recordings

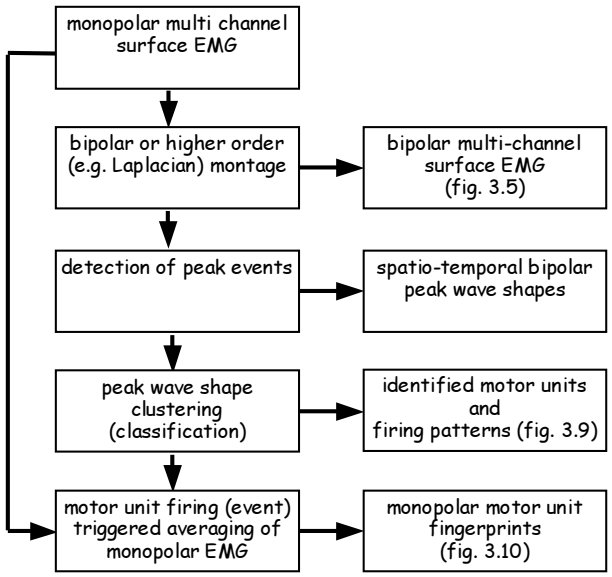

An example of a registration with a series of electrodes with the flexible grids applied to the face (as illustrated in figure 3.8C) is presented in figure 3.9C. The bipolar signals were recorded during voluntary contraction of the m. depressor labii inferioris. The neuromuscular junctions can be found slightly beneath the third trace from below. Due to the distinct amplitude distributions of the motor unit action potentials, also in fiber direction, the activity of five motor units can be discerned visually in this array of signals. These examples illustrate that the spatial surface EMG dynamics contain information that is missing in the temporal quality of the signals and that is even indispensable when disentangling motor unit activity from the surface EMG.

Motor units decomposition from surface EMG

In needle EMG recording, it is possible to follow the firing pattern of a few motor units during isometric contraction at low force levels (Stålberg et al. 1996). Needle EMG based decomposition performance increases by using spatial information with a three-needle electrode (De Luca et al. 1993). The spatial profile of surface EMG motor unit action potentials appears to be specific for a certain motor unit (figure 3.9). The recognition of motor units using surface EMG appears possible when using the motor unit's unique configuration of the spatial potential distribution over the skin (Kleine et al. 2000a; Wood et al. 2001). Practically, the first step of classifying motor unit firings needs surface EMG

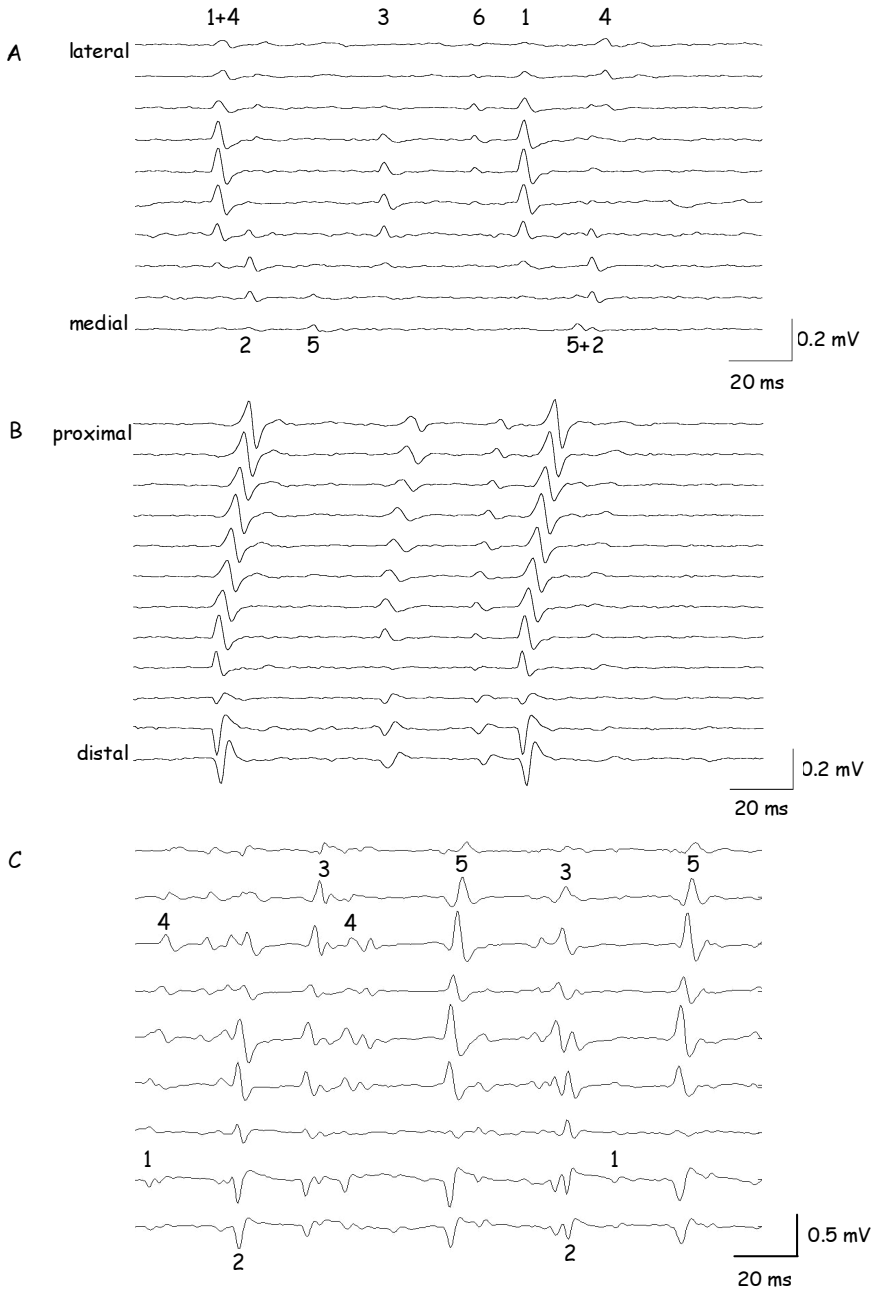

Figure 3.9: surface EMG patterns from a selection of electrodes from high-density EMG grids. A: a subject contracted the m. biceps brachii to a low force level of about 5% MVC. The signals are obtained with the grid of figure 3.8A. Ten bipolar signals (adjacent distal – proximal electrodes) perpendicular to the fiber direction show the variability of amplitude over the muscle in medial lateral direction. Visually traceable motor unit action potentials are numbered. B: twelve (13 minus 1) bipolar signals in the fiber direction from the same time segment as in A clearly show the position of the endplate at the 3rd row from below and the propagation of action potentials along the muscle fiber in two directions from there. A and B are adapted from Kleine et al. (2000a). C: nine bipolar signals from the depressor m. labii inferioris (figure 3.8C, one column of the medial grid), obtained during its contraction at an intermediate force level. The endplate zone is slightly below the electrodes of the third lowest trace. Again, visually traceable motor unit action potentials are numbered.

signals in a bipolar montage with short (3-6 mm) interelectrode distance, leading to signals as shown in figure 3.9. An early attempt used two surface EMG channels in addition to a needle recording as described by Kakuda et al. (1991). Using the 126-channel surface EMG grid, up to six simultaneously active motor units could be detected (Kleine et al. 2000a). What follows is a motor unit classification using a so-called clustering algorithm (table 3.1). Similar motor unit action potential profiles are grouped together until the spatio-temporal patterns of grouped motor unit action potential events have acceptable similarity, whereby also physiological firing patterns should arise. In that way a specific selected group of motor unit action potentials can be classified as being the activity of a separate motor unit over time.

The motor unit fingerprint

A spatial profile of a motor unit action potential is most characteristic in a monopolar montage (figure 3.6, left column). However, motor unit firing events can barely be distinguished in monopolar recordings, let alone be classified in the way described above. The uptake area of monopolar signals is too large with numerous components from distant activity (figure 3.3) contained in the signal. The solution to this dilemma is a noninvasive variation of “spike triggered averaging”, as applied in the macro EMG technique (Stålberg, 1983) and also in the combination of needle EMG with surface EMG techniques (Farina et al. 2002). The identification of motor unit firing events requires spatially distributed surface EMG recordings in a bipolar or higher order montage (figure 3.5 and 3.9). After having identified and classified motor unit firing events in bipolar EMG signals as described in the previous section, monopolar motor unit action potentials can be averaged out of the originally recorded monopolar surface EMG signals (table 3.1). In that way monopolar action potentials of one particular motor unit, obscured in the ongoing signal by the interference of other motor unit action potentials, can be visualized.

Two examples of complete motor unit templates in a monopolar montage (2x60 channels) are given in figure 3.10. These templates are called motor unit fingerprints. These fingerprints were constructed from data obtained in the setting as presented in figure 3.8C, when a subject was contracting the m. depressor anguli oris (motor unit 1) and the m. depressor labii inferioris (motor unit 2), respectively. The data reveal the different positions of the motor units and their largely different topography. In these monopolar fingerprints, the locations of the neuromuscular junctions are less clear than in a bipolar montage (compare figure 3.6, right column; figure 3.9B,C). The facial musculature is exemplified since multiple muscles are differently arranged in a small area and the multi-electrode grid can be used to determine the position and orientation of underlying motor units. The fingerprint of motor unit

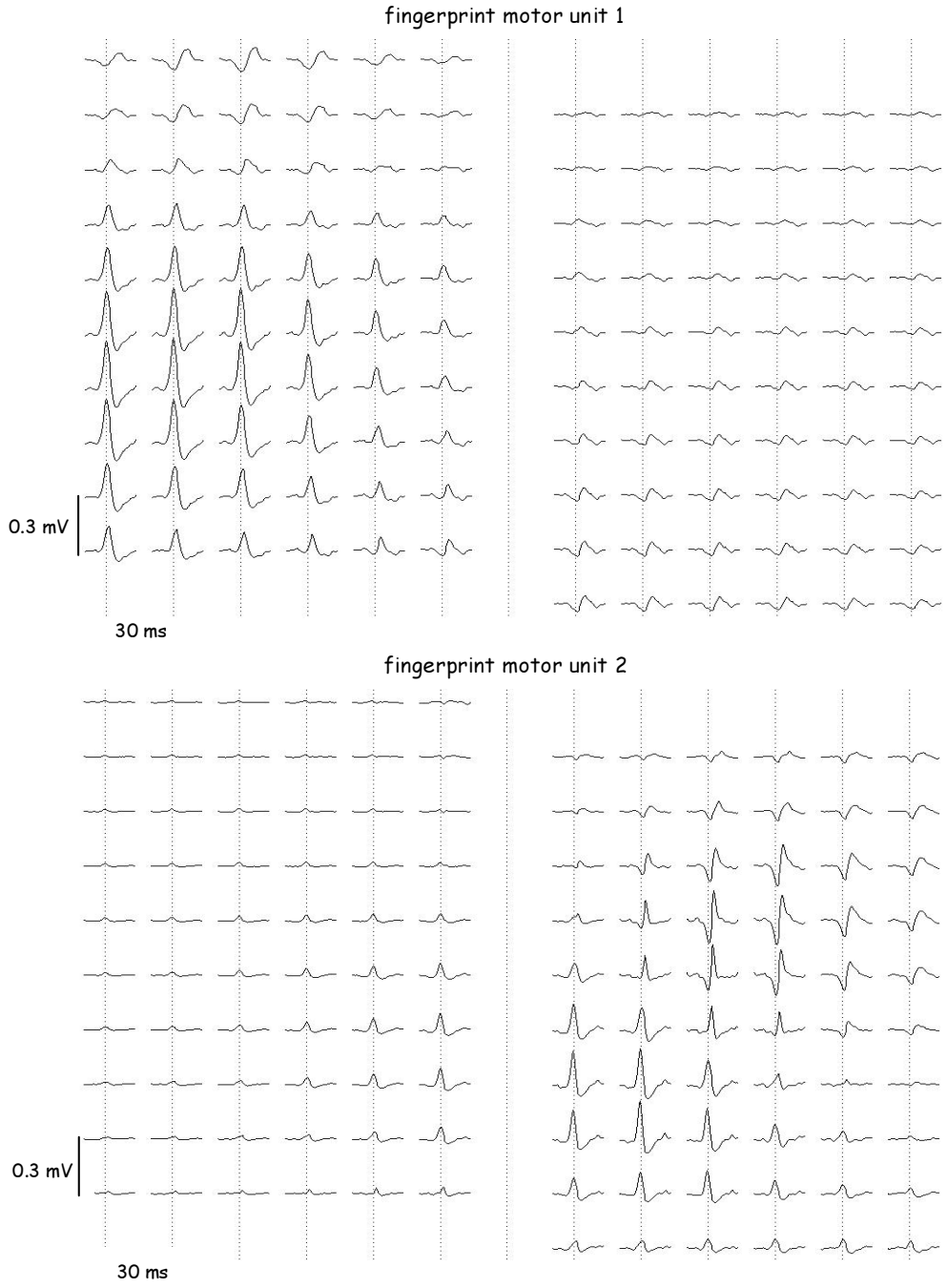

Figure 3.10: three-dimensional motor unit fingerprints recorded from two different motor units. The signals are represented in monopolar montage. The fingerprints were constructed from a subject contracting the right m. depressor anguli oris (motor unit 1) or the m. depressor labii inferioris (motor unit 2), respectively. The left and right displayed grid segments are obtained from the lateral and the medial grids in figure 3.8C. Note the amplitude profile in medio-lateral (left-right) direction (especially in motor unit 1). The propagating component and the non-propagating final component can be recognized in proximal-distal (vertical) direction in motor unit 1. In motor unit 2, the fiber direction is oblique (right-upper to left-below in the medial grid as can be expected from the fiber direction of the m. depressor labii inferioris). Adapted from Lapatki et al. (2004).

2 shows an oblique orientation, as can be expected from the fiber direction of the m. depressor labii inferioris.

Motor unit physiology, anatomy, histology and surface EMG

Obviously, there is an intrinsic relation between EMG signals and the underlying motor unit properties. These relations are in many cases (both in needle EMG and surface EMG) indirectly, i.e. no direct interpretation of motor unit parameters is possible from the EMG signals. Needle EMG literature and practice proves that these relations are most useful, however. A number of studies relate the basic conditions of pathological muscle (neuropathic, myopathic) to the global surface EMG signal characteristics (Huppertz et al. 1997; Uesugi et al. 1999). Apparently, surface EMG bears, as needle EMG, information on basic abnormalities in muscle disease. Literature on data on single motor units from surface EMG in pathology is scarce. The rather contra-intuitive advantage of the spatial surface motor unit action potential distribution over needle EMG motor unit action potentials is that information on a motor unit's physiology, anatomy and histology can be obtained rather directly from the surface motor unit action potential fingerprint. A further survey will be given. The location of the neuromuscular junction can be detected from the bipolar montage by polarity inversion of the action potential, by propagation in two opposite directions and by bipolar motor unit waveforms with low amplitude (figure 3.6, 2nd trace in the bipolar montage). The width of the neuromuscular junction can be estimated from the number of electrodes with reduced and/or irregular amplitude. The resolution of that estimation is restricted by the interelectrode distance (4 or 5 mm in the grids of figure 3.8). The mean propagation velocity of a surface motor unit action potential can best be determined from the bipolar traces. A high velocity might denote muscle fibers with large diameters and vice versa. The location of the motor unit can be derived from the amplitude profile (see also figure 3.9A and 3.10). The motor unit is located below the column with the highest amplitude surface motor unit action potentials. The depth of the motor unit can be deduced from an amplitude decline of the action potential in the direction perpendicular on the muscle fibers (figure 3.9A) (Roeleveld et al. 1997d). The amplitude or, even better, the signal area of the monopolar motor unit waveform (as in macro EMG), appears to be a good indicator of the (electrical) motor unit size (also see below) (Roeleveld et al. 1997b). Sometimes, the mean half-length of the fibers in a motor unit can also be deduced from motor unit fingerprints. The duration of the propagation of action potentials between endplate and tendon region must then be combined with the mean propagation velocity U. In figure 3.6, the duration is the time segment between the vertical lines.

Other characteristics of muscle and motor unit from surface EMG

Motor units size estimation from high-density surface EMG

The 'size' of the motor unit contains important information for the clinical neurophysiologist. Changes in this 'electrical size' reflect alterations due to reinnervation or loss of muscle fibers, e.g. due to a myopathic process. The motor unit size can be represented in different ways. In needle EMG, usually, the duration of the motor unit action potential is measured or, alternatively, the area of the motor unit action potential can be calculated. Since its size is an essential property of a motor unit, we investigated the possibility of measuring this feature of the motor unit from the monopolar motor unit fingerprints non-invasively with surface EMG (Roeleveld et al. 1997b, 1998). As in macro EMG, and as already argued from a theoretical point of view, estimation of motor unit size from a monopolar montage appears to be superior to other montages. The technique of using a bipolar montage for identification and subsequent averaging of the monopolar motor unit action potentials as presented in table 3.1 can be fruitfully used for this work. The size of the motor unit can be estimated from the measured amplitude (or area) of the largest surface motor unit action potential in a fingerprint. A major question is how well do these monopolar action potentials represent the motor unit size. Essentially, the depth of the motor unit influences the motor unit action potential amplitude and wave shape. It was proposed to use the spatial characteristics of the motor unit fingerprint to solve this problem (Roeleveld et al. 1997d). Superficial motor units give rise to a fast decline in amplitude with distance from the motor unit. Deep motor units show much less relative amplitude decline (figure 3.9A). Using these differences, the depth of a motor unit can be estimated, allowing for “depth correction” of the amplitude. To test this, motor unit action potentials were measured using macro needle EMG and surface EMG electrodes simultaneously. It turned out that good correlation coefficients (in the order of 0.85) were found between the area and amplitudes of macro EMG and surface EMG measured action potentials (Roeleveld et al. 1997b). Extensions of this work for motor units that were enlarged due to a neurogenic condition essentially confirmed this relationship (Roeleveld et al. 1998). Wood et al. (2001) also reported enlarged surface EMG action potentials in motor neuron disease. When performing motor unit decomposition starting with bipolar or higher order filtered surface EMG montages, correcting for motor unit depth appeared not to be of great practical importance. Motor units that give rise to clear-cut bipolar motor unit action potential signals cannot be expected to be located deep below the muscle surface. Recent results in our group revealed the usefulness of disentangling motor unit fingerprints with high-density surface EMG for the improvement of the various techniques of motor unit number estimation (Blok et al. submitted).

Table 3.2: Clinical applications of surface EMG

Central nervous system	Peripheral nervous system
	Evoked activity
	• CMAP (amplitude/area)
• Timing	• Motor unit number estimation
• Movement patterns	
• Central drive/ synchronization	*Voluntary activity*
• Involuntary movements	• Amplitude/frequency
• Central fatigue	• Fatigue
• Tremor	• Endplate localization
• Gait disorders	• Muscle fiber conduction velocity
	• MUP variables: amplitude and duration
	• Follow-up studies

adapted from Zwarts et al. 2000. CMAP, compound motor unit action potential.

Motor control

Historically, the majority of surface EMG applications was related to motor control questions. A precise analysis of the relative timing of activation patterns by the central nervous system using surface EMG, has been a major tool in numerous rehabilitation and ergonomic studies. In that context, the surface EMG is used as a marker for the way in which the central nervous system controls muscles during different tasks, e.g. walking or running (De Luca, 1997). In the same way, analysis of movement disorders such as tremor, dystonia or myoclonus can be performed with surface EMG. The high temporal resolution of activity measured on different muscles simultaneously, makes surface EMG a superior tool in the analysis of complex movements and movement disorders. In such approaches, the muscle is regarded as a single entity and a common effector of the central nervous system. Placing the electrodes in a bipolar or double differential configuration with an interelectrode distance up to 2 cm usually suffices to measure the activity of the muscle under investigation without excessive cross-talk (De Luca & Merletti, 1988; Blanc et al. 1999; Van Vugt & Van Dijk, 2001).

Motor control within a muscle also can be a complicated phenomenon and unraveling requires the recognition and measurement of single motor units (Van Bolhuis et al. 1997). Surface motor unit action potential decomposition algorithms were already introduced (Kleine et al. 2000a; Wood et al. 2001). In a study of the influence of sub-threshold transcranial magnetic stimulation on the firing sequences of single motor units, such algorithm was used to demonstrate impaired inhibition of the motor cortex in Parkinson's patients (Kleine et al. 2001a). This study of transcranial magnetic stimulation induced firing events, derived from surface EMG, presents methodologically a unique combination of two noninvasive techniques by which neuronal firing events can both be influenced and quantified.

Substantial evidence can be found in recent literature that motor unit pairs show a varying, modest but consistent, degree of so-called short time synchronization of firing events. The extent of the synchronization depends on the complexity of the task (Schmied et al. 2000), and on the level of fatigue. Synchronization can be interpreted as a reflection of common parts of the central drive to the muscle, transported and generated by corticospinal neurons and possibly by spinal reflex mechanisms. It may, therefore, contain essential information on motor control mechanisms. The synchronization of motor unit firing events can influence the surface EMG characteristics substantially. Moreover, simulations show that these central drive influences on frequency and amplitude are electrode location dependent (Kleine et al. 2001b).

Motor unit types and motor unit recruitment

The mean propagation velocity of muscle fibers in a motor unit can potentially be used to type the motor unit. Since the propagation velocity is related to the diameter of the fibers, motor units with thicker fibers can possibly be distinguished from those with thinner fibers. In this way, the process of motor unit recruitment, as well as the separate fatigue processes of type I and type II motor units could be followed in time. This appears not as straightforward as suggested sometimes. It will be shown that a differentiation in recruited motor unit populations seems possible for the tibialis anterior muscle, as described in chapter 6.

Basic limitations and advantages of surface EMG

Figure 3.11 gives an overview of the applications of needle versus surface EMG techniques in relation to the level of investigation (Zwarts et al. 2000). It is obvious that for phenomena at the level of the muscle fiber, the needle EMG electrode is indispensable. At the level of the motor unit, an overlap exists between the two techniques with respect to several important characteristics such as size and number of motor unit action potentials. Presently, the use of needle EMG is well embedded in clinical neurophysiology, it is a fast and versatile tool for assessing motor unit changes in disease. Although it requires advanced software analysis, surface EMG offers valuable complementary information about the muscle, to that obtained with needle EMG. For example, one of the most important variables in EMG, the motor unit size, can be reliably estimated using multichannel surface EMG. Table 3.2 provides an overview of applications of surface EMG. It is worthwhile to further explore the surface EMG possibilities, for example its use in children or for follow-up studies (Stegeman et al. 2000b), whereby the noninvasive character is very appealing. Applications concerning topographical information of the motor unit and the activity distribution over the muscle clearly belong to the domain of surface EMG. They, too, await further exploration. At present, a number of pathophysiological mechanisms concerning motor unit action

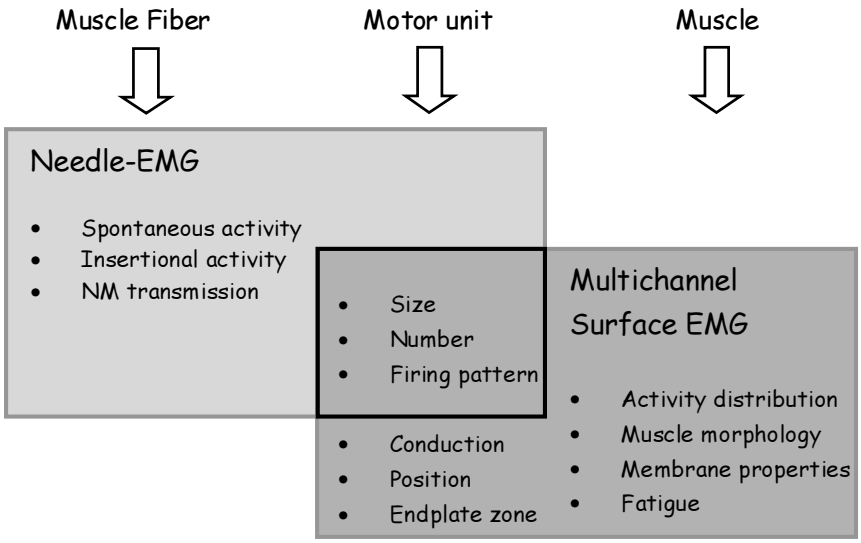

Figure 3.11: overview of the applications of needle and surface EMG at different levels (fiber, motor unit and muscle). NM, neuromuscular.

potentials have escaped the keen eye of the needle electromyographer due to the topographic character of the pathology.

Surface EMG now has a thorough and extensive theoretical background. Multichannel surface EMG provides some of the classic but also particularly new information regarding the neuromuscular system in health and disease. Its main advantage lies in the noninvasive addition of spatial information to our view of the motor unit. The exploration of the possibilities of this technique has only just begun.

Acknowledgements

The discussions with Joleen Blok, Gea Drost, Hans van Dijk and Bert Kleine are gratefully acknowledged. The development of the high-density surface EMG system and the Anvolcon model was made possible by a grant from The Technology Foundation, Utrecht, The Netherlands (Grant NGN 3818).

References

Andreassen S & Arendt-Nielsen L. Muscle fiber conduction velocity in motor units of the human anterior tibial muscle: a new size-principle parameter. *J Physiol* 391: 561-571, 1987.

Arendt-Nielsen L & Zwarts MJ. Measurement of muscle fiber conduction velocity in human - techniques and applications. *J Clin Neurophysiol 6*: 173-190, 1989.

Blanc Y, Coletti Moja M, Dimanico U, Merlo A & Nazarro M. Crosstalk evaluation during voluntary muscle contraction. In: *Proceedings Fourth General Workshop.* European concerted action (SENIAM, BIOMED II), edited by Hermens HJ & Freriks B. Enschede: Roessingh, 1999, p. 12-16.

Blok JH, Stegeman DF & Van Oosterom A. A three-layer volume conductor model and software package for applications in surface electromyography. *Ann Biomed Eng* 30: 566-577, 2002a.

Blok JH, Van Asselt S, van Dijk JP & Stegeman DF. On an optimal pasteless electrode to skin interface in surface EMG. In: *Sensors and sensor placement.* European concerted action (SENIAM, BIOMED II), edited by Hermens HJ & Freriks B. Enschede: Roessingh, 1998, p. 71-76.

Blok JH, Van Dijk JP, Drost G, Zwarts MJ & Stegeman DF. A high-density multichannel surface electromyography system for the characterization of single motor units. *Rev Sci Instr* 73: 1887-1897, 2002b.

Blok JH, Van Dijk JP, Zwarts MJ & Stegeman DF. Topographical information improves motor unit number estimation. *Submitted.*

Broman H, Bilotto G & De Luca CJ. A note on the noninvasive estimation of muscle fiber conduction velocity. *IEEE Trans Biomed Eng* 32: 341-344, 1985.

Buchthal F, Guld C & Rosenfalck P. Multielectrode study of the territory of a motor unit. *Acta Physiol Scand* 39: 83-104, 1959.

De Luca CJ. Myoelectric manifestations of localized muscle fatigue. *CRC Crit Rev Bioengin* 11: 251-279, 1984.

De Luca CJ. The use of electromyography in biomechanics. *J Appl Biomech* 13: 135-153, 1997.

De Luca CJ & Merletti R. Surface myoelectric signal cross-talk among muscles of the leg. *Electroenceph Clin Neurophysiol* 69: 568-575, 1988.

De Luca CJ, Roy AM & Erim Z. Synchronization of motor-unit firings in several human muscles. *J Neurophysiol* 70: 2010-2023, 1993.

Dimitrov GV & Dimitrova NA. Fundamentals of power spectra of extracellular potentials produced by a skeletal muscle fibre of finite length. Part I: Effect of fibre anatomy. *Med Eng Phys* 20: 580-587, 1998a.

Dimitrov GV & Dimitrova NA. Fundamentals of power spectra of extracellular potentials produced by a skeletal muscle fibre of finite length. Part II: Effect of parameters altering with functional state. *Med Eng Phys* 20: 702-707, 1998b.

Disselhorst-Klug C, Silny J & Rau G. Improvement of spatial resolution in surface-EMG: a theoretical and experimental comparison of different spatial filters. *IEEE Trans Biomed Eng* 44: 567-574, 1997.

Drost G, Blok JH, Stegeman DF, van Dijk JP, van Engelen BG & Zwarts MJ. Propagation disturbance of motor unit action potentials during transient paresis in generalized myotonia: a high-density surface EMG study. *Brain* 124: 352-360, 2001.

Dumitru D. Physiologic basis of potentials recorded in electromyography. *Muscle Nerve* 23: 1667-1685, 2000.

Dumitru D & King JC. Far-field potentials in muscle: a quantitative investigation. *Arch Phys Med Rehabil* 73: 270-274, 1992.

Dumitru D, King JC & Zwarts MJ. Determinants of motor unit potential duration. *Clin Neurophysiol* 110: 1876-1882, 1999.

Dumitru D, Stegeman DF & Zwarts MJ. Electric sources and volume conduction and appendix-the leading/trailing dipole model and near-field/far-field waveforms. In: *Electrodiagnostic Medicine*, edited by Dumitru D, Amato AM and Zwarts MJ. Philadelphia: Hanley and Belfus, Inc., 2002, p. 27-67.

Falla D, Dall'Alba P, Rainoldi A, Merletti R & Jull G. Location of innervation zones of sternocleidomastoid and scalene muscles: a basis for clinical and research electromyography applications. *Clin Neurophysiol* 113: 57-63, 2002.

Farina D, Arendt-Nielsen L, Merletti R & Graven-Nielsen T. Assessment of single motor unit conduction velocity during sustained contractions of the tibialis anterior muscle with advanced spike triggered averaging. *J Neurosci Methods* 115: 1-12, 2002.

Farina D, Fortunato E & Merletti R. Noninvasive estimation of motor unit conduction velocity distribution using linear electrode arrays. *IEEE Trans Biomed Eng* 47: 380-388, 2000.

Farina D & Merletti R. A novel approach for precise simulation of the EMG signal detected by surface electrodes. *IEEE Trans Biomed Eng* 48: 637-646, 2001.

Gootzen TH, Vingerhoets DJ & Stegeman DF. A study of motor unit structure by means of scanning EMG. *Muscle Nerve* 15: 349-357, 1992.

Hagg GM. Interpretation of EMG spectral alterations and alteration indexes at sustained contraction. *J Appl Physiol* 73: 1211-1217, 1992.

Henneman E, Somjen G & Carpenter DO. Functional significance of cell size in spinal motoneurons. *J Neurophysiol* 28: 560–580, 1965.

Huppertz HJ, Disselhorst-Klug C, Silny J, Rau G & Heimann G. Diagnostic yield of noninvasive high spatial resolution electromyography in neuromuscular diseases. *Muscle Nerve* 20: 1360-1370, 1997.

Kakuda N, Nagaoka M & Tanaka R. Discrimination of different motor units by spike-triggered averaging of surface electromyograms. *Neurosci Lett* 122: 237-240, 1991.

Kleine BU, Blok JH, Oostenveld R, Praamstra P & Stegeman DF. Magnetic stimulation induced modulations of motor unit firings extracted from multi-channel surface EMG. *Muscle Nerve* 23: 1005-1015, 2000a.

Kleine BU, Praamstra P, Stegeman DF & Zwarts MJ. Impaired motor cortical inhibition in Parkinson's disease: motor unit responses to transcranial magnetic stimulation. *Exp Brain Res* 138: 477-483, 2001a.

Kleine BU, Schumann NP, Stegeman DF & Scholle HC. Surface EMG mapping of the human trapezius muscle: the topography of monopolar and bipolar surface EMG amplitude and spectrum parameters at varied forces and in fatigue. *Clin Neurophysiol* 111: 686-693, 2000b.

Kleine BU, Stegeman DF, Mund D & Anders C. The influence of motoneuron firing synchronization on surface EMG characteristics in dependence of electrode position. *J Appl Physiol* 91: 1588-1599, 2001b.

Krogh-Lund C & Jørgensen K. Changes in conduction velocity, median frequency, and root mean square-amplitude of the electromyogram during 25% maximal voluntary contraction of the triceps brachii muscle, to limit of endurance. *Eur J Appl Physiol Occup Physiol* 63: 60-69, 1991.

Lateva ZC, Dimitrov GV & Dimitrova NA. Power spectra of single infinite fibre extracellular potentials recorded by a bipolar electrode. *Med Biol Eng Comput* 28: 537-543, 1990.

Lange F, Van Weerden TW & Van Der Hoeven JH. A new surface electromyography analysis method to determine spread of muscle fiber conduction velocities. *J Appl Physiol* 93: 759-764, 2002.

Lapatki BG, Stegeman DF & Jonas IE. A surface EMG electrode for the simultaneous observation of multiple facial muscles. *J Neurosci Methods* 123: 117-128, 2003.

Lapatki BG, Van Dijk JP, Jonas IE, Zwarts MJ & Stegeman DF. A thin, flexible multielectrode grid for high-density surface EMG. *J Appl Physiol* 96: 327-336, 2004.

Lindstrøm L & Peterson I. Power spectrum of EMG signals and its applications. In: *Progress in clinical neurophysiology, vol. 10: Computer-aided electromyography*, edited by Desmedt JE. Basel: Karger, 1983, p. 1-51.

Linssen WHJP, Jacobs M, Stegeman DF, Joosten EMG & Moleman J. Muscle fatigue in McArdle's disease. Muscle fibre conduction velocity and surface EMG frequency spectrum during ischaemic exercise. *Brain* 113: 1779-1793, 1990.

Linssen WHJP, Stegeman DF, Joosten EMG, Merks HJH, Laak ter HJ, Binkhorst RA & Notermans SLH. Force and fatigue of human type I muscle fibres. A surface EMG study in patients with congenital myopathy and type I fibre predominance. *Brain* 114: 2123-2132, 1991.

Lowery MM, Stoykov NS, Taflove A & Kuiken TA. A multiple-layer finite-element model of the surface EMG signal. *IEEE Trans Biomed Eng* 49: 446-454, 2002.

Macefield VG, Fuglevand AJ, Howell JN & Bigland-Ritchie B. Discharge behaviour of single motor units during maximal voluntary contractions of a human toe extensor. *J Physiol* 528: 227-234, 2000.

Masuda T, Miyano H & Sadoyama T. A surface electrode array for detecting action potential trains of single motor units. *Electroencephalogr Clin Neurophysiol* 60 : 435-443, 1985.

Masuda T & Sadoyama T. The propagation of single motor unit action potentials detected by a surface electrode array. *Electroencephalogr Clin Neurophysiol* 63: 590-598, 1986.

Masuda T & Sadoyama T. Skeletal muscles from which the propagation of motor unit action potentials is detectable with a surface electrode array. *Electroencephalogr Clin Neurophysiol* 67: 421-427, 1987.

McGill KC & Lateva ZC. A model of the muscle-fiber intracellular action potential waveform, including the slow repolarization phase. *IEEE Trans Biomed Eng* 48: 1480-1483, 2001.

Merletti R, Farina D, Gazzoni & Schieroni MP. Effect of age on muscle functions investigated with surface electromyography. *Muscle Nerve* 25: 65-76, 2002.

Merletti R, Lo Conte L, Avignone E & Guglielminotti P. Modeling of surface myoelectric signals--Part I: Model implementation. *IEEE Trans Biomed Eng* 46: 810-820, 1999a.

Merletti R, Roy SH, Kupa E, Roatta S & Granata A. Modeling of surface myoelectric signals--Part II: Model-based signal interpretation. *IEEE Trans Biomed Eng* 46: 821-829, 1999b.

Miller RG, Kent-Braun JA, Sharma KR & Weiner MW. Mechanisms of human muscle fatigue. Quantitating the contribution of metabolic factors and activation impairment. *Adv Exp Med Biol* 384: 195-210, 1995.

Monster AW & Chan H. Surface electromyogram potentials of motor units; relationship between potential size and unit location in a large human skeletal muscles. *Exp Neurol* 67: 280-297, 1980.

Prutchi D. A high-resolution large array (HRLA) surface EMG system. *Med Eng Phys* 17: 442-454, 1995.

Roeleveld K, Blok JH, Stegeman DF & Van Oosterom A. Volume conduction models for surface EMG; confrontation with measurements. *J Electromyogr Kinesiol* 7: 221-232, 1997a.

Roeleveld K, Sandberg A, Stålberg EV & Stegeman DF. Motor unit size estimation of enlarged motor units with surface electromyography. Muscle Nerve 21: 878-886, 1998.

Roeleveld K, Stegeman DF, Falck B & Stålberg EV. Motor unit size estimation: confrontation of surface EMG with macro EMG. *Electroencephalogr Clin Neurophysiol* 105: 181-188, 1997b.

Roeleveld K, Stegeman DF, Vingerhoets HM & Van Oosterom A. Motor unit potential contribution to surface electromyography. *Acta Physiol Scand* 160: 175-183, 1997c.

Roeleveld K, Stegeman DF, Vingerhoets HM & Van Oosterom A. The motor unit potential distribution over the skin surface and its use in estimating motor unit location. *Acta Physiol Scand* 161: 465-472, 1997d.

Rongen GA, Dijk JP, Ginneken EE, Stegeman DF, Smits P & Zwarts MJ. Repeated ischaemic isometric exercise increases muscle fibre conduction velocity in humans: involvement of Na(+)-K(+)-ATPase. *J Physiol* 540: 1071-1078, 2002.

Rosenfalck P. Intra- and extracellular potential fields of active nerve and muscle fibres. *Suppl Acta Physiol Scand* 321: 1-168, 1969.

Sadoyama T & Masuda T. Changes of the average muscle fiber conduction velocity during a varying force contraction. *Electroencephalogr Clin Neurophysiol* 67: 495-497, 1987.

Schmied A, Pagni S, Sturm H, Vedel JP. Selective enhancement of motoneurone short-term synchrony during an attention-demanding task. *Exp Brain Res* 133: 377-390, 2000.

Stålberg E. Propagation velocity in human muscle fibers in situ. *Acta Physiol Scand* 287, 1-112, 1966.

Stålberg E. Macro EMG. *Muscle Nerve* 6: 619-630, 1983.

Stålberg E. Single fiber EMG, macro EMG and scanning EMG. New ways of looking at the motor unit. *CRC Crit Rev Clin Neurobiol* 2: 125-167, 1986.

Stålberg E & Falck B. The role of electromyography in neurology. *Electroencephalogr Clin Neurophysiol* 103: 579-598, 1997.

Stålberg E, Nandedkar SD, Sanders DB & Falck B. Quantitative motor unit potential analysis. *J Clin Neurophysiol* 13: 401-422, 1996.

Stegeman DF, Blok JH, Hermens HJ & Roeleveld K. Surface EMG models: properties and applications. *J Electromyogr Kinesiol* 10: 313-326, 2000a.

Stegeman DF, Dumitru D, King JC & Roeleveld K. Near- and far-fields: source characteristics and the conducting medium in neurophysiology. *J Clin Neurophysiol* 14 : 429-442, 1997.

Stegeman DF & Linssen WH. Muscle fibre membrane electrophysiology and surface EMG: A simulation study. *J Electromyogr Kinesiol* 2, 130-140, 1992.

Stegeman DF, Roeleveld K & Blok JH. EMG topography as an instrument in clinical neurophysiology: a unipolar recording approach. In: *Proceedings first general workshop.* European concerted action (SENIAM, BIOMED II), edited by Hermens HJ, Merletti R & Freriks B. Enschede: Roessingh, 1996, p. 73-76.

Stegeman DF, Zwarts MJ, Anders C & Hashimoto T. Multi-channel surface EMG in clinical neurophysiology. *Suppl Clin Neurophysiol* 53: 155-162, 2000b.

Uesugi H, Sonoo M, Stalberg E, Matsumoto K, Stalberg S & Karlsson L. A new technique of analysing surface EMG on voluntary contraction which can differentiate between neurogenic and myopathic change: a proposal of 'clustering index'. *Clin Neurophysiology* 110: S249, 1999.

Trontelj JV, Stalberg EV. Single fiber EMG and spectral analysis of surface EMG in myotonia congenita with or without transient weakness. *Muscle Nerve* 18: 252-254, 1995.

Van Bolhuis BM, Medendorp WP & Gielen CC. Motor unit firing behavior in human arm flexor muscles during sinusoidal isometric contractions and movements. *Exp Brain Res* 117, 120-130, 1997.

Van der Hoeven van der JH, Links TP, Zwarts MJ & Weerden van TW. Muscle fiber conduction velocity in the diagnosis of familial hypokalemic periodic paralysis-invasive versus surface determination. *Muscle Nerve* 17: 898-905, 1994.

Van der Hoeven JH, Zwarts MJ & Weerden van TW. Muscle fiber conduction velocity in amyotrophic lateral sclerosis and traumatic lesions of the plexus brachialis. *Electroenceph Clin Neurophysiol* 89: 304-310, 1993.

Van Dijk JP, Stegeman DF & Zwarts MJ. Possibilities and limitations of conduction velocity distribution estimation. In: *The state of the art on signal processing methods for surface electromyography.* European concerted action (SENIAM, BIOMED II), edited by Hermens HJ. Enschede: Roessingh, 1999, p. 211-217.

Van Vugt JP & Van Dijk JG. A convenient method to reduce crosstalk in surface EMG. *Clin Neurophysiol* 112: 583-592, 2001.

Wallinga W, Meijer SL, Alberink MJ, Vliek M, Wienk ED & Ypey DL. Modelling action potentials and membrane currents of mammalian skeletal muscle fibres in coherence with potassium concentration changes in the T-tubular system. *Eur Biophys J* 28: 317-329, 1999.

Wood SM, Jarratt JA, Barker AT & Brown BH. Surface electromyography using electrode arrays: a study of motor neuron disease. *Muscle Nerve* 24: 223-230, 2001.

Zwarts MJ & Arendt-Nielsen L. The influence of force and circulation on average muscle fibre conduction velocity during local muscle fatigue. *Eur J Appl Physiol* 58: 278-283, 1988.

Zwarts MJ, Drost G & Stegeman DF. Recent progress in the diagnostic use of surface EMG for neurological diseases. *J Electromyogr Kinesiol* 10: 287-291, 2000.

Zwarts MJ & Van Dijk JP. Methods to determine muscle fiber conduction velocity. In: *State of the art on modelling methods for surface electromyography.* European concerted action (SENIAM, BIOMED II), edited by Hermens HJ, Stegeman DF, Blok JH & Freriks B. Enschede: Roessingh, 1998, p. 85-89.

Zwarts MJ, Van Weerden TW & Haenen HT. Relationship between average muscle fiber conduction velocity and EMG power spectra during isometric contraction, recovery and applied ischemia. *Eur J Appl Physiol Occup Physiol* 56: 212-216, 1987.

Zwarts MJ, Weerden van TW, Links TP, Haenen HTM & Oosterhuis HJG. The muscle fiber conduction velocity and power spectra in familial hypokalemic periodic paralysis. *Muscle Nerve* 11: 166-173, 1988.

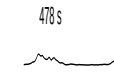

4

pH heterogeneity in tibial anterior muscle during isometric activity studied by ^{31}P NMR spectroscopy*

Abstract

The occurrence of pH heterogeneity in human tibial anterior muscle (TA) during sustained isometric exercise is demonstrated by applying phosphor nuclear magnetic resonance (^{31}P NMR) spectroscopy in a study of 7 healthy subjects. Exercise was performed at 30 and 60% of maximal voluntary contraction (MVC) until fatigue. The ^{31}P NMR spectra, as localized by a surface coil and improved by proton irradiation, were obtained at a high time resolution (16 s). They reveal the simultaneous presence of two pH pools during most experiments. Maximum difference in the two pH levels during exercise was 0.40 ± 0.07 (30% MVC, n=7) and 0.41 ± 0,03 (60% MVC, n=3). Complementary two-dimensional ^{31}P spectroscopic imaging (2D ^{31}P SI) experiments in one subject supported the supposition that the distinct pH pools reflect the metabolic status of the main muscle fiber types. The relative size of the inorganic phosphate (P_i) peak in the spectrum attributed to the type II fiber pool increases with decreasing pH levels. This phenomenon is discussed in the context of the size principle stating that the smaller (type I) motor units are recruited first.

Introduction

pH-heterogeneity in human muscle tissue during exercise and recovery, as monitored by ^{31}P NMR spectroscopy, has been addressed in several studies (Achten et al. 1990; Mizuno et al. 1994a; Mizuno et al. 1994b; Park et al. 1987; Vandenborne et al. 1991; Vandenborne et al. 1993; Yoshida & Watari, 1994; Yoshida et al. 1996). A shift of the frequency of the P_i

*Houtman CJ, Heerschap A, Zwarts MJ & Stegeman DF. *J Appl Physiol* 91: 191-200, 2001.

signal, relative to that of phosphocreatine (PCr) in the ^{31}P NMR spectrum, corresponds to a change in the intracellular pH. The occurrence of a broadened, or even split, resonance of inorganic phosphate during exercise is often ascribed to the different metabolic behavior of slow and fast-twitch fibers involved in the exercise. Slow-twitch (type I) fibers mainly use aerobic energy sources and therefore produce few protons, resulting in a relatively unaffected tissue pH. Fast-twitch (type II) fibers are better equipped for anaerobic glycolysis. This is accompanied by a more extensive production of protons. If this proton production is not balanced by its removal and/or buffering, the pH will decline, resulting in a shift of the P_i peak.

Fiber type-related pH heterogeneity has been reported for wrist flexion muscles (Mizuno et al. 1994a; Mizuno et al. 1994b; Park et al. 1987), for calf muscles (Achten et al. 1990; Vandenborne et al. 1991; Vandenborne et al. 1993), and for the m. biceps femoris (Yoshida & Watari, 1994; Yoshida et al. 1996). In these experiments cyclic concentric exercises were used. Mostly, a graded exercise at low frequency (1/6-1/4 Hz) was chosen (Mizuno et al. 1994a; Mizuno et al. 1994b; Park et al. 1987; Vandenborne et al. 1993). This type of exercise ensures the supply of oxygen to muscles contributing to the exercise. Also cyclic concentric exercise at highest frequency possible (2-3 Hz) was used to guarantee the recruitment of all motor units, the functional building blocks of a muscle (Vandenborne et al. 1991; Vandenborne et al. 1993). Vandenborne et al. (1993) applied a NMR localization method, to distinguish between the contributions of the three different calf muscles to the sampled signal.

Slow-twitch (type I) motor units and fast-twitch (type II) motor units differ in size. According to the size principle, as ascribed by Henneman (1981), motor units are recruited from small to large. Combining the size principle with the development of P_i peaks is an alternative approach to study pH heterogeneity. Because the size principle is disputed in non-isometric exercises (e.g. Howell et al. 1995), we studied pH heterogeneity during sustained isometric exercise at two different loads (30 and 60% MVC). At first during a 30% MVC level only the relative small slow-twitch (type I) motor units are recruited. In the course of the fatiguing contraction at 30% MVC new motor units, including the relative large fast-twitch (type II), are indispensable. This would induce a changeover to the simultaneous activity of both fiber types. At 60% MVC, the muscle is used under ischemic conditions (Kent-Braun et al. 1993, Sjøgaard et al. 1988). At this exercise level motor units of both types are expected to be active from the beginning (Enoka, 1995). This lead to the hypothesis that (i) pH heterogeneity will emerge in the course of an exercise at 30% MVC, (ii) pH heterogeneity will emerge soon after the start of an exercise at 60% MVC.

We selected the tibialis anterior muscle for this study, because it has no synergists for its performance, excluding the possibility that the measured force is produced by more than

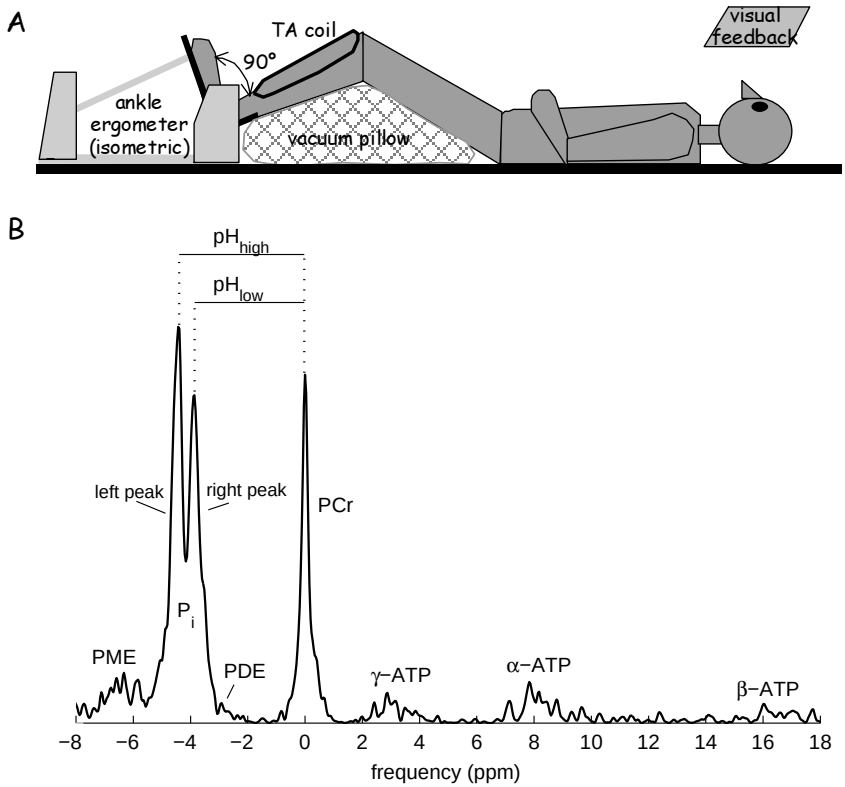

Figure 4.1A: experimental set up. The subject lies in a supine position on the table. The U-shaped coil is placed over the tibialis anterior muscle (TA) of the left leg. The left foot is strapped in the ergometer. The left leg is slightly bent and supported by vacuum pillows. The angle between foot and lower leg is 90°. The subject gets visual feedback of the force and is encouraged verbally during exercise. B: example of a phosphor nuclear magnetic resonance (^{31}P NMR) spectrum (2 acquisitions, repetition time = 7 s) measured 68 s after the start of a 60% MVC exercise (subject 6, see also figure 4.2). Compared with a NMR spectrum obtained at rest, the phosphocreatine (PCr) peak is decreased, the inorganic phosphate (P_i) peak is increased and doubled. pH values are derived from the frequency of the P_i peaks relative to that of the PCr peak. The area of a peak is a measure for the tissue level of the corresponding molecule. PME, phosphomonoesters; PDE, phosphodiesters; pH_{high} and pH_{low}, values derived from, respectively, left (low-field) and right (high-field) P_i peaks.

one muscle. The measurements only use coil localization to visualize as many as possible temporal details (temporal resolution 16s). In one of the seven subjects the coil profile and the spatial distribution of the P_i peaks during exercise have been investigated.

Methods

Subjects

Seven healthy men and women participated in the study, aged 22-48 (table 4.1). All subjects were regularly engaged in low to moderate aerobic exercise. They were informed on the purpose of the experiments and gave their written consent. The protocol was approved by the local ethics committee of the University Medical Center Nijmegen.

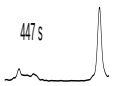

Table 4.1: Subject and force parameters

	Sex	Age, yr	100% MVC before 60% MVC, N	Duration of 60% MVC, s	100% MVC before 30% MVC, N	Duration of 30% MVC, s
Subject 1	m	25	282	81	268	608
Subject 2	f	31	214	112	241	387
Subject 3	m	47	318	167	312	660
Subject 3, SI					298	690
Subject 4	m	33	277	151	317	348
Subject 5	m	27	258	114	273	376
Subject 6	f	22	256	96	207	580
Subject 7	m	23	336	80	295	660
Means ± SD		30 ± 9	277 ± 41	114 ± 34	276 ± 38	539 ± 144

MVC, maximal voluntary contraction; m, male; f, female; SI, spectroscopic imaging data.

Exercise

Subjects had a supine position on the investigation table with their left leg slightly bent and supported with vacuum pillows (figure 4.1A). For the 2D ^{31}P SI measurements, the exercising leg was straightened to enable its horizontal alignment with respect to the static magnetic (B_0) field. The angle of the left lower leg compared to the left foot was always 90 degrees and the foot was fixed with straps in a pedal. Subjects were supplied with visual feedback of the force and were verbally encouraged during exercise. All subjects performed both exercise protocols, separated by at least two days.

The ergometer was home built, was specially designed for use in the magnet and was both applicable for dorsal and plantar ankle flexion. The force signal was digitally stored at a sample rate of 100 Hz. To enable synchronization afterwards, a trigger signal of the NMR system was registered on the force system. The NMR data points were assigned to the midpoint of the two ^{31}P NMR excitation pulses, applied for each measurement.

The exercise consisted of an isometric plantar ankle flexion until fatigue at 30 or 60% MVC. After offset correction, two MVC measurements were done, from which the maximum was used (table 4.1). The subject was permitted to deviate ±3% at 30% MVC or ±5% at 60% MVC. If he or she could no longer meet this condition (despite encouraging), exercise was stopped. MVC measurements and exercise were separated by at least 30 minutes. ^{31}P NMR data were collected during rest (3 minutes), exercise (table 4.1) and recovery (15 minutes).

Nuclear Magnetic Resonance

All experiments were performed on a 1.5 T whole-body system (Magnetom SP, Siemens Medical Systems Inc. Erlangen, Germany). The surface coil was home built and specially designed to detect signals from the TA. It consisted of two concentric loops: 25 cm x 8½ cm (tuned to the proton (^{1}H) frequency) and 20 cm x 3½ cm (tuned to the ^{31}P frequency). It was carefully placed over the TA and fixed with tape. Before ^{31}P NMR data collection, a series of

five transversal ^{1}H NMR images (gradient-recalled echo: echo time = 6 ms, repetition time = 70 ms, thickness = 10 mm, distance factor = 0.4) were made to validate the correct placement of the surface coil. In case of the 2D ^{31}P SI measurements, this series was extended to 15 transversal ^{1}H NMR images divided over the length of the coil, to control the horizontal position of the lower leg and consequently that of the TA. After the last 2D ^{31}P SI measurement this series of 15 ^{1}H NMR images was repeated, to confirm an unchanged leg position.

The homogeneity of the B_0 field was adjusted using the proton signal from water, resulting in a peak width at half-height of ≤ 0.5 ppm. To overcome inhomogeneity of the radio frequency (B_1) field, an amplitude-modulated adiabatic 90° pulse (sincos), with a length of 2.56 ms, was used for excitation. The spectral excitation of this pulse was constant over a frequency range of 1000 Hz (≈ 39 ppm), which is sufficient to map all resonances present in skeletal ^{31}P NMR spectra.

For optimal signal to noise ratio per unit time we used a repetition time (TR) of seven seconds, according to Ernst & Anderson (1966) (TR=1.25 T_1) and to Thomsen et al. (1989) (muscle T_1(PCr, P_i, ATP) ≤ 5.5 s), with T_1 as spin-lattice relaxation time. Two acquisitions were averaged per measurement. Including data storage, the time resolution became 16 s. The free induction decay (FID) was low-pass filtered at 5 kHz and sampled during 512 ms at a sample frequency of 4 kHz. During data collection, high-level (10 W) WALTZ4 proton irradiation was applied to decouple the ^{31}P-^{1}H spin coupling (Luyten et al. 1989). During the remaining time, low-level (0.6 W) WALTZ4 proton irradiation was applied to amplify the ^{31}P NMR signal by the nuclear Overhauser effect (Brown et al. 1995).

For localization of the ^{31}P NMR signal, 2D ^{31}P SI, without slice selection, with a matrix size of 8 x 8 was applied in the transversal direction. Each volume of interest had a nominal resolution of 1.5 x 1.5 cm². In the third dimension the view of the surface coil dictated the localization (~20 cm). Acquisition time was 7.57 minutes (≈ 8 x 8 x 7 s), taking one acquisition for every phase encoding step.

Data analysis

The data-analyzing method VARPRO (Van der Veen et al. 1988) was used as fitting procedure. The first three data points of each FID were not included in the Fourier transformation to avoid the broad baseline component arising from the tibia bone. Starting values for the peak position and line width of PCr and P_i were given. The peaks were assumed to have a Lorentzian line shape. If the P_i resonance split into two resonances, equal line widths were not assumed since the origin of this phenomenon is part of the study. To avoid improper use of prior knowledge, a broadened P_i peak was analyzed in two ways:

Table 4.2: 60% MVC, pH slopes, maximum differences and end-of-exercise values.

	Slope of pH_{high} $x10^{-3}$ s^{-1}	Slope of pH_{low} $x10^{-3}$ s^{-1}	Max(pH_{high} minus pH_{low})	pH_{high} at end-of-exercise	pH_{low} at end-of-exercise
Subject 3	-1,1	-4,8	0,43	6,98	6,55
Subject 5			0,38	6,50	6,12
Subject 6	-7,3	-11,9	0,42	6,58	6,16
Means ± SD	-4,2 ± 4,4	-8,4 ± 5,0	0,41 ± 0,03	6,69 ± 0,26	6,28 ± 0,24

pH_{high} and pH_{low} are derived from, respectively, the left (low-field) and right (high-field) P_i peak. Slopes, maximum difference and end-of-exercise values are derived from fitted line pieces through the data points (see text).

as one peak and as two independent peaks. In the evaluation of the results the lower bound of the theoretical statistical errors, the Cramer-Rao (CR) lower bound, was used. The result with the lowest CR lower bound in the calculated parameters (peak area, line width and frequency) was accepted as the best fit. Sometimes, both results came up with CR lower bounds of more than 60% of the parameter values. Then the P_i peak was excluded from the fit procedure.

Intracellular pH was calculated from the chemical shift of P_i based on the equation pH = 6.75 + log(δ-3.26)/log(5.75-δ), were δ equals the chemical shift of the P_i peak in parts per million (ppm), relative to PCr. The curves of the pH were fitted by piecewise linear regression. Continuity was assumed, except for the transition of one pH to two pH's and vice versa. The distribution of data points over the successive regression lines was optimized by minimizing the sum of the residuals of the lines. This method is described by Vieth (1989) for the combination of two regression lines. We extended this method to an arbitrary number of line pieces.

The 2D ^{31}P SIs were analyzed with LUISE, a data-analyzing program supplied by Siemens. No zero filling, filtering, or offset correction was used in the k space (the spatial frequency space). The shift of the matrix grid was equal for both 2D ^{31}P SI 's (rest and exercise). The first 2D ^{31}P SI was depicted on ^{1}H NMR images measured before exercise, and the last 2D ^{31}P SI was depicted on ^{1}H NMR images measured after exercise.

Preprocessing of the spectra shown in this paper (figure 4.1B, 4.2B, 4.3B & 4.4B) was as follows. Before Fourier transformation, the first three data points of the FID were skipped, an asymmetric Gauss window (center 25 ms, width 100 ms) was applied and zero filling was performed to 4,096 data points.

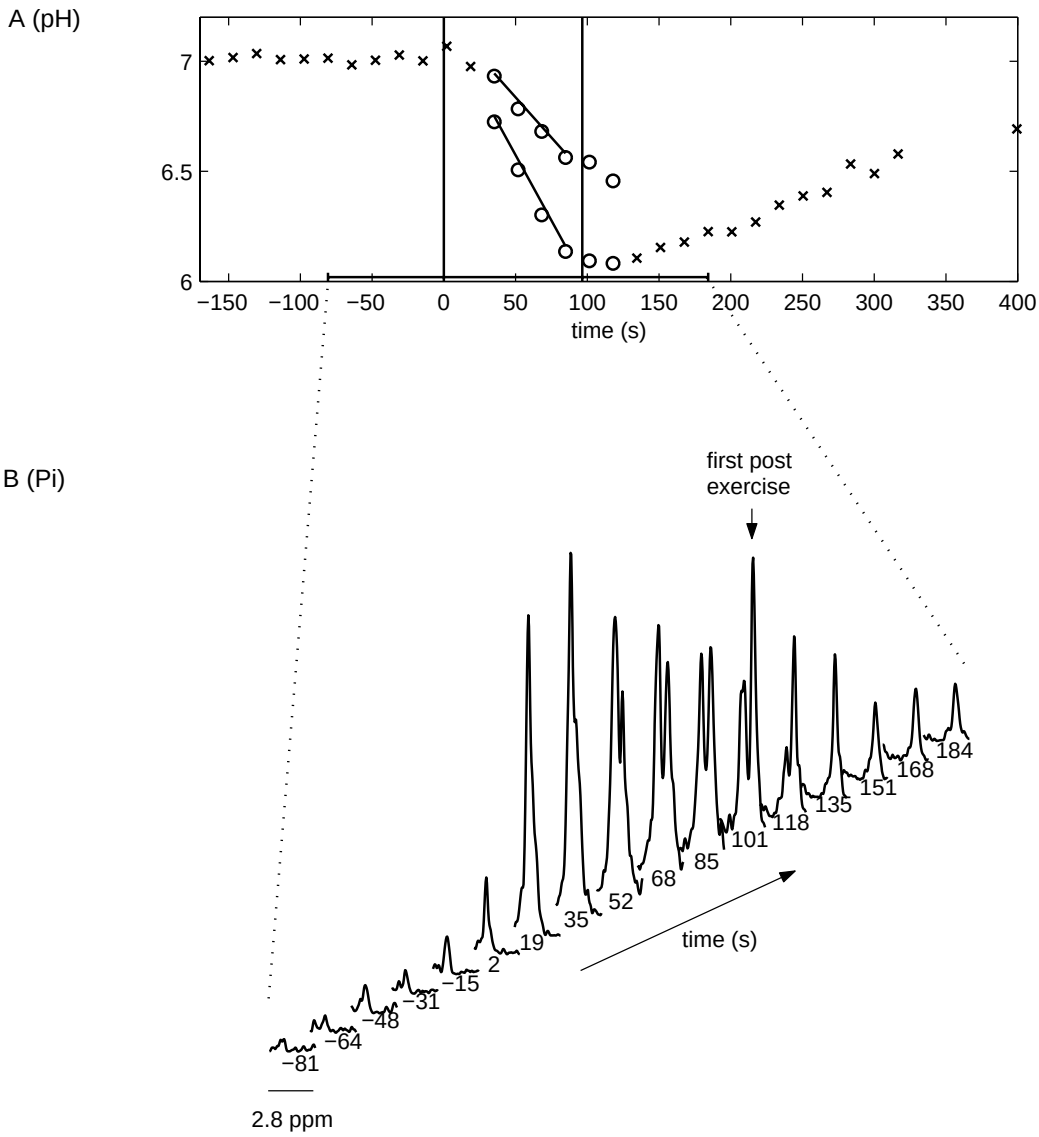

Figure 4.2: results of pH analysis and ^{31}P NMR spectra of subject 6, performing a 60% MVC exercise. A: pH, Start (at 0 s) and end of exercise (at 96 s) are marked with vertical lines. One (x) or two (o) P_i peaks were analyzed. Lines through the data points are fitted as described in the text. Horizontal bar, just over the time scale, indicates the time interval corresponding to the spectral selection shown in B for the region with P_i peaks. B: P_i peak region of sequential spectra. Numbers below the spectra represent time (in s). Note the gradual appearance of two P_i peaks during exercise leading to two different pH levels (A&B), the decrease of the two pH levels and simultaneous increase of the relative size of the right P_i peak (A&B), and the relative quick recovery (= disappearance) of the left P_i peak (B).

Results

Exercise

Maximum voluntary contraction ranged between 207 and 336 N. The duration of the exercises varied between 80-167 s for 60% MVC and between 348-660 s for 30% MVC

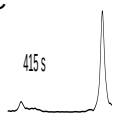

Table 4.3: 30% MVC, pH slopes, pH differences and end-of-exercise values.

	Slope of pH_{high} $x10^{-3}$ s^{-1}	Slope of pH_{low} $x10^{-3}$ s^{-1}	Max(pH_{high} minus pH_{low})	pH_{high} at end-of-exercise (if two)	pH_{low} at end-of-exercise (if two)	pH at end-of-exercise (if one)
Subject 1	-0,7	-2,6	0,42			6,24
Subject 2	-1,8	-1,8	0,34			6,25
Subject 3	-0,1	0,2	0,48	7,01	6,61	
Subject 4	-0,8	-2,9	0,30			6,45
Subject 5	-0,6	-0,5	0,36	6,79	6,46	
Subject 6	0,0	-0,6	0,46			6,38
Subject 7	-0,9	-1,6	0,41			6,41
Means ± SD	-0,7 ± 0,6	-1,4 ± 1,1	0,40 ± 0,07	6,90 ± 0,16	6,54 ± 0,11	6,35 ± 0,10

pH_{high} and pH_{low} are derived from respectively the left (low-field) and right (high-field) Pi peak. Slopes, maximum difference and end-of-exercise values are derived from fitted line pieces through the data points (see text).

(table 4.1). Although toe extension muscles did not contribute to the delivered force, subjects tended to extend their toes when it became hard to maintain the desired force. This means that the extensor digitorum longus (EDL) and the extensor hallucis longus were also activated and could potentially contribute to the ^{31}P NMR signal. However, the extensor hallucis longus is situated distal to the TA and therefore did not contribute to the ^{31}P NMR signal. The influence of the EDL was studied with the 2D ^{31}P SI results (see below).

^{31}P NMR spectroscopy with only surface coil localization, 60% MVC

An example of a ^{31}P NMR spectrum of the TA obtained during a 60% MVC exercise is shown in figure 4.1B. A doubling of the P_i peak is clearly visible. Such a doubling of the P_i NMR signal was evident in three subjects. The other four subjects showed a clear broadening of the line width of the P_i peak during exercise and early recovery. In three of these subjects a second P_i peak was visible in the first spectrum after the end of exercise.

The data of three subjects in which doubled P_i peaks were analyzed, are summarized in table 4.2. The values were derived from the fitted line pieces through the data points as described. The slopes of pH_{high} and pH_{low}, the maximum difference between pH_{high} and pH_{low} during exercise, and the pH levels at the end of exercise are given. For pH_{high} and pH_{low} the mean ± SD slopes are respectively (- 4.2 ± 4.4) * 10^{-3} and (-8.4 ± 5.0) * 10^{-3} pH units/s and the mean of the maximum difference in pH levels during exercise is 0.41 ± 0.03 pH units. The mean ± SD values at the end of exercise are respectively 6.69 ± 0.26 and 6.28 ± 0.24. No slopes are given for subject 5, because two P_i peaks could only be analyzed just before the end of exercise and during recovery.

Figure 4.2A shows the results for the pH analysis before, during and after an exercise at 60% MVC performed by subject 6. Figure 4.2B show stack plots of spectra for the P_i peak region for the same period. During exercise, gradually two P_i peaks appear. With lowering of the pH levels, the relative size of the right (high-field) P_i peak increases (figure 4.2A&B). This

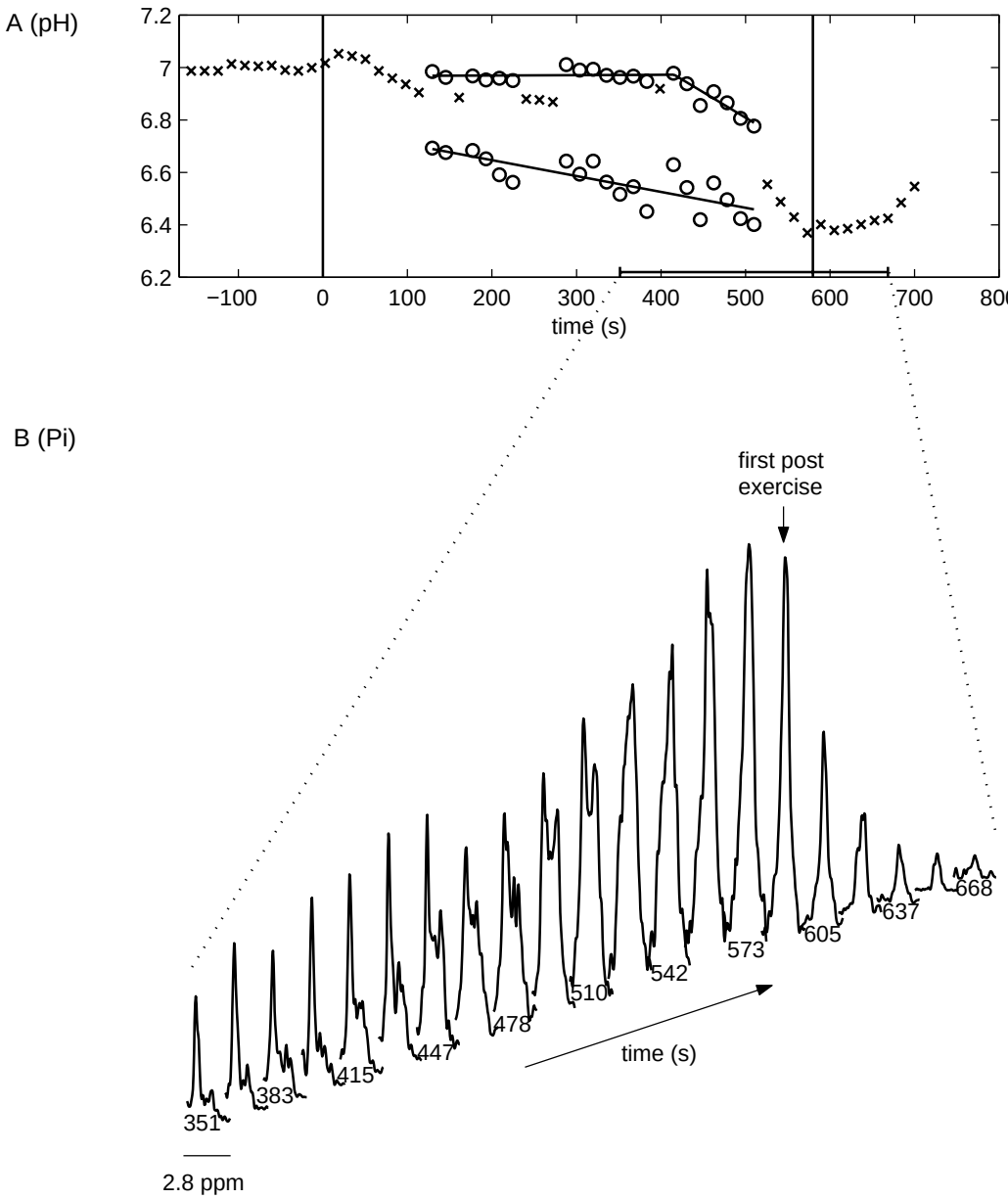

Figure 4.3: results of pH analysis and ^{31}P NMR spectra of subject 6, performing a 30% MVC exercise. A: pH. Start (at 0 s) and end of exercise (at 580 s) are marked with vertical lines. One (x) or two (o) P_i peaks were analyzed. Lines through data points are fitted as described in the text. Horizontal bar, just over the time scale, indicates the time interval corresponding to the spectral selection shown in B for the region with P_i peaks. B: P_i peak region of sequential spectra. Numbers below the spectra represent time (in s). Note the appearance of two different pH levels during exercise corresponding to two P_i peaks(A and B), the accelerated decrease of pH_{high} and the increase of the relative size of the right P_i peak between 415 s and 510 s (A and B), and the merging of both P_i peaks between t=510 s and 573 s, leading to one low pH level (A and B).

P_i peak corresponds to pH_{low}. The subsequent recovery of the left (low-field) P_i peak is remarkably quicker than the recovery of the right P_i peak (figure 4.2B).

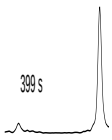

^{31}P NMR spectroscopy with only surface coil localization, 30% MVC

All seven subjects showed doubled P_i peaks during the 30% MVC exercise. The results of the pH analysis for all subjects are summarized in table 4.3. The values were derived from fitted line pieces through the data points as described. Of each subject the slopes of pH_{high} and pH_{low}, the maximum difference in pH_{high} and pH_{low} during exercise, and the pH levels at the end of exercise are given. If pH_{high} or pH_{low} consisted of two line pieces, the slope from the first line piece is given. The mean ± SD slopes for pH_{high} and pH_{low} are respectively (-0.7 ± 0.6) and (-1.4 ± 1.1) * 10^{-3} pH units/s, the mean of the maximum difference in pH levels is 0.40 ± 0.07 pH units. The mean pH values (± SD) at the end of exercise are 6.90 ± 0.16 and 6.54 ± 0.11 for respectively pH_{high} and pH_{low} and 6.34 ± 0.09 if only one P_i peak is left at the end of exercise.

Figure 4.3A shows the results for the pH analyses during rest, exercise and recovery at 30% MVC as analyzed from the data of subject 6. Figure 4.3B shows the P_i peak region of the spectra, corresponding to the most remarkable changes in peak area distribution over both P_i peaks, and to the course of the peak after the end of exercise. pH heterogeneity appears during a large part of the exercise, but is absent in the first and last spectra during exercise (figure 4.3A). The relative size of the right P_i peak (corresponding to pH_{low}) increases as the highest pH level decreases (figure 4.3A&B, between 415 and 510 s). pH_{high} declines faster than pH_{low} so that the two P_i peaks merge in one large peak, corresponding to one low pH level (figure 4.3A&B, starting after 510 s).

Figure 4.4A shows the results of pH analyses of rest, exercise and recovery at 30% MVC, performed by subject 3. Figure 4.4B shows the P_i region of the spectra during the final eight minutes of exercise. For clarity, every 2nd available spectrum is skipped in this presentation. Again two P_i peaks appear. In this subject these two peaks last until the end of exercise and in addition, the peaks and the calculated pH values stabilize during a long period compared to the other subjects. This behavior was the reason to select this subject for the spectral imaging session presented below which has a much lower time resolution (8 minutes).

Two-dimensional phase encoded ^{31}P spectroscopic imaging

The 2D ^{31}P SI measurement required an acquisition time of 8 minutes. Too much shifting of the P_i peaks during these 8 minutes would cause a spread and flattening of the P_i peaks. Therefore, the 2D ^{31}P SI measurements were performed on subject 3, who showed two stable pH levels during 30% MVC in the measurement with only surface coil localization (figure 4.4A). Two 2D ^{31}P SI measurements were acquired in one session. The first was measured during rest, immediately preceding the exercise. The signal intensities reflect the sensitivity profile of the ^{31}P coil (figure 4.5A). Four of the 64 voxels contained almost all signal intensity. These voxels cover the TA (3½ voxel) and part of the EDL (½ voxel).

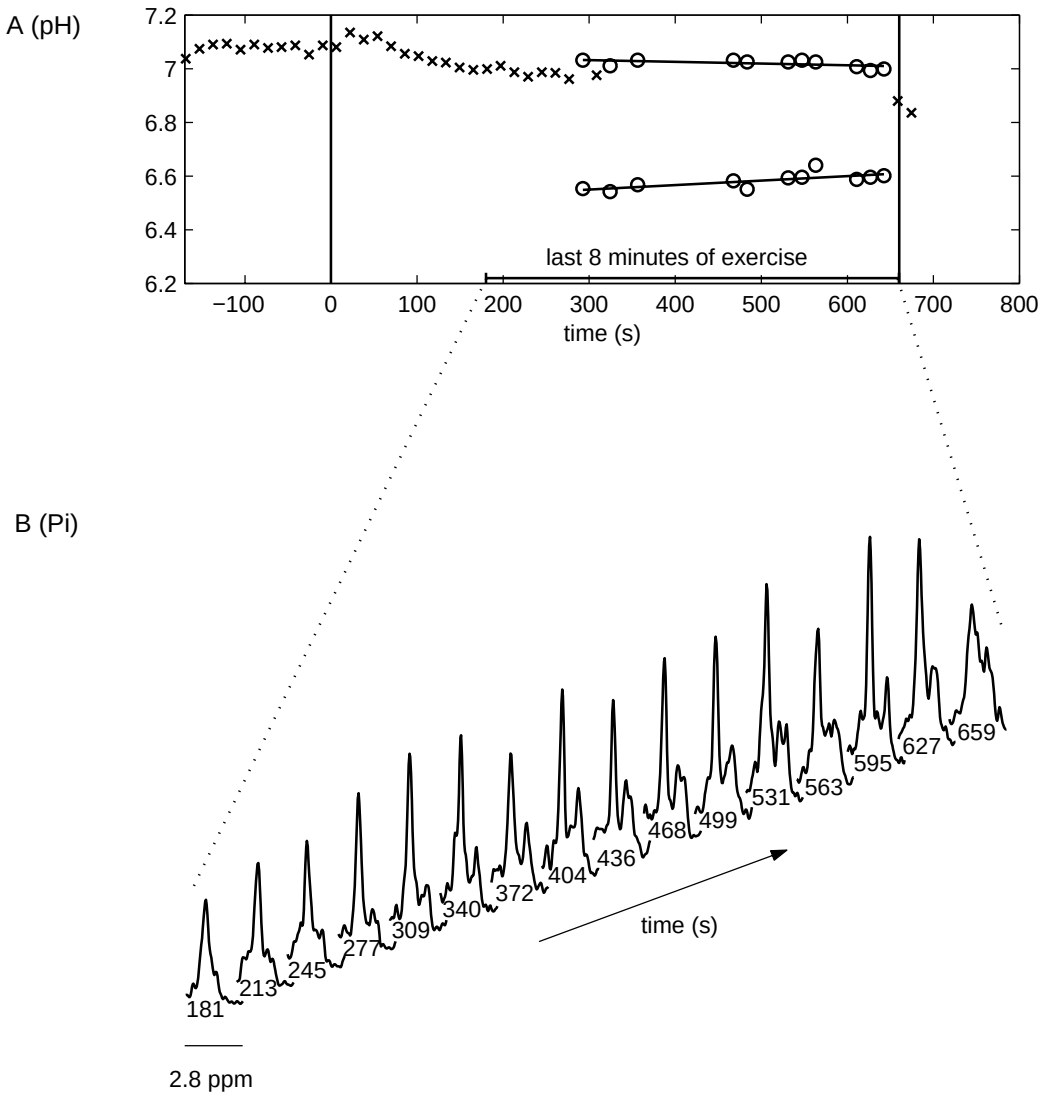

Figure 4.4: results of pH analysis and ^{31}P NMR spectra of subject 3, performing a 30% MVC exercise. The same exercise was performed by this subject to obtain the 2D ^{31}P SIs (figure 4.5). A: pH, Start (at 0 s) and end of exercise (at 660 s) are marked with vertical lines. One (x) or two (o) P_i peaks were analyzed. Lines through the data points are fitted as described in the text. Horizontal bar, just over the time scale, indicates the last eight minutes of exercise and corresponds with the spectral selection shown in B for the region with P_i peaks. B: P_i peak region of sequential spectra. Numbers below the spectra represent time (in s). Every second spectrum is shown for clarity. Note the visibility of two stable P_i peaks leading to two constant pH levels during the last 6½ minutes of the exercise.

Because the signal intensity is higher in the most ventral voxels, more than 7/8 of the total signal intensity originates from the TA. The signal intensity of PCr is highest in the medial ventral (left upper) voxel.

The second 2D ^{31}P SI (figure 4.5B) was measured during the last 8 minutes of an exercise at 30% MVC. In this 2D ^{31}P SI the highest intensity of PCr is now observed for the lateral ventral (right upper) voxel. The medial ventral (left upper) voxel, in which PCr is most

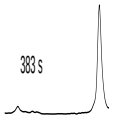

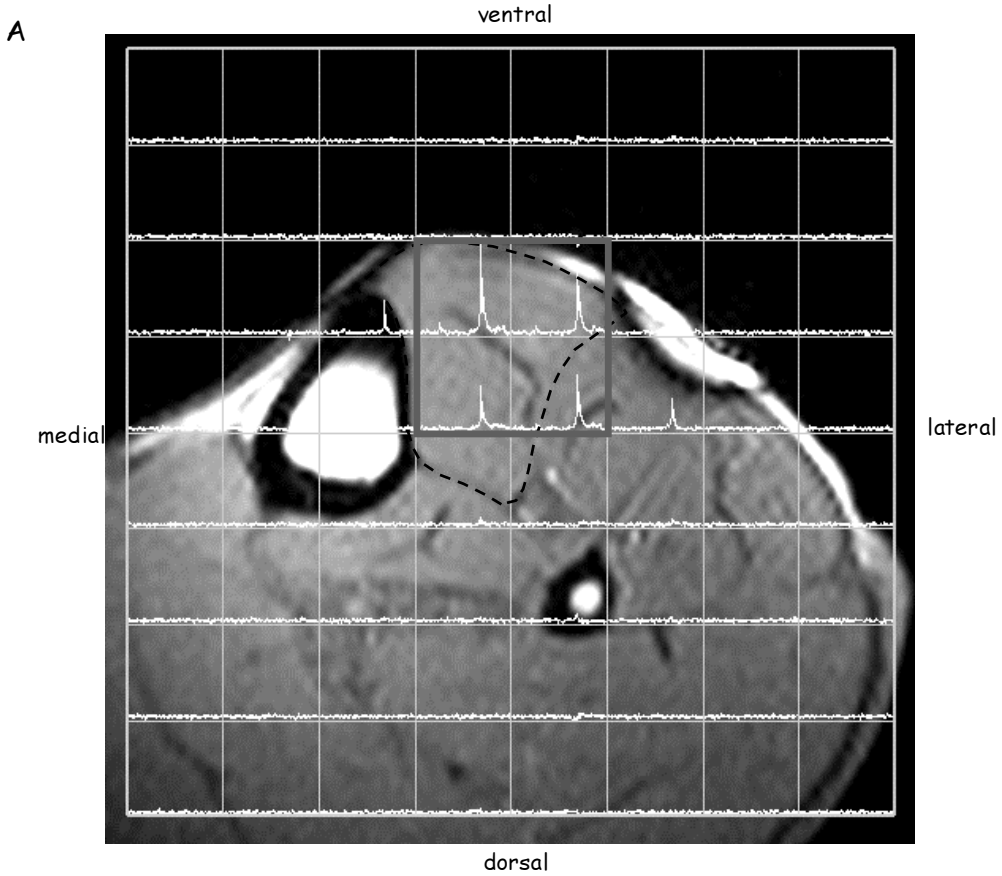

Figure 4.5A: ^{31}P two-dimensional phase encoded spectroscopic imaging (2D ^{31}P SI) of the left lower leg of subject 3 during rest, preceding a 30% MVC exercise. In each voxel, that part of the spectrum containing P_i and PCr is shown. TA is outlined with a broken line. Note that four of the 64 voxels contain most of the ^{31}P NMR signal (outlined with a solid line). These four voxels cover mainly the TA and partly the extensor digitorum longus muscle. The highest PCr peak occurs in the medial ventral (left upper) side of these four voxels. Large white area on left of the NMR ^{1}H image is the inner side of the tibia bone. Small white spot is the inner side of the fibula bone. Long white area on right is an artifact of the ^{1}H coil (high flux area).

declined, shows a doubled inorganic phosphate peak. Five voxels clearly reveal increased inorganic phosphate peaks. Figure 4.5C shows enlargements of the corresponding spectra obtained during rest and during exercise. Obviously, a pH gradient from lateral (pH level of 7.0 in the lateral voxels) to medial (lowest pH levels of 6.3 and 6.7 in the most medial voxel) is present. A summation of all five spectra (not shown) during exercise results in two P_i peaks at pH 7.0 and 6.5, which is similar to the pH levels measured with only surface coil localization in the same subject (figure 4.4A). As expected, there is a good reproducibility within one subject (Miller et al. 1995).

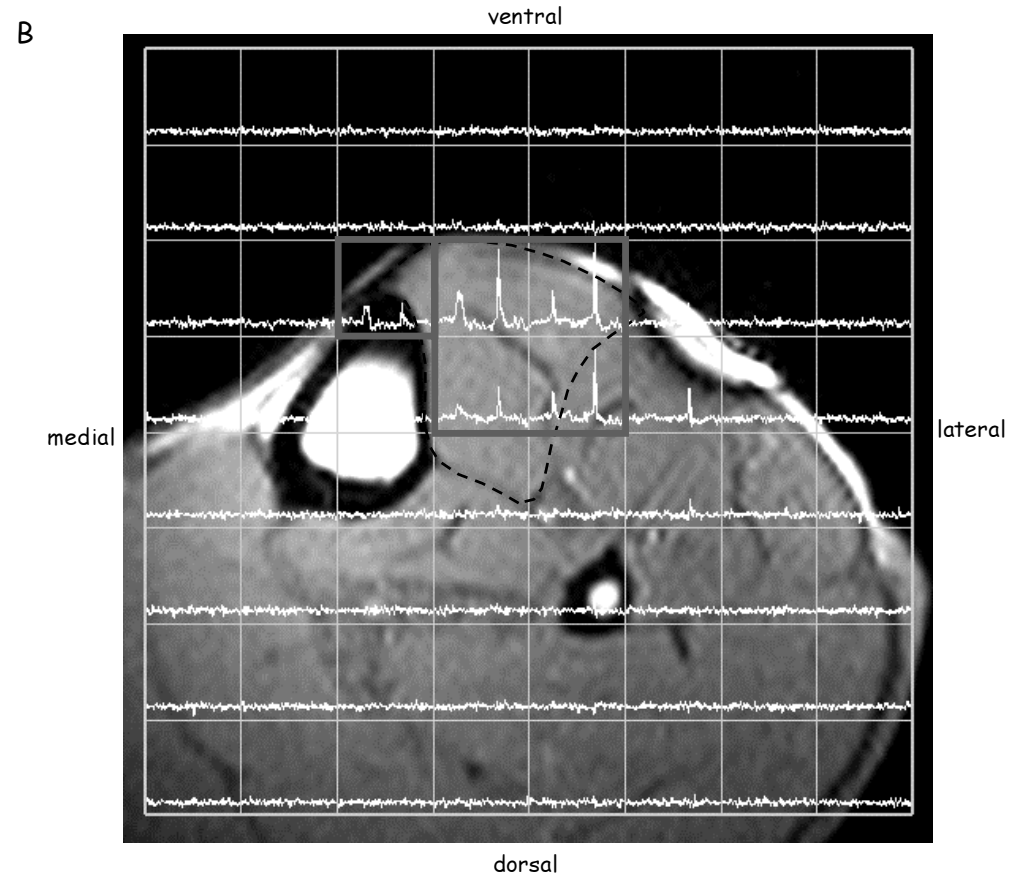

B: 2D ^{31}P SI of the same left lower leg as in A measured during the last eight minutes of the fatiguing 30% MVC exercise after measuring A. TA is outlined with a broken line. In each voxel, the same part of the spectrum as in A is shown; however, the y-axis rescaled. Note that the P_i peak is increased in five voxels (outlined with a solid line). The PCr peak is highest in the lateral ventral (right upper) voxel, and the P_i peak is broadened in the medial (left) voxels covering the TA.

Discussion

pH heterogeneity within the tibialis anterior muscle

This study reveals pH heterogeneity in the TA during sustained isometric exercise at both sides of the anaerobic threshold (30 vs. 60% MVC). This pH heterogeneity is not caused by the contributions of different muscles in the leg, because the only other muscle within the field of view of the coil (the EDL), which was sometimes activated by the subjects, contributes to less than 1/8 of the total ^{31}P NMR signal.

The combination of the two 2D ^{31}P SIs, measured during rest and during exercise at 30% MVC respectively, shows that during exercise PCr is more decreased at the medial side than at the lateral side of the TA. In this medial part of the muscle, a doubling of the inorganic phosphate peak occurs during the last 8 minutes of exercise. Whether the resulting two P_i peaks were present simultaneously during the eight minutes acquisition

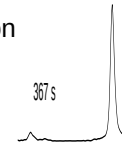

time, or one after the other can not be concluded from these data. The ^{31}P NMR data, acquired with only surface coil localization, however, show that the two pH levels occur simultaneously during the last 6½ minutes of the exercise, in this subject. Therefore, the doubled P_i peak must be ascribed to two pH compartments in the medial part of the TA. The size of these compartments has to be smaller than the nominal voxel size of 1.5 x 1.5 x 20 cm^3. As argued by Vandenborne et al. (1993), differences between intra- and extracellular pH, or intracellular pH differences are unlikely to be the origin of the distinct P_i peaks. Remaining sources are difference in activation or a partial limitation of the oxygen supply, both within a voxel size of 1.5 x 1.5 x 20 cm^3. We have no anatomical indications for two distinct areas of blood supply within this voxel. Neither do we have anatomical indications for two distinct areas of muscle activation otherwise than on the level of muscle fiber types. Therefore, the following discussion proceeds from the most probable interpretation linking the left (pH_{high}) peak to the slow-twitch (type I) motor units in the muscle and the right (pH_{low}) one to the fast-twitch (type II) motor units.

pH gradient within the tibialis anterior muscle

The fact that the pH shows a declining gradient from lateral to medial within the TA is possibly caused by differences in blood supply (Sjøgaard et al. 1988). The compliance of the tibia bone is smaller than the compliance of the membrane surrounding the anterior compartment. During a sustained isometric exercise this could possibly lead to a gradient in intramuscular pressure. If beside that the mean arterial blood pressure and the local metabolic vasodilatation are assumed to be homogeneously distributed over the whole TA, then blood flow is lowest closest to the tibia bone.

Comparing 60% and 30% MVC

Directly after the start of exercise, a small transient increase of pH is visible in all experiments with only coil localization (also in figure 4.2A, 4.3A & 4.4A). This reflects the proton consumption of PCr, which initially is the main energy source in these experiments (DeGroot et al. 1993).

In both exercise levels, the decrease of the pH_{low} is roughly twice as fast as that of pH_{high} (table 4.2 & 4.3). These pH slopes can be used as a measure of glycolytic activity (Kemp & Radda, 1994). The factor of two corresponds well with the difference of phosphofructokinase activity in fiber types I and II, also a measure of glycolytic activity (Essen et al. 1975).

Recovery of both P_i peaks could only be followed in two cases, because the P_i peaks tend to disappear quickly in the noise after exercise. In these two cases (both after 60% MVC), the P_i peak ascribed to the type I fibers disappears much faster than the one ascribed to the type II fibers. This can be explained by the pH dependency of the recovery of P_i (Iotti et al.

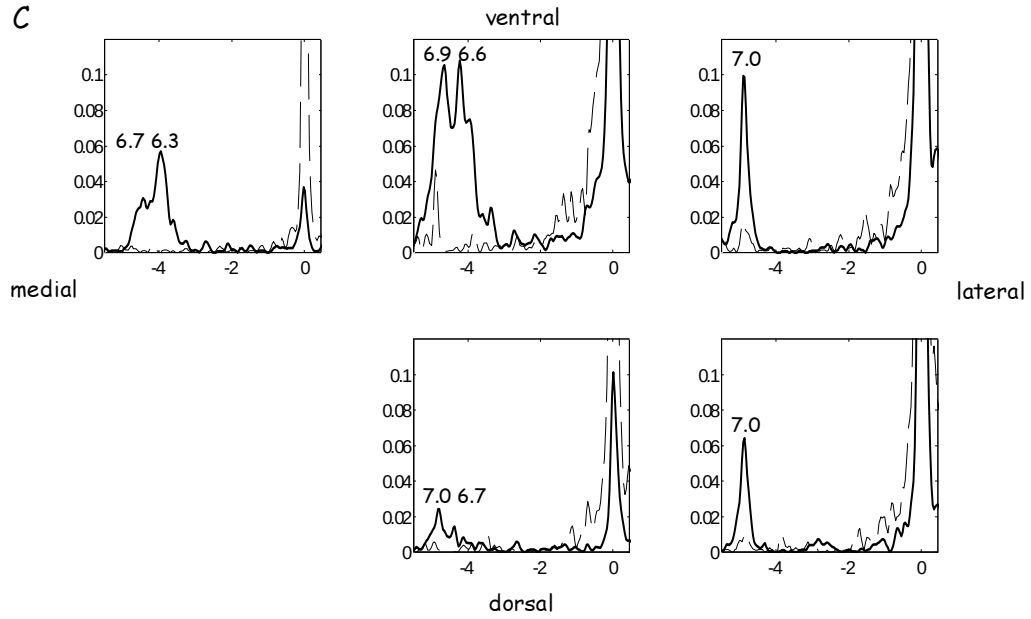

C: enlargements of five voxels covering the TA (outlined with a solid line in B). Dashed lines originate from the 2D ^{31}P SI measured during rest; solid lines are from the 2D ^{31}P SI measured during 30% MVC exercise. Scaling of the x- and y-axis is the same for all. Numbers at the P_i peaks are the corresponding pH levels. Note the doubled P_i peaks in the medial (left) voxels. Further, note the pH gradient from lateral (right) side to medial (left) side of the TA.

1993), and the higher oxydative capacity of the type I fibers (Quistorff et al. 1992) and is in agreement with the observations of others (Achten et al. 1990; Mizuno et al. 1994a; Mizuno et al. 1994b; Park et al. 1987; Vandenborne et al. 1991; Yoshida & Watari, 1994; Yoshida et al. 1996).

The pH heterogeneity is more difficult to measure during 60% MVC than during 30% MVC exercise, although the pH differences at the end of exercise are similar (table 4.2 & 4.3). An obvious explanation is that less data points are available for a 60% MVC exercise. Moreover, a faster shifting of both P_i peaks limits proper analysis.

Distribution of peak areas of inorganic phosphate

A number of issues is relevant in relating the distribution of peak areas to the recruitment of motor units.

1. Johnson et al. (1973) and Polgar et al. (1973) investigated fiber type distribution and sizes in young, healthy, male subjects. In the superficial region of the TA they found a mean percentage of type I fibers of 73% and a mean cross section of type I and type II fibers of respectively $2.4*10^{-9}$ m^2 and $3.4*10^{-9}$ m^2. So, it is assumed that 64% of the TA cross section consists of type I fibers.

2. With increasing central neural drive, motor units are recruited according the size principle of Henneman (1981), whereby smaller type I motor units become active before larger type II motor units.
3. Vandenborne et al. (1995) showed that, in contrast to results of experiments on animals, human muscle with predominantly type I fibers had the same PCr content as muscle with predominantly type II fibers. Thus, it is assumed that type I fibers and type II fibers have the same PCr content in rest.
4. PCr consumption might be higher in type II fibers, because PCr also acts as a proton buffer (Zandt in 't, et al. 1999).
5. If local ischemia arises, a part of the inorganic phosphate is trapped by mitochondria and becomes invisible for ^{31}P NMR (Iotti et al. 1996). Especially already recruited motor units will "lose" some of their P_i signal. From the size principle it can be predicted that the peak area of type I fibers is most affected.

In the theoretical case that all motor units will be equally recruited during the whole isometric exercise, around or somewhat less than 64% of the PCr consumption is attributed to type I motor units (see above, issue 1, 3 & 4). If two P_i peaks can be discerned, one expects a somewhat larger left peak. If ischemia occurs, a decrease of P_i in all active fibers is expected, leading to a proportional decrease of both P_i peaks (issue 5). Possibly the uptake of P_i in the mitochondria is larger in type I fibers, because of a larger mitochondrial density in that fiber type. In that case a larger decrease of the left P_i peak is expected.

During sustained isometric exercise at 30 or 60% MVC, the prediction is more complicated because only a part of the motor units is recruited at the start of exercise. Fatigue and/or a deterioration of blood supply forces the system to recruit more motor units. Even at sustained isometric exercise at 30% MVC, deterioration of blood supply may occur, caused by an increase of intramuscular pressure (Crenshaw et al. 1997). Two P_i peaks appear as soon as most type I units and a part of the type II units are recruited (issue 2) and intracellular protons accumulate. A relatively larger left P_i peak and a smaller right P_i peak are expected. The difference between the peak areas depends on the number of type II motor units that is necessary at that time and on the level of ischemia (issue 5). The more type II units involved, the larger the right P_i peak; the more ischemia, the smaller the left P_i peak.

Our results (figure 4.2, 4.3 & 4.5C) nicely illustrate that an increase of the relative size of the right P_i peak coincides with a notable decrease of pH_{high} and pH_{low}. This is in particular clear during the last part of the exercise at 30% MVC, where (in most of our subjects) a striking increase of the right P_i peak occurs in coincidence with an accelerated decline of pH_{high}. All together this points to a deteriorating of blood supply combined with anaerobic glycolysis. This fits well to the mechanisms sketched above: the lower the blood flow, the less efficient

type I fiber contributions and thus the more type II motor units have to be recruited, according to the size principle, to maintain the expected force.

Yoshida & Watari (1994) showed the development of P_i peaks in one subject, during a progressive dynamic exercise at an intermediate frequency (0.8 Hz) of the m. biceps femoris. Their results (figure 4.5) shows that a substantial increase of the low pH peak area coincides with a shift of both P_i peaks towards the PCr peak (after 3-3½ minutes of exercise). Although their exercise is non-isometric, and thus the size principle is disputed (e.g. Howell et al. 1995), the development of P_i peak areas and positions suggests an orderly recruitment of motor units.

Conclusions

This study reveals pH heterogeneity in the TA during sustained isometric exercise below and above anaerobic threshold. The fact that the spatial pH distribution shows a declining gradient from lateral to medial within the TA (one subject) is attributed to intramuscular differences in blood supply. The pH dependency of relative sizes of both P_i peaks, in the temporally and spatially characterized ^{31}P NMR data, can be explained by the size principle of motor unit type-related orderly recruitment of motor units.

Acknowledgements

The indispensable technical support from Erik van den Boogert, Erik van den Bergh and Hans van Dijk is particularly acknowledged.

References

Achten E, van Cauteren M, Willem R, Luypaert R, Malaisse W, van Bosch G, Delanghe G, de Meirleir K & Osteaux M. ^{31}P-NMR spectroscopy and the metabolic properties of different muscle fibers. *J Appl Physiol* 68: 644-649, 1990.

Brown TR, Stoyanova R, Greenberg T, Srinivasan R & Murphy-Boesch J. NOE enhancements and T_1 relaxation times of phosphorylated metabolites in human calf muscle at 1.5 Tesla. *Magn Reson Med* 33: 417-421, 1995.

Crenshaw AG, Karlsson S, Gerdle B & Friden J. Differential responses in intramuscular pressure and EMG fatigue indicators during low- vs.high-level isometric contractions to fatigue. *Acta Physiol Scand* 160: 353-361, 1997.

DeGroot M, Massie BM, Boska M, Gober J, Miller RG & Weiner MW. Dissociation of [H^+] from fatigue in human muscle detected by high time resolution ^{31}P-NMR. *Muscle Nerve* 16: 91-98, 1993.

Enoka RM. Morphological features and activation patterns of motor units. *J Clin Neurophysiol* 12: 538-559, 1995.

Ernst RR & Anderson WA. Application of Fourier transform spectroscopy to magnetic resonance. *Rev Sci Instrum* 37: 93-102, 1966.

Essen B, Jansson E, Henriksson J, Taylor AW & Saltin B. Metabolic characteristics of fiber types in human skeletal muscle. *Acta Physiol Scand* 95: 153-165, 1975.

Henneman E. Recruitment of motor units: the size principle. In: *Motor Unit Types, Recruitment and Plasticity in Health and Disease*, edited by J. E. Desmedt. Basel: Karger, 1981, p. 26-60.

Howell JN, Fuglevand AJ, Walsch ML & Bigland-Ritchie B. Motor unit activity during isometric and concentric-eccentric contractions of the human first dorsal interosseus muscle. *J Neurophysiol* 74: 901-904, 1995.

Iotii S, Lodi R, Frassineti C, Zaniol P & Barbiroli B. In vivo assesment of mitochondrial functionality in human gastrocnemius muscle by ^{31}P MRS. *NMR in Biomed* 6: 248-253, 1993.

Iotti S, Lodi R, Gottardi G, Zaniol P & Barbiroli B. Inorganic phosphate is transported into mitochondria in the absence of ATP biosynthesis: an in vivo ^{31}P NMR study in the human skeletal muscle. *Biochem Bioph Res Co* 225: 191-194, 1996.

Johnson MA, Polgar J, Weightman D & Appleton D. Data on the distribution of fiber types in thirty-six human muscles. An autopsy study. *J Neurol Sci* 18: 111-29, 1973.

Kemp GJ & Radda GK. Quantitative interpretation of bioenergetic data from ^{31}P and ^{1}H magnetic resonance spectroscopic studies of skeletal muscle: an analytical review. *Magn Reson Quart* 10(1): 43-63, 1994.

Kent-Braun JA, Miller RG & Weiner MW. Phases of metabolism during progressive exercise to fatigue in human skeletal muscle. *J Appl Physiol* 75: 573-580, 1993.

Luyten PR, Bruntink G, Sloff FM, Vermeulen JWAH, van der Heijden JI, den Hollander JA & Heerschap A. Broadband proton decoupling in human ^{31}P NMR spectroscopy. *NMR Biomed* 1: 177-183, 1989.

Miller, RG, Carson PJ, Moussavi RS, Green A, Baker A, Boska MD & Weiner MW. Factors which influence alterations of phosphates and pH in exercising human skeletal muscle: measurement error, reproducibility, and effects of fasting, carbohydrate loading, and metabolic acidosis. *Muscle Nerve* 18: 60-67, 1995.

Mizuno M, Horn A, Secher NH & Quistorff B. Exercise-induced ^{31}P-NMR metabolic response on human wrist flexor muscles during partial neuromuscular blockade. *Am J Physiol* 267: R408-R414, 1994a.

Mizuno M, Secher NH & Quistroff B. ^{31}P-NMR spectroscopy, rsEMG and histochemical fiber types of human wrist flexor muscles. *J Appl Physiol* 76: 531-538, 1994b.

Park JH, Brown RL, Park CR, McCully K, Cohn M, Haselgrove J & Chance B. Functional pools of oxidative and glycolytic fibers in human muscle observed by ^{31}P magnetic resonance spectroscopy during exercise. *Proc Natl Acad Sci USA.* 84: 8976-8980, 1987.

Polgar J, Johnson MA, Weightman D & Appleton D. Data on fiber size in thirty-six human muscles. An autopsy study. *J Neurol Sci* 19: 307-318, 1973.

Quistorff B, Johansen L & Sahlin K. Absence of phosphocreatine resynthesis in human calf muscle during ischemic recovery. *Biochem J* 291: 681-686, 1993.

Sjøgaard G, Savard G & Juel C. Muscle blood flow during isometric activity and its relation to muscle fatigue. *Eur J Appl Physiol* 57: 327-335, 1988.

Thomsen C, Jensen KE & Henriksen O. In vivo measurements of T_1 relaxation times of ^{31}P-metabolites in human skeletal muscle. *Magn Reson Imaging* 7: 231-234, 1989.

Vandenborne K, McCully K, Kakihira H, Prammer M, Bolinger L, Detre JA, de Meirleir K, Walter G, Chance B & Leigh JS. Metabolic heterogeneity in human calf muscle during maximal exercise. *Proc Natl Acad Sci USA* 88: 5714-5718, 1991.

Vandenborne K, Walter G, Leigh JS & Goelman G. pH heterogeneity during exercise in localized spectra from single human muscles. *Am J Physiol* 265: C1332-C1339, 1993.

Vandenborne K, Walter G, Ploutz-Snyder L, Staron R, Fry A, de Meirleir K, Dudley GA & Leigh JS. Energy-rich phosphate in slow and fast human skeletal muscle. *Am J Physiol* 268: C869-C876, 1995.

Van der Veen JWC, de Beer R, Luyten PR & van Ormondt D. Accurate quantification of in vivo ^{31}P NMR signals using the variable projection method and prior knowledge. *Magn Reson Med* 6: 92-98, 1988.

Vieth E. Fitting piecewise linear regression functions to biological responses. *J Appl Physiol* 67: 390-396, 1989.

Yoshida T & Watari H. Exercise-induced splitting of the inorganic phosphate peak: investigation by time-resolved ^{31}P-nuclear magnetic resonance spectroscopy. *Eur J Appl Physiol Occup Physiol* 69: 465-73, 1994.

Yoshida T, Watari H & Tagawa K. Effects of active and passive recoveries on splitting of the inorganic phosphate peak determined by ^{31}P-nuclear magnetic resonance spectroscopy. *NMR Biomed* 9: 13-19, 1996.

Zandt HJA in 't, Oerlemans F, Wieringa B & Heerschap A. Effects of ischemia on skeletal muscle energy metabolism in mice lacking creatine kinase monitored by in vivo ^{31}P nuclear magnetic resonance spectroscopy. *NMR Biomed* 12: 327-334 1999.

5

An additional phase in PCr use during sustained isometric exercise at 30% MVC in the tibialis anterior muscle*

Abstract

The occurrence of an abrupt acceleration in phosphocreatine (PCr) hydrolysis in the tibial anterior muscle (TA) during the last part of a sustained isometric exercise at 30% maximal voluntary contraction (MVC) until fatigue, is demonstrated in 7 out of 8 healthy subjects by applying in vivo phosphor nuclear magnetic resonance (^{31}P NMR) spectroscopy at 1.5 T field strength. This additional third phase in PCr hydrolysis, is preceded by a common biphasic pattern (first fast then slow) in PCr use. The NMR spectra, as localized by a surface coil and improved by proton (^{1}H) irradiation, were collected at a time resolution of 16 s. Mean rates of PCr hydrolysis during exercise were –0.44 ± 0.19% s^{-1}, -0.07 ± 0.04% s^{-1}, and -0.29 ± 0.10% s^{-1} for the three successive phases. The increased rate of PCr hydrolysis, and also the loss of fine force control evident in the force records are consistent with increased involvement of large, fast-fatigable units later in the contraction.

Introduction

With increasing central neural drive, motor units are recruited according to the size principle, whereby smaller type I motor units become active before larger type II motor units (Henneman, 1981). Type I muscle fibers are fatigue resistant, well circulated and rely mostly on aerobic energy production. Type II muscle fibers are stronger, less vascularized and rely mostly on anaerobic energy production.

***Houtman CJ, Heerschap A, Zwarts MJ & Stegeman DF**. *NMR Biomed* 15: 270-277, 2002.

The size principle is especially demonstrated during isometric contractions of a relatively short duration (Milner-Brown et al. 1973). Although less documented, it is possible that the size principle is also valid during sustained submaximal isometric exercises, which start with the activation of a subpool of motor units (Fallentin et al. 1993). Because of the short duration of the contractions used to investigate the size principle, restrictions of blood flow are not an issue. During sustained isometric contractions, however, blood flow is only sufficient to maintain homeostasis at contraction levels below 10% MVC (Sjøgaard et al. 1988). To what extent the blood flow within the muscle changes during sustained isometric contraction will depend on the balance between the intramuscular pressure (increased by water accumulation (Crenshaw et al. 1997)) and the increased mean arterial pressure (Fallentin & Jørgensen, 1992).
A high demand and a compromised blood flow will fatigue already activated motor units in the course of a sustained isometric contraction. It is likely that (i) additional motor units will be recruited and (ii) the order of recruitment will be given by the size principle. In chapter 4 we related this to changes in tissue pH and inorganic phosphate (P_i) levels, assessed by ^{31}P NMR spectroscopy. In this chapter the hydrolysis of PCr in combination with the development of pH and the force recording during a fatiguing isometric exercise of the TA are studied. In these experiments, we discovered an unusual third phase in PCr consumption during the last part of the exercise.

Methods

Subjects

Six healthy men and two healthy women, aged 22-47 (mean: 30), participated in the study. All subjects were regularly engaged in low to moderate aerobic exercise. They were informed of the purpose of the experiments and gave their written consent. The ethics committee of the University Medical Center Nijmegen approved the protocol.

Exercise

Subjects had a supine position on the investigation table of the NMR system with their left leg slightly bent and supported with vacuum pillows. The angle of the ankle joint was 90 degrees and the left foot was fixed with straps in a pedal. Subjects were supplied with visual feedback of the force and they were verbally encouraged during exercise.

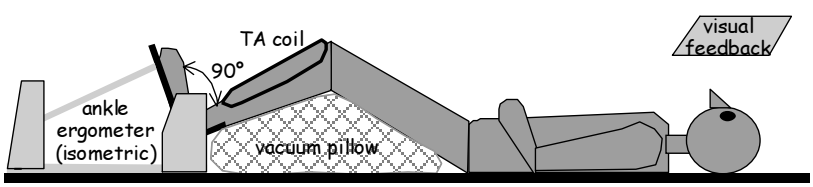

Figure 5.1: experimental set-up.

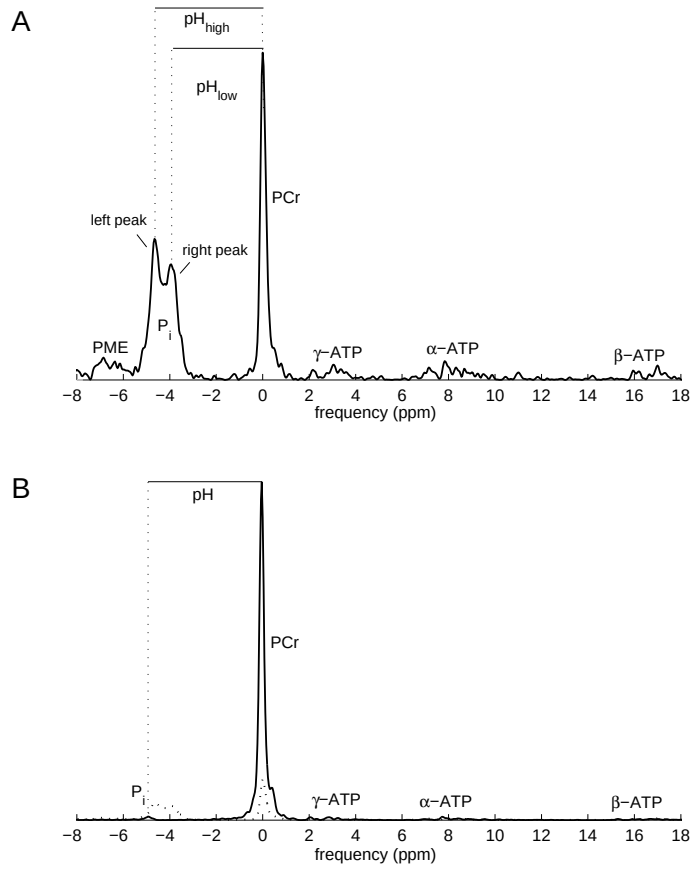

Figure 5.2: examples of phosphor nuclear magnetic resonance (^{31}P NMR) spectra of the tibialis anterior muscle (TA) of subject 6 (2 acquisitions, repetition time = 7 s) measured 510 s after the start of a 30% MVC exercise (A) and in rest 124 s before the start of exercise (B). Spectrum A is repeated in spectrum B as dotted line.

The ankle flexion/extension ergometer was home-built, and especially designed for use in the magnet, both applicable for dorsal and plantar ankle flexion. Force data were sampled at 100 Hz and digitally stored. To enable synchronisation afterwards, a trigger signal of the NMR system was co-registered with the force data. The NMR data points assigned to the midpoint of the two ^{31}P NMR excitation pulses, applied for each measurement.

The exercise consisted of an isometric dorsal ankle flexion until fatigue at 30% MVC. After offset correction, two MVC measurements were done, from which the maximum was taken. The feedback to the subjects consisted of an array of colored LED's: green in the middle, red at both sides. This area of green LED's had a width of 30 ± 3% MVC. The subject had to keep the force as stable as possible in the middle of the green area. If he or she could no longer reach the green area (despite encouragement), exercise was stopped. MVC measurements and exercise were separated by at least 30 minutes. ^{31}P NMR data were collected during rest (3 minutes), exercise (table 5.I) and recovery (15 minutes).

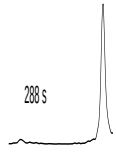

Nuclear Magnetic Resonance

All experiments were performed on a 1.5 T whole-body system (Magnetom SP, Siemens Medical Systems Inc. Erlangen, Germany). The RF surface coil was home-built and specially designed for the TA. It consisted of two concentric loops: one 25 cm x 8½ cm (tuned to the ^{1}H frequency) and one 20 cm x 3½ cm (tuned to the ^{31}P frequency). It was carefully placed over the TA and fixed with tape.

Before ^{31}P NMR data collection, a series of five transversal ^{1}H NMR images (gradient-recalled echo: echo time = 6 ms, repetition time = 70 ms, thickness = 10 mm, distance factor = 0.4) was made to confirm the correct placement of the surface coil.

The homogeneity of the static magnetic (B_0) field was adjusted using the proton signal from water, resulting in a peak width at half-height of ≤ 0.5 ppm. To overcome inhomogeneity of the radio frequency (B_1) field, an amplitude-modulated adiabatic 90° pulse (sincos) with a length of 2.56 ms, was used for excitation. The spectral excitation of this pulse was constant over a frequency range of 1000 Hz (≈ 39 ppm), which is sufficient to map all resonances present in skeletal ^{31}P NMR spectra.

For optimal signal to noise ratio per unit time we used a repetition time (TR) of seven seconds, according to Ernst & Anderson (1966) (TR = 1.25 T_1), and to Thomsen et al. (1989) (muscle T_1(PCr, P_i, ATP) ≤ 5.5 s), with T_1 as spin-lattice relaxation time. Two acquisitions were averaged per measurement. Including data storage, the time resolution became 16 s. The free induction decay (FID) was sampled during 512 ms at a sample frequency of 4 kHz and low-pass filtered at 5 kHz. During data collection, high-level (10 W) WALTZ4 proton irradiation was applied to decouple the ^{31}P-^{1}H spin coupling (Luyten et al. 1989). During the remaining time, low-level (0.6 W) WALTZ4 proton irradiation was applied to amplify the ^{31}P signal by the nuclear Overhauser effect (Brown et al. 1995).

Data analysis

To fit the data, the VARPRO data-analyzing method (van der Veen et al. 1988) was used. The first three data points of each FID were skipped, to avoid the broad baseline component arising from the tibia bone. Starting values for the peak position and line width of PCr and P_i were given. The peaks were assumed to have a Lorentzian line shape. To avoid improper use of prior knowledge, a broadened P_i peak was analyzed in two ways: as one peak and as two independent peaks, the latter indicating the existence of two different pH levels within the muscle (chapter 4). In the evaluation of the results the lower bound of the theoretical statistical errors, the Cramer-Rao (CR) lower bound, was used. The result with the lowest CR lower bound in the calculated parameters (peak area, line width and frequency) was accepted as the best fit. Sometimes, both results came up with CR lower bounds of more than 60% of the parameter values. Then the P_i peak was excluded from the fit procedure.

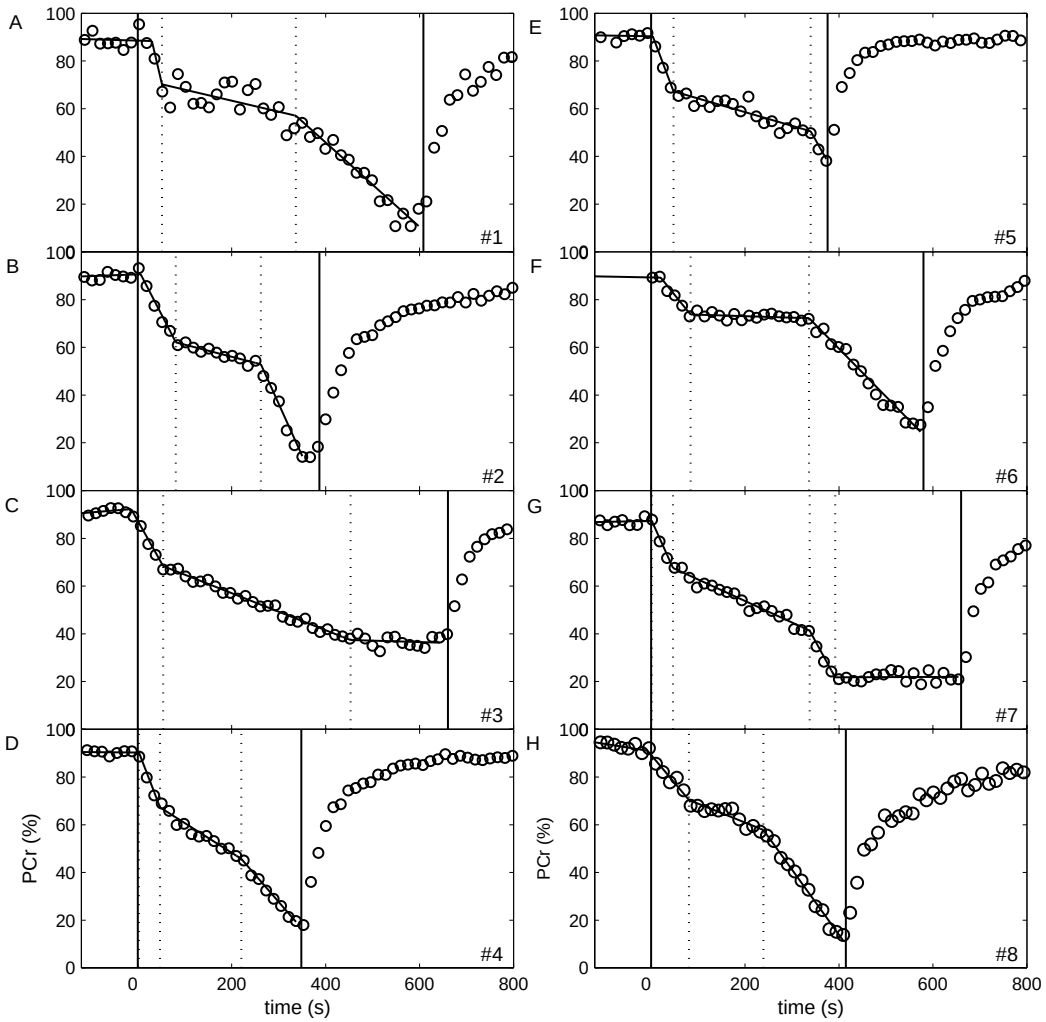

Figure 5.3: the results of phosphocreatine (PCr) analyses of all subjects. PCr peak area is expressed as percentage of the sum of PCr and inorganic phosphate (P_i) during rest, preceding the exercise. The solid vertical lines represent beginning and end of exercise; the broken vertical lines define the different phases in rate of PCr consumption. Fitted lines are included. Subject numbers are indicated in the bottom right corners.

Intracellular pH was calculated from the chemical shift of P_i based on the equation $pH = 6.75 + \log(\delta-3.26)/\log(5.75-\delta)$, were δ equals the chemical shift of the P_i peak in parts per million (ppm), relative to PCr.

The curves of PCr and pH, during rest and exercise, were fitted by piecewise linear regression. Continuity is assumed, except for the transition of one pH to two pH's and vice versa. The distribution of data points over the successive regression lines is optimized by minimizing the sum of the residuals of the lines. This method is described by Vieth (1989) for the combination of two regression lines. We extended this method to an arbitrary pre-set number of line pieces.

Table 5.1: Rates of PCr consumption

	dPCr/dt, % s^{-1}				
	I	II	III	III*	IV
Subject 1	-0,84	-0,05	-0,18		
Subject 2	-0,38	-0,05	-0,44		
Subject 3	-0,35	-0,08		-0,0058	
Subject 4	-0,51	-0,12	-0,23		
Subject 5	-0,52	-0,06	-0,35		
Subject 6	-0,24	-0,01	-0,20		
Subject 7	-0,44	-0,09	-0,36		0,0010
Subject 8	-0,23	-0,08	-0,27		
Means ± SD	-0,44 ± 0,19	-0,07 ± 0,04	-0,29 ± 0,10		

phosphocreatine (PCr) is expressed as percentage of the sum of PCr and inorganic phosphate (P_i) at rest, preceding exercise. The successive phases in PCr hydrolyses are labeled as I, II, III, IV.

Results

Exercise

The range of maximal voluntary contraction force of the volunteers was 207-317 N (mean: 271 N). The duration of the 30% MVC exercises was 348-660 s (mean: 504 s).

^{31}P NMR spectroscopy data

Figure 5.1 shows examples of ^{31}P NMR spectra measured before and during exercise with peaks for ATP, PCr and P_i. The P_i peak during exercise is doubled, which points to two pH compartments within the muscle.

The decrease of PCr during exercise was tri- (or four)phasic in all our eight subjects (figure 5.2). The P_i peak doubled during exercise, in spectra of all eight subjects, which corresponds to two different, but simultaneous occurring pH levels within the muscle (figure 5.3). Compared to each other, the mean PCr consumption rates, measured as the slopes of the regression lines, can be classified as high, low and moderate for respectively phases I, II and III (see table 5.I).

Phase I coincidences with a transient increase of pH (figure 5.3). During phase II and III two P_i peaks occur. The pH levels derived from the left (low-field) and right (high-field) P_i peaks are named pH_{high} and pH_{low}, respectively. They reflect different rates of proton production: successively a low and a high rate for pH_{high} and a continuously moderate rate for pH_{low} (figure 5.3). In the force recording, fluctuations are observed which increase towards the end of exercise (figure 5.4).

One of the subjects (#7) shows the similar triphasic pattern in PCr changes, except for an extra fourth phase during which PCr stays at a very low but constant level (figure 5.2G). As for the other subjects, first pH shows a transient increase, subsequently followed by a

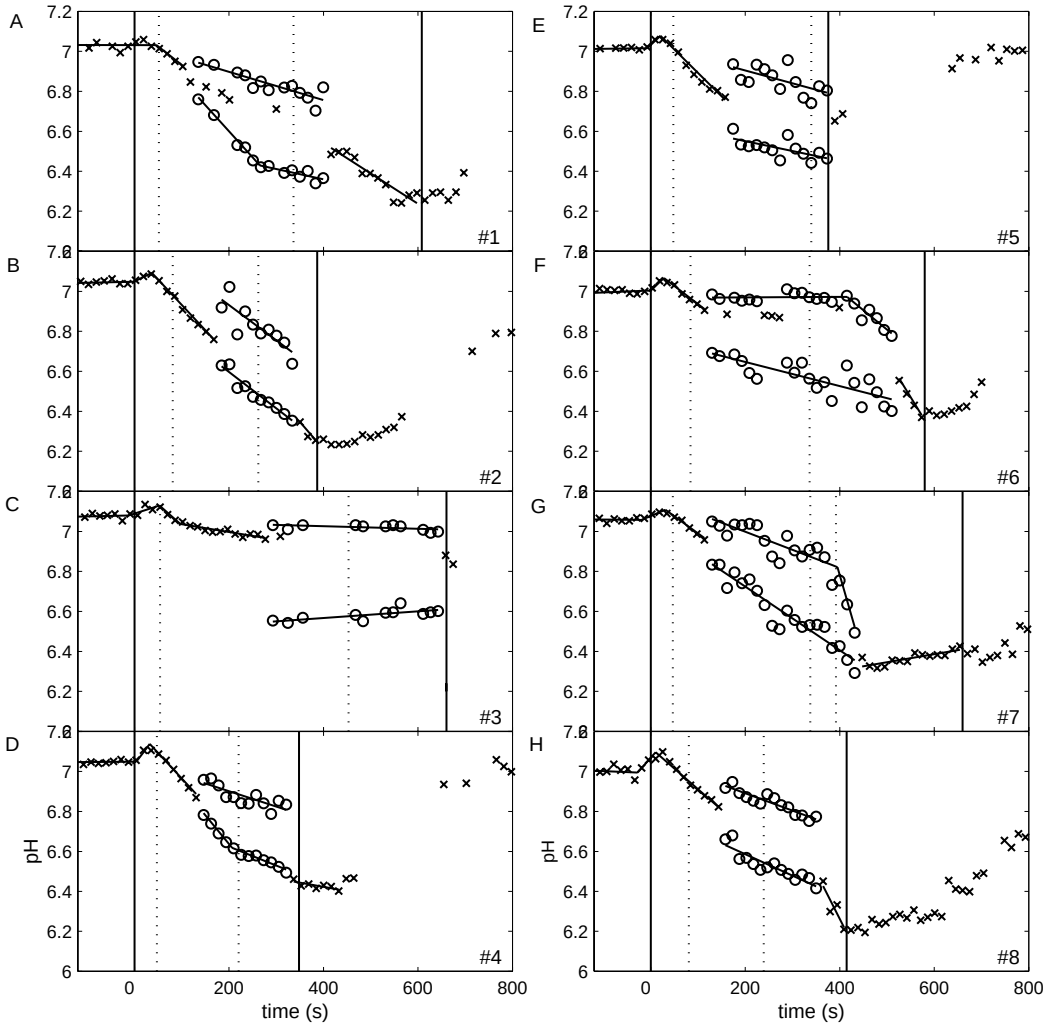

Figure 5.4: results of pH analyses of all subjects. If P_i peaks are recognized, (thus two pH values can be derived,) the symbol o is used instead of the symbol x. The solid vertical lines represent beginning and end of exercise; the broken vertical lines define the different phases in rate of PCr consumption. Fitted lines are included. Subject numbers are indicated in the bottom right corners.

splitting in pH_{high} and pH_{low} and an accelerated decrease of pH_{high} , by which both pH's merges into one low pH level. Next, during the extra fourth phase, pH slightly recovers (figure 5.3G). Strikingly large fluctuations are observed in the force recording during the last minutes of exercise in this subject (figure 5.4G).

The results from subject 3 are also deviating from a clear-cut common triphasic pattern. A striking long phase II (figure 5.2C) is observed, with more or less the same characteristics as described above. The last phase (III*), however, is different: PCr stays at a constant medium level and pH levels remain unchanged until the end of exercise (figure 5.3C). In this subject the force fluctuation increase gradually until the end of exercise (figure 5.4C). Because of

the different character of this last phase compared to the seven other subjects, it is placed apart as "III*" in table 5.I.

Discussion

Triphasic pattern in PCr hydrolysis

This study reveals a triphasic pattern in PCr hydrolyses in the TA during a sustained isometric exercise at a level (i) below the aerobic threshold of the muscle (around 40–50% MVC (Kent-Braun et al. 1993)), (ii) where the mean arterial pressure initially is evidently higher than the intra muscular pressure (Sjøgaard et al. 1988), and (iii) where only a part of the motor unit pool initially is recruited (Feiereisen et al. 1997). Muscle fibers of newly recruited motor units will initially rely on the most rapid energy supplier (and proton consumer) PCr. The first 1-1½ minute of exercise (phase I) is therefore characterized by a rapid decrease of PCr accompanied with a transient increase of the pH (DeGroot et al. 1993). In the following phase II, PCr consumption slows down as sign of an increased participation of glycolysis and oxidative metabolism, and of no or only little recruitment of extra motor units. The occurrence of two distinct pH levels during this phase is most likely attributed to the contributions of type I (pH_{high}) and type II (pH_{low}) motor units (chapter 4, Vandenborne et al. 1993).

The recruitment of additional motor units, in the course of a sustained isometric exercise at low-medium levels, follows probably the size principle (Fallentin et al. 1993). This means that motor units are activated in an orderly sequence, starting with the smallest (type I) ones (Henneman, 1981). During the last phase (III), it seems likely that large type II motor units are recruited, while the motor units that were recruited first start to fatigue. Both the increased rate of PCr hydrolysis, and the loss of fine force control evident in the force records are consistent with such an increased involvement of large, type II motor units later in the contraction. The analysis of the peak areas of the P_i peak (ascribed to respectively type I and type II muscle fibers) leads to the same interpretation (chapter 4). Probably deterioration of blood supply plays a role, since the phase II –III transition happens most of the times rather abrupt. The anatomical position of the TA may favour this process. Together with the extensor digitorum longus muscle and the hallucis longus muscle, the TA is situated in the anterior compartment. The tibia bone, the interosseus membrane and the anterior intermuscular septum enclose this compartment. This stiff surrounding may enhance the increase of the intramuscular pressure during sustained exercise by water accumulation (Crenshaw et al. 1997), and therefore enhance the possibility of a deterioration of the microcirculation.

The accelerated decrease of pH_{high} in the course of phase III might be caused by a shift to an anaerobic state of the type I fibers. This points as well to a deteriorated blood supply

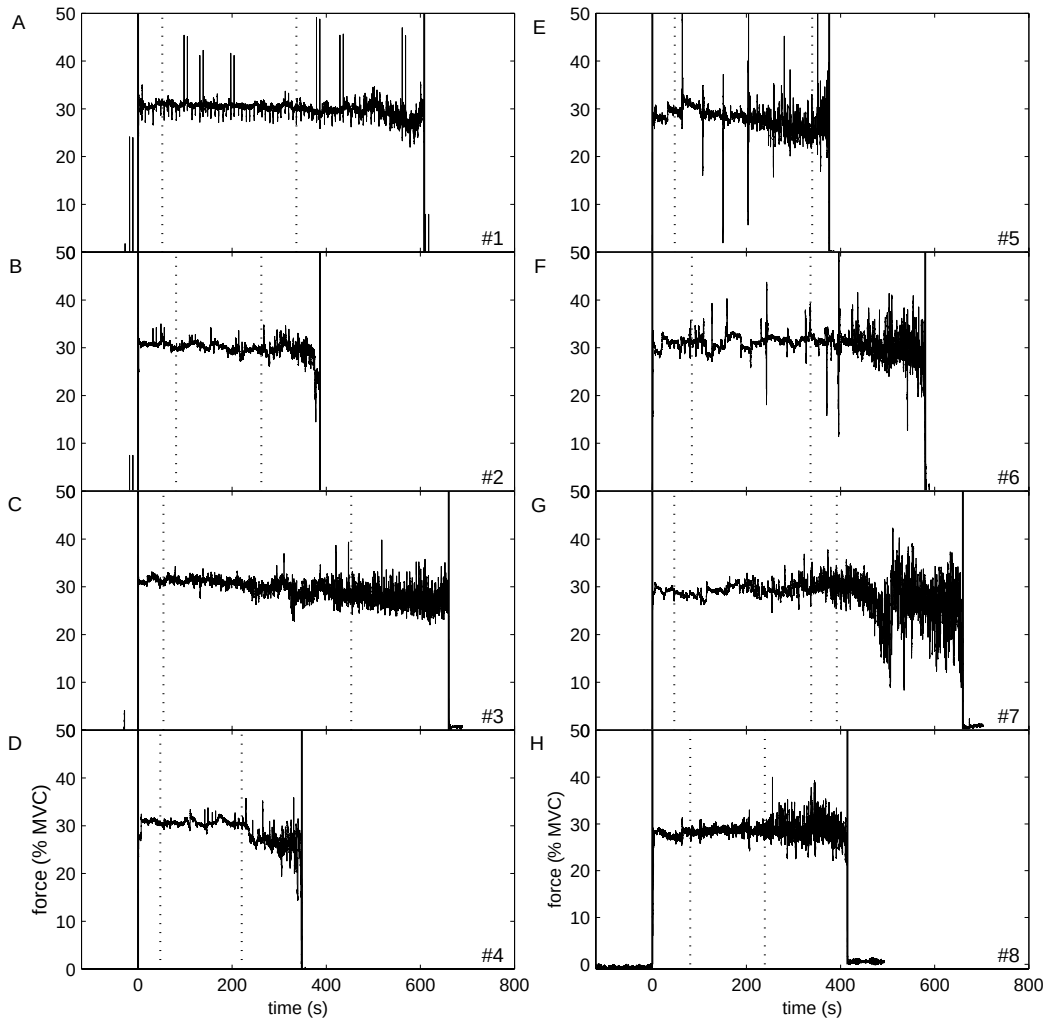

Figure 5.5: the exerted force expressed as percentage of maximal voluntary contraction for all subjects. The solid vertical lines represent beginning and end of exercise; the broken vertical lines define the different phases in rate of PCr consumption. Subject numbers are indicated in the bottom right corners.

during the last part of the exercise. The fact that (if our suggestion is true) ischemia occurs earlier in type II fibers than in type I fibers, can be explained by the better vascularization in the latter ones.

Biphasic pattern in PCr hydrolysis

An abrupt acceleration in PCr hydrolysis followed by a decrease of pH_{high} towards the end of exercise (phase III) has not been described before. A biphasic pattern of PCr decrease is a common observation during cyclic exercises at a constant load (i.e. Mattei et al. 1997; Molé et al. 1985; Taylor et al. 1983; Vandenborne et al. 1991; Yoshida & Watari, 1993). An acceleration of PCr hydrolyze late in the exercise can not be expected if all motor units would have been recruited from the beginning, as in exercises at maximal contraction rate

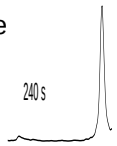

(Vandenborne et al. 1991). In exercise at a low duty cycle, the blood circulation is stimulated, making the recruitment of extra motor units late in the exercise probably less necessary. Another factor can be that the exercises described in (Mattei et al. 1997; Molé et al. 1985; Taylor et al. 1983; Vandenborne et al. 1991; Yoshida & Watari, 1993) have been executed during a fixed period of time and not until fatigue.

The TA was previously monitored by Vestergaard-Poulsen et al. (1995) using ^{31}P NMR spectroscopy in isometric exercises at 5, 10 and 30% MVC until exhaustion. The results of one of their subjects performing at 30% MVC showed a biphasic hydrolysis of PCr similar to results obtained by cyclic exercises (i.e. Mattei et al. 1997; Vandenborne et al. 1991). However, the mean endurance time of their five subjects is 264 ± 244 s, which is much lower than the mean endurance time of our subjects (504 s, range 348-660 s, n=8). This could possibly point to a lower grade of exhaustion in their subjects. They also showed (in their figure 5.2) the hydrolysis of the same subject performing at 10% MVC, with a duration of about 800 s. After a rapid initial decrease (20 s), the hydrolysis of PCr remains constant during 5 minutes and is then followed by a continuous decrease during the last 7 minutes of exercise. This approaches a triphasic pattern.

Deviating pattern in PCr hydrolysis

The general triphasic pattern is not seen in all our subjects. In subject 3 (figure 5.2C, 5.3C & 5.4C) PCr and the pH levels stabilize until the end of exercise. This points to an unchanged supply of glycogen/glucose and oxygen and an unchanged efflux of protons, which is only conceivable when the microcirculation is maintained. Obviously, extra recruitment of (larger) motor units takes not place in this case. If indeed only a part of the motor unit pool is activated until the end of exercise, and the mean muscle PCr value stays at a medium level, than the PCr will be relatively low in the active fibres during these last minutes of exercise.

Another subject (#7, figure 5.2G, 5.3G & 5.4G) shows the possibility to continue exercise with very low PCr and pH levels. A study of Zwarts & Arendt-Nielsen (1988) showed that the average muscle fibre conduction velocity, related to fatigue induced changes, improved during maximum exercise when force declined below 30–50% MVC. They explained it by assuming a restart of the occluded circulation. Due to the fluctuations of the force profile in our subject (#7) during the last minutes of exercise, the circulation might be improved in the short phases of low force, when the intramuscular pressure is smaller than the blood pressure. Taylor et al. (1986) described one subject who continued cyclic finger flexion for ten minutes, while pH is about 6.0 and PCr is only 10% of its resting level. It should be concluded from that case and from our present observation that very low pH and PCr values often coincide with exhaustion, but cannot be considered as its inevitable cause.

Conclusions

A third phase of increased PCr utilisation in the TA during sustained 30% MVC is observed in seven of eight subjects. This phase is characterised by an additional recruitment of type II motor units, when already recruited motor units are fatigued. A deterioration of the microcirculation in the muscle, enforced by the stiff compartment in which the TA is situated, may play a role in this process.

Acknowledgements

The indispensable technical support from Erik van den Boogert and Hans van Dijk is particularly acknowledged.

References

Brown TR, Stoyanova R, Greenberg T, Srinivasan R & Murphy-Boesch J. NOE enhancements and T_1 relaxation times of phosphorylated metabolites in human calf muscle at 1.5 Tesla. *Magn Reson Med* 33: 417-421, 1995.

Crenshaw AG, Karlsson S, Gerdle B & Friden J. Differential responses in intramuscular pressure and EMG fatigue indicators during low- vs.high-level isometric contractions to fatigue. *Acta Physiol Scand* 160: 353-361, 1997.

DeGroot M, Massie BM, Boska M, Gober J, Miller RG & Weiner MW. Dissociation of [H^+] from fatigue in human muscle detected by high time resolution ^{31}P-NMR. *Muscle Nerve* 16: 91-98, 1993.

Ernst RR & Anderson WA. Application of Fourier transform spectroscopy to magnetic resonance. *Rev Sci Instrum* 37: 93-102, 1966.

Fallentin N & Jørgensen K. Blood pressure response to low level static contractions. *Eur J Appl Physiol* 64: 455-459, 1992.

Fallentin N, Jorgensen K & Simonsen EB. Motor unit recruitment during prolonged isometric contractions. *Eur J Appl Physiol Occup Physiol* 67: 335-341, 1993.

Feiereisen P, Duchateau J & Hainaut K Motor unit recruitment order during voluntary and electrically induced contractions in the tibialis anterior. *Exp Brain Res* 114:117-123, 1997.

Henneman E. Recruitment of motor units: the size principle. In: *Motor Unit Types, Recruitment and Plasticity in Health and Disease*, edited by J. E. Desmedt. Basel: Karger, 1981, p. 26-60.

Kent-Braun JA, Miller RG & Weiner MW. Phases of metabolism during progressive exercise to fatigue in human skeletal muscle. *J Appl Physiol* 75: 573-580, 1993.

Luyten PR, Bruntink G, Sloff FM, Vermeulen JWAH, van der Heijden JI, den Hollander JA & Heerschap A. Broadband proton decoupling in human ^{31}P NMR spectroscopy. *NMR Biomed* 1: 177-183, 1989.

Mattei JP, Bendahan D, Erkintalo M, Harle JR, Weiller PJ, Roux H & Cozzone PJ. P-31 magnetic resonance spectroscopy demonstrates unaltered muscle energy utilization in polymyalgia rheumatica. *Arthritis Rheum* 40: 1817-1822, 1997.

Milner-Brown HS, Stein RB & Yemm R. The orderly recruitment of motor units during voluntary isometric contractions. *J Physiol Lond* 230: 359-370, 1973.

Molé PA, Coulson RL, Caton JR, Nichols BG & Barstow TJ. In vivo ^{31}P -NMR in human muscle: transient patterns with exercise. *J Appl Physiol* 59: 101-104, 1985.

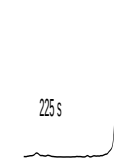

Sjøgaard G, Savard G & Juel C. Muscle blood flow during isometric activity and its relation to muscle fatigue. *Eur J Appl Physiol* 57: 327-335, 1988.

Taylor DJ, Bore PJ, Styles P, Gadian DG & Radda GK. Bioenergetics of intact human muscle. A ^{31}P nuclear magnetic resonance study. *Mol Biol Med* 1: 77-94, 1983.

Taylor DJ, Styles P, Matthews PM, Arnold DA, Gadian DG, Bore P & Radda GK. Energetics of human muscle: exercise-induced ATP depletion. *Magn Reson Med* 3: 44-54, 1986.

Thomsen C, Jensen KE & Henriksen O. In vivo measurements of T_1 relaxation times of ^{31}P-metabolites in human skeletal muscle. *Magn Reson Imaging* 7: 231-234, 1989.

Vandenborne K, McCully K, Kakihira H, Prammer M, Bolinger L, Detre JA, de Meirleir K, Walter G, Chance B & Leigh JS. Metabolic heterogeneity in human calf muscle during maximal exercise. *Proc Natl Acad Sci USA* 88: 5714-5718, 1991.

Vandenborne K, Walter G, Leigh JS & Goelman G. pH heterogeneity during exercise in localized spectra from single human muscles. *Am J Physiol* 265: C1332-C1339, 1993.

Van der Veen JWC, de Beer R, Luyten PR & van Ormondt D. Accurate quantification of in vivo ^{31}P NMR signals using the variable projection method and prior knowledge. *Magn Reson Med* 6: 92-98, 1988.

Vestergaard-Poulsen P, Thomsen C, Sinkjær T & Henriksen O. Simultaneous ^{31}P NMR spectroscopy and EMG in exercising and recovering human skeletal muscle: a correlation study. *J Appl Physiol* 79: 1469-1478, 1995.

Vieth E. Fitting piecewise linear regression functions to biological responses. *J Appl Physiol* 67: 390-396, 1989.

Yoshida T, Watari H. ^{31}P -nuclear magnetic resonance spectroscopy study of the time course of energy metabolism during exercise and recovery. *Eur J Appl Physiol Occup Physiol* 66: 494-499, 1993.

Zwarts MJ & Arendt-Nielsen L. The influence of force and circulation on average muscle fibre conduction velocity during local muscle fatigue. *Eur J Appl Physiol* 58: 278-283, 1988.

6

Changes in muscle fiber conduction velocity indicate recruitment of distinct motor unit populations*

Abstract

To obtain more insight into the changes in mean muscle fiber conduction velocity (MFCV) during sustained isometric exercise at relatively low contraction levels, we performed an in-depth study of the human tibialis anterior (TA) muscle using multichannel surface electromyography (EMG). The results show an increase in MFCV after an initial decrease of MFCV at 30 or 40% maximum voluntary contraction (MVC) in all of the five subjects studied. With a peak velocity (PV) analysis we calculated the distribution of conduction velocities of action potentials in the bipolar EMG signal. It shows two populations of PVs occurring simultaneously halfway through the exercise. The MFCV pattern implies the recruitment of two different populations of motor units. Due to the lowering of MFCV of the first activated population of motor units, the newly recruited second population of motor units becomes visible. It is most likely that the MFCV pattern can be ascribed to the fatiguing of already recruited predominantly type I motor units, followed by the recruitment of fresh, predominantly type II, motor units.

Introduction

A decrease of the MFCV measured with surface EMG during sustained isometric exercise at relatively high contraction levels (40-100% MVC) is often reported (i.e. Arendt-Nielsen & Mills, 1988; Krogh-Lund, 1993; Masuda et al. 1999; Zwarts et al. 1987). During sustained isometric exercises at relatively low contraction levels (10-30% MVC), the MFCV appears to

***Houtman CJ, Stegeman DF, Van Dijk JP, and Zwarts MJ**. *J Appl Physiol* 95: 1045-1054, 2003.

remain constant or even to increase during the exercise (Arendt-Nielsen et al. 1989; Krogh-Lund, 1993; Krogh-Lund & Jørgensen, 1991, 1992 & 1993; Zwarts & Arendt-Nielsen, 1988). With increasing central neural drive, motor units are expected to be recruited according to the size principle, whereby smaller motor units become active before larger motor units (Henneman, 1981). This motor unit size dependent recruitment order can be thought to go in parallel with orderly recruitment of type I and type II motor units, the latter in general being larger (Polgar et al. 1973). For example in voluntary isometric ramp contractions of the TA, motor units are recruited in order of increasing size (Feiereisen et al, 1997). Also, during sustained low level contractions, inducing local muscle fatigue, motor units seem to be recruited according to the size principle (Fallentin et al, 1993). For the TA, this was supported by the phosphor nuclear magnetic resonance (^{31}P NMR) spectroscopy studies of Houtman et al. (chapter 4 and 5). These studies show a striking increase of metabolic activity most probably of type II fibers in the second half of a sustained isometric exercise at 30% MVC, while the metabolic activity of these fibers was relatively low in the first half. It is explained by an additional recruitment of type II motor units towards the end of exercise. Besides the orderly recruitment of motor units, larger motor units consist of muscle fibers with (initially) higher propagation velocities than smaller motor units (Andreassen & Arendt-Nielsen, 1987; Gantchev et al. 1992). So, two processes can be expected to influence the MFCV in opposite directions: fatigue of already recruited motor units leads to a MFCV decrease, whereas recruitment of fresh large units leads to an increase of the MFCV.

If the recruitment of motor units is as orderly as suggested by our NMR spectroscopy studies (chapter 4 and 5), also a clear-cut pattern in the MFCV development of the TA could be expected. Namely, an MFCV decrease in the first part of a sustained 30% MVC exercise, followed by an increase of MFCV and probably by a decrease again towards the end of exercise.

The MFCV consist of the contributions of different (motor unit) action potentials in the surface EMG. Lange et al. (2002) showed that the spread in MFCV followed a normal (Gaussian) distribution in the m. biceps brachii at different contraction levels (0-100% MVC) of short duration (1,5 s). Fatigue of motor units and a shift in motor unit recruitment from type I units at the start of exercise to type II units towards the end should be reflected in a spread of MFCV. We also developed a method to calculate the conduction velocities of action potentials in the bipolar surface EMG, to add information about the composition of the MFCV during long lasting exercises.

For proper analyses the correct placement of surface electrodes is very important (Hogrel et al. 1998). Therefore we applied a multichannel surface EMG method, which enables the choice of the best quality signals post hoc.

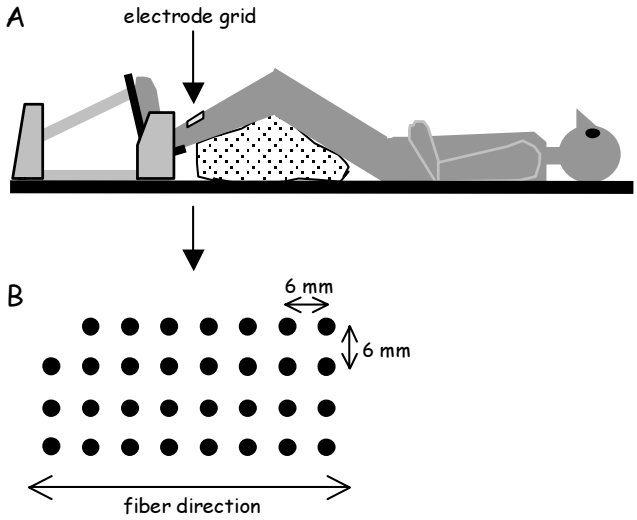

Figure 6.1A: experimental set up. B: schematic presentation of the electrode matrix.

Methods

Subjects

Five healthy subjects, aged 24-37, participated in the study (table 6.1). All subjects were regularly engaged in moderate to high aerobic exercise. They were informed of the purpose of the experiments and gave their written consent. The ethics committee of the University Medical Center Nijmegen approved the protocol.

Exercise

Subjects had a supine position on the investigation table with their left leg slightly bent and supported with a vacuum pillow (figure 6.1A). The angle between the left lower leg and the left foot was 90 degrees, and the foot was secured to a foot plate by using Velcro straps. Subjects were supplied with visual feedback of the force and were verbally encouraged during exercise. The ankle ergometer system used was home built and was applicable both for dorsal and plantar ankle flexion. The force signal was digitally stored, together with an externally generated time code signal, at a sampling rate of 100 Hz.

After offset correction for the force, two MVC measurements were done, from which the maximum was used to calculate the force level (table 6.1). MVC measurements and exercise were separated by at least 10 minutes. The subject had to maintain the desired force level, within a bandwidth of ±3% MVC. When he or she could no longer meet this condition, despite encouragement, exercise was stopped. The exercise consisted of an isometric dorsal ankle flexion until fatigue at 30% MVC in all subjects, and, based on their results at this 30% MVC level, also at 40% MVC in subject #3 and #5. Measurements were separated by 2-14 days.

Table 6.1: Subject and force parameters

	Sex	Age, yr	100% MVC prior to exercise, N	Duration of exercise, s	Force, %
Subject 1	m	28	319	409	30
Subject 2	m	29	336	316	30
Subject 3	f	24	225	722	30
			228	405	40
Subject 4	f	31	177	484	30
Subject 5	m	37	243	510	30
			236	298	40

MVC, maximum voluntary contraction; m, male; f, female.

Surface EMG

For skin surface recordings, 31 gold-coated electrodes, with a diameter of 1.52 mm were used (type 'serrated contact'; Farnell, Inc., (Blok et al. 1998)). They were fixed into an electrode holder with interelectrode distances of 6 mm, in a 4 x 8 configuration (figure 6.1B), with one empty corner. First, the skin was shaved and electrode cream was rubbed into the skin. After the superfluous cream was carefully removed from the skin surface, the holder was placed with the four columns of 7-8 electrodes parallel to the muscle fiber direction on the distal part of the TA, where the muscle fibers are situated parallel to the skin surface. Additionally, a 10 mm diameter gold-coated conventional EEG electrode filled with electrode gel was attached to the knee as common reference allowing so-called monopolar recording from all 31 "active" electrodes. A ground electrode was attached to the ankle.

The monopolar signals were amplified, band pass filtered (3-800 Hz), and simultaneously analog-to-digital converted (16 bits with a resolution of 0.5 μV/bit at a rate of 4000 samples/s/channel) using a multichannel amplifier system (Mark 6, Biosemi Inc., Amsterdam, The Netherlands). A second gold-coated EEG electrode placed on the upper part of the TA acted as a sense electrode allowing the use of the "driven right leg" principle for common mode rejection improvement (Metting van Rijn et al. 1990). Data were stored for off-line analysis on the hard disk of a 180 MHz Pentium PC. To synchronize the data with the force recording afterward, the externally generated time code signal, was also registered on one of the amplifier's channels.

Time series analysis of surface EMG signal

Bipolar signals were derived by subtracting two monopolar signals from electrodes at consecutive positions along the four columns (fiber direction). The column with the overall highest amplitudes and the shortest durations of the individual peaks was chosen for further analysis. The bipolar surface EMG signals of this column were baseline-corrected and divided in successive epochs of 2.048 seconds. For each of these epochs the following

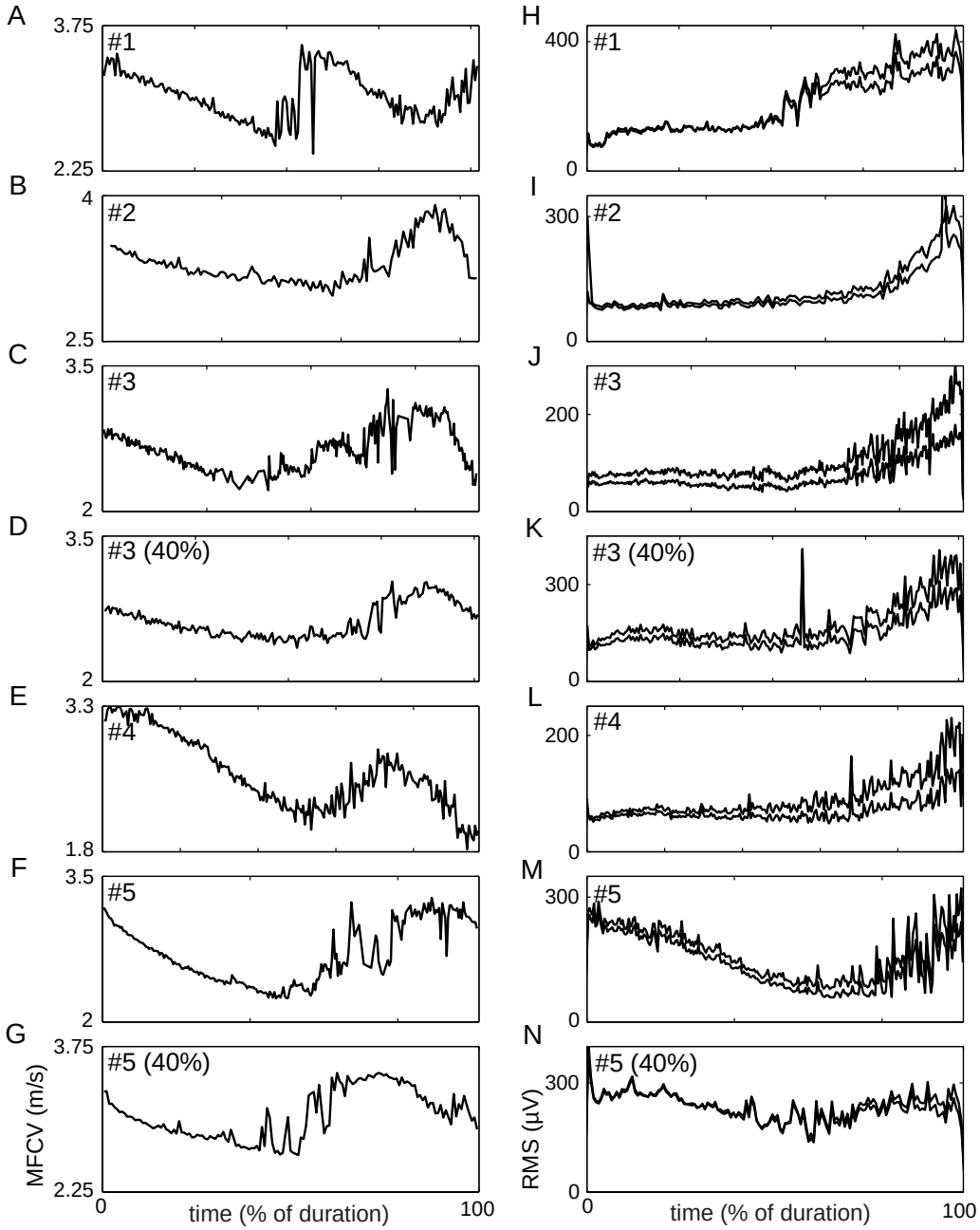

Figure 6.2A-G: the mean muscle fiber conduction velocity (MFCV) for the seven experiments (five subjects, two levels: subject numbers and force levels of 40% maximum voluntary contraction (MVC) are indicated at top left). The x-axes are rescaled to the duration of the exercise. The range of the y-axis is 1.5 m/s in all cases but differs in offset. H-N: the root mean square (RMS) amplitude development of the two consecutive signals used for MFCV determination for the same seven experiments. Subject numbers and force levels of 40% MVC are indicated at top left. The y-axes are optimized for each amplitude profile. The x-axes are rescaled to the duration of the exercise.

parameters were calculated, the root mean square (RMS) voltage (as a measure of the mean amplitude), the median frequency (Fmed), and the MFCV using the phase difference

method (see below). The MFCV calculations were based on two consecutive bipolar signal pairs along the column (over a distance of 6 mm in the fiber direction). Signal pairs showing a maximum cross correlation coefficient less than 0.9 were excluded from the MFCV calculations. MFCV values tend to increase, when observed close to the motor endplate or close to the muscle tendon transition (Hogrel et al. 1998). Therefore, the pair of consecutive bipolar signals with the overall lowest MFCV values was selected for presentation and also for the subsequent analysis of velocities of individual peaks.

Velocity analysis of individual peaks

The PV method calculates the conduction velocities of action potentials in the surface EMG signal, which gives additional information about the composition of the MFCV. For each of the before mentioned 2s epochs, the peaks were selected and then the associated delay for each peak to travel between the two adjacent electrodes (a known distance apart) was estimated.

Peak selection

The selected pair of two consecutive signals was given the polarity whereby the largest (depolarization) action potentials were oriented upwards. These action potentials were called peaks. Each peak larger than 30 µV was detected. This threshold value was based on the noise level of the bipolar surface EMG signal in rest preceding exercise. The amplitude and timing of each peak were stored. Around the maximum of each peak, a square window of 16 ms was placed. Such a window was large enough to contain the whole peak, unless peaks were very broadened. In that case the window was widened to 32 ms. The Fmed value of the associated 2s signal segment was used as an objective criterion for window width. The window was doubled if Fmed was less than 40 Hz, because the frequency content of the surface EMG signal decreases as the peak width broadens. In this study Fmed was only used for this purpose. If the distance between two consecutive peaks was smaller than half of the window size, the largest peak would be counted twice, and if a small peak was located on the flank of another peak, the flank would be selected as maximum instead of the peak. Therefore, double counted peaks and peaks with their maximum values appearing close (3 samples) to the time border of a peak window were excluded.

Velocity calculation

First, each of the 16 or 32 ms peak signals were weighted with a Hanning window. The MFCV previously determined for the 2s signal segment was used as a first estimate of the delay between two corresponding peaks detected at the two adjacent electrode pairs. The

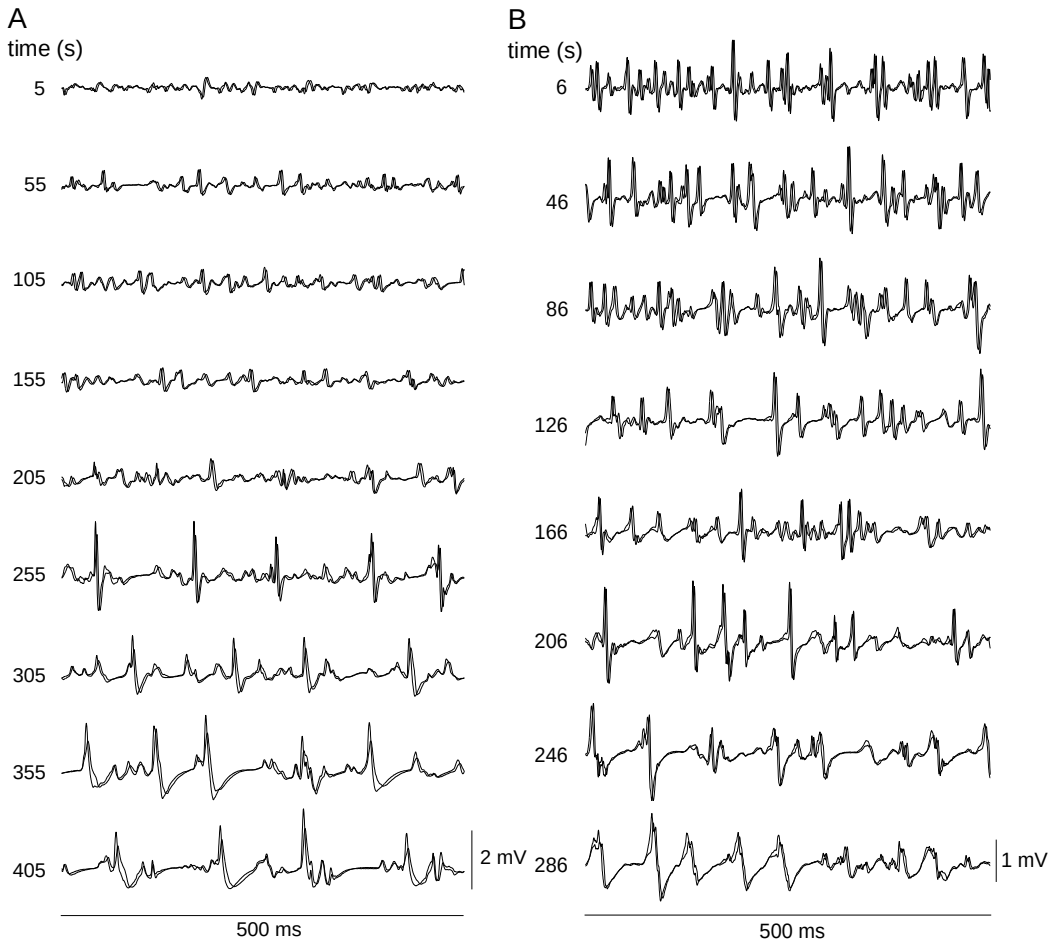

Figure 6.3A: ensemble of bipolar surface electromyogram (EMG) signals, each with a duration of 500 ms from subject 1, who performed an exercise at 30% MVC and started at indicated times (t) of 5, 55, 105, 155, 205, 255, 305, 355, and 405 s. B: ensemble of bipolar surface EMG signals, each with a duration of 500 ms from subject 5, who performed an exercise at 40% MVC and started at indicated t = 6, 46, 86, 126, 166, 206, 246, and 286 s.

peaks were pre-aligned according to this MFCV based delay. For a further estimate of the delay the phase difference method was used (see below).

MFCV and PV: phase difference method

The method is based on a property of the Fourier transform: assuming a constant time delay T between two identical signals, the phase difference φ between the Fourier transformed signals will be proportional to the frequency. This property can be used to align waveforms (McGill & Dorfman, 1984) and/or to determine the time delay with, in principle, an unlimited temporal resolution. The steps for this procedure were as follows:

For the two baseline-corrected bipolar signal segments (detected at the two adjacent electrode pairs) the cross correlation was calculated. The shift at which the maximum cross correlation occurs is a rough estimate in sample point resolution of the delay. The pre

alignment of the signals with this delay, avoids >2π phase differences in the next step. Both, now roughly aligned, signals were Fourier transformed. This results in a description of the data in phase and power as functions of frequency. We assumed that the signals are identical except for a delay T. We calculated this delay by fitting a straight line through the phase difference between both signals φ as function of frequency ω (φ= T ω). Frequencies at which almost no power is measured, overcontribute to this phase difference function. Therefore the power distributions were used as a weighting factor in the linear regression. At each frequency value, the smallest of the two power functions was taken. The least square error method was used as a fitting procedure. The resultant delay used to calculate MFCV or PV was the sum of the (initial) time-domain delay (limited by the sampling resolution) and the finely estimated delay (determined from the phase-based method).
MFCV was calculated using 2.048 s of two bipolar surface EMG signals from the adjacent electrode pairs. PV values were estimated using two pre-aligned filtered bipolar surface EMG signals of 16 or 32 ms from adjacent electrode pairs (containing roughly one peak).

Results

Exercise

MVC force ranged between 177 and 336 N. The duration of the exercises varied between 298 and 722 s (table 6.1).

Two periods of MFCV decrease

From the left column of figure 6.2 it can be concluded that all five subjects show two different periods of MFCV decrease in the course of the exercise both for 30 and 40% MVC (figure 6.2A-G). After an initial decrease, MFCV starts to fluctuate. The mean trend of MFCV then increases. This increase is accompanied or followed by an increase of amplitude and by gradually increasing fluctuations in amplitude (figure 6.2H-N). The MFCV then starts to decrease again towards the end of the exercise, although sometimes a final increase in the MFCV profile during the last minute of exercise can be observed (figure 6.2A&G). Only subject #5 (figure 6.2M&N) does not fully follow the described surface EMG amplitude profile (initially almost constant and increased in the second half of the exercise). The pattern of MFCV development is most clear in subjects #1, #2 and #4 at 30% MVC, and in subject #3 and #5 at 40% MVC (figure 6.2A, B, D, E & G). At 30% MVC, the period of fluctuating increase of MFCV is longer in subjects #3 and #5 (figure 6.2C&F). The experiments were therefore repeated in these subjects at a slightly higher force level.

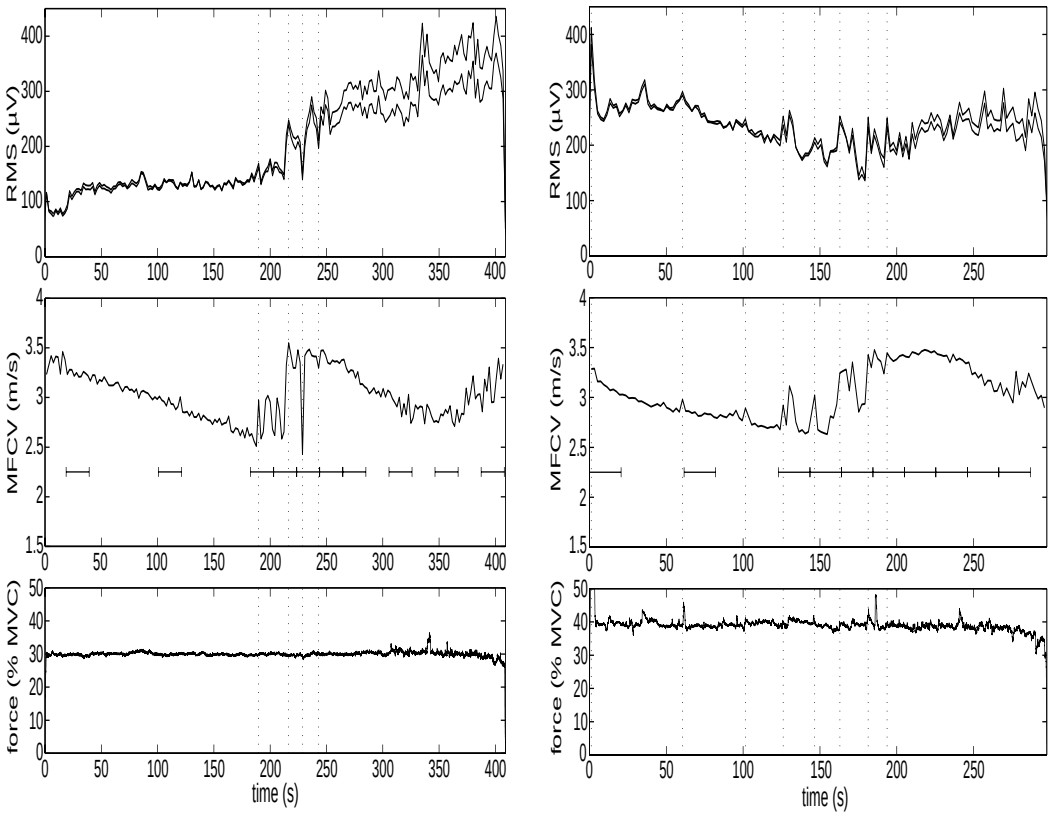

Figure 6.4A: amplitude (RMS), MFCV and force development for subject 1, who performed an exercise at 30% MVC. Aa: RMS values of both accompanying bipolar surface EMG signals. Ab: lowest MFCV of the selected column of electrodes (parallel to the fiber direction); vertical dotted lines point to coincidences in amplitude and MFCV shifts at, respectively, t = 190, 216, 229 and 243 s (see text); thin horizontal bars (Ab) indicate the time intervals used to derive the histograms shown in figure 6.5A. B: amplitude (RMS), MFCV, and force for subject 5, who performed an exercise at 40% MVC. Presentation as in A; vertical dotted lines point to coincidences in amplitude and MFCV shifts at, respectively, t = 1, 61, 102, 126, 147, 163, 181 and 194 s; thin horizontal bars (Bb) indicate the time intervals used to derive the histograms shown in figure 6.5B.

Representative examples

Two representative examples will be presented more extensively: the exercise at 30% MVC performed by subject #1 (figure 6.2A&H) and the exercise at 40% MVC performed by subject #5 (figure 6.2G&N). All other cases were analyzed in the same way. An exhaustive presentation of all cases would not add insight, however. For these experiments segments of the raw bipolar signal (figure 6.3), amplitude, MFCV and force values together in one figure (figure 6.4), histograms of the PVs (figure 6.5) and PVs presented on one segment of the raw bipolar signal (figure 6.6) are shown.

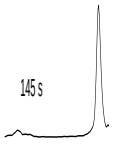

Bipolar signals

Figure 6.3A & 6.3B show segments of bipolar surface EMG signal pairs of 500 ms at different times during the selected exercises. In figure 6.3A larger peaks occur in the second half of the exercise. Visual inspection of the surface EMG signals show that these large peaks concern one or only a few motor units. Their large peak sizes contribute to an increased RMS amplitude towards the end of exercise. In figure 6.3B the initial density of peaks and their relative amplitude is higher than in figure 6.3A. (Note the scaling differences). The density of peaks decreases, and the peak amplitudes hardly change with time, which are the apparent reasons for the relative high initial value and the limited dynamical range for the RMS curve in figure 6.2N.

MFCV, amplitude and force

Figure 6.4A shows the results for MFCV and amplitude in more detail for subject #1 at 30% MVC, with the force curve added. MFCV fluctuates strongly during the transition from low to high MFCV values (between 190 and 245 s). The amplitude slowly increases, but also shows large jumps during the same period. A number of simultaneous jumps of amplitude and MFCV are striking, e.g. at t = 190 s, t = 216 s, t = 229 s and t = 243 s (marked with dotted lines). From about t = 330 s, the decrease in MFCV levels off and changes into an increase until the end of exercise. The amplitude shows increased variability again during this period. The force recording remains remarkably flat during the whole period and tends to become slightly more variable towards the end of exercise.

Figure 6.4B shows the more detailed results for subject #5 at 40% MVC. Again, transiently higher values of MFCV correspond to simultaneous bumps in the amplitude profile (marked with dotted lines at t = 1, 61, 102, 126, 147, 163, 181 and 194 s). The amplitude shows an unusual decrease during the first two minutes of exercise. This coincides with the decrease of peak density (figure 6.3B). During the transition from low to high MFCV values (between about 125 s – 195 s), the RMS data can be seen to decrease further being transiently interrupted by high peaks. The MFCV follows the same pattern: a further decrease interrupted by substantial larger values. During the last half minute of the exercise, a transient irregular pattern of slightly higher MFCV values is observed. As in subject #1, the amplitude shows large fluctuations during the latter period. The fluctuations in the force seem to have a minimal correlation with the surface EMG variables (RMS and MFCV).

Peak velocities

The PV histograms in figure 6.5, each representing selected periods of 20 seconds, are calculated to throw additional light on what determines the observed MFCV changes. The changes in PV distribution for both subjects demonstrate the shift of an initial population towards lower values without much change in the histogram shape (figure 6.5Aa-b & Ba-b).

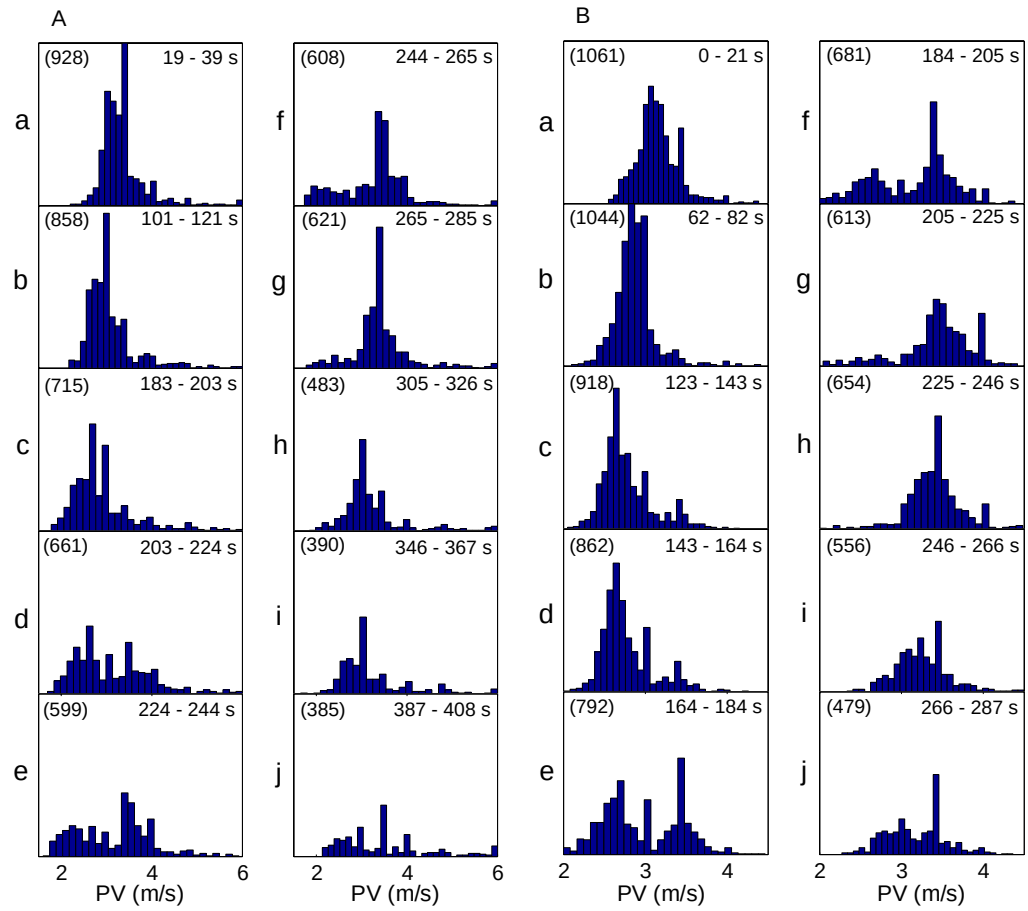

Figure 6.5A: peak velocity (PV) distribution analysis of subject 1, who performed an exercise at 30% MVC. To improve clarity, the results of 10 successive PV analyses (a-j; see indicated time segments at top right) are presented in one histogram. The scales of x- and y-axes are fixed. The total number of peaks analyzed is indicated between brackets at top left of each histogram. B: PV analysis of subject 5, who performed an exercise at 40% MVC. Presentation is as in A.

A second PV population emerges with a slightly higher mean velocity than the mean at the beginning of the exercise (figure 6.5Ab-d & Bc-e). The first histogram shifts further towards lower values, while the number of detected peaks belonging to this population decreases. At the same time, the number of peaks belonging to the second population increases (figure 6.5Ad-g & Bd-g). When the first distribution has almost disappeared, the second one shifts toward lower values (figure 6.5Ag-h & Bg-i). Towards the end of the exercise the histogram widens (figure 6.5Ai-j & Bi-j).

The peak amplitudes (not shown) show a large variability. On average, the amplitudes of the peaks belonging to the first population are smaller than these belonging to the second population. But peaks with high velocities do not always have the largest amplitudes (see figure 6.6 for selected signal examples of 500 ms).

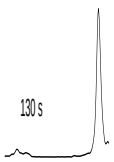

Discussion

Two population of motor units

The results show, as expected from our ^{31}P NMR spectroscopy results, an increase of MFCV after an initial decrease at 30 or 40% MVC in all of the five subjects studied. After this increase, MFCV decreases again towards the end of exercise. This MFCV pattern shows the recruitment of (at least) two different populations of motor units. Due to the lowering of MFCV of the first activated population of motor units, the newly recruited second population of motor units becomes visible. The initial MFCV of the second population is 2-14% (mean: 8%) higher than the initial MFCV of the first population, for all subjects except subject #4, (figure 6.2F). According to the size principle (Fallentin et al. 1993; Feiereisen et al. 1997; Henneman, 1981), there will be a higher fraction of type II motor units in the later-recruited population of motor units. If the first population consists only of fresh type I and the second population only of fresh type II motor units a mean increase in MFCV of 21-23% could be expected on the basis of fiber diameter distributions (Henriksson-Larsen, 1985; Henriksson-Larsen et al. 1985; Polgar et al. 1973) and the apparently linear relationship between the conduction velocities and the diameters of muscle fibers (Blijham et al. 2002; Nandedkar & Stålberg, 1983). The increase of the initial MFCV of the second population compared with that of the first represents a larger percentage (but not 100%) of type II motor units in the latter population. The atypical behavior of subject #4 can be explained by the fact that the MFCV is a weighted-average value of the contributions of all active motor units: freshly recruited and already fatigued. Moreover, the surface EMG signals are collected locally, and can thus be influenced by local physiological differences.

Our former studies (chapter 4 and 5) show a striking increase of metabolic activity of (most probably) the type II fibers in the second half of a sustained isometric exercise at 30% MVC, whereas the metabolic activity of these fibers was small in the first half. It was explained by an extra recruitment of type II motor units towards the end of exercise. Based on these former experiments the explanation of our present results becomes more explicit: it is most likely that the first population can be ascribed to type I motor units and the latter to type II motor units. In that line of reasoning, the MFCV is mainly determined by contributions of type I motor units during the first part of the exercise, and mainly by contributions from type II motor units during the second part of the exercise in spite of the fact that type II motor units are relatively scarce in the TA muscle (±27%, Johnson et al. (1973)). The transition periods are characterized by an intermingled activation of both types as illustrated by figure 6.6.

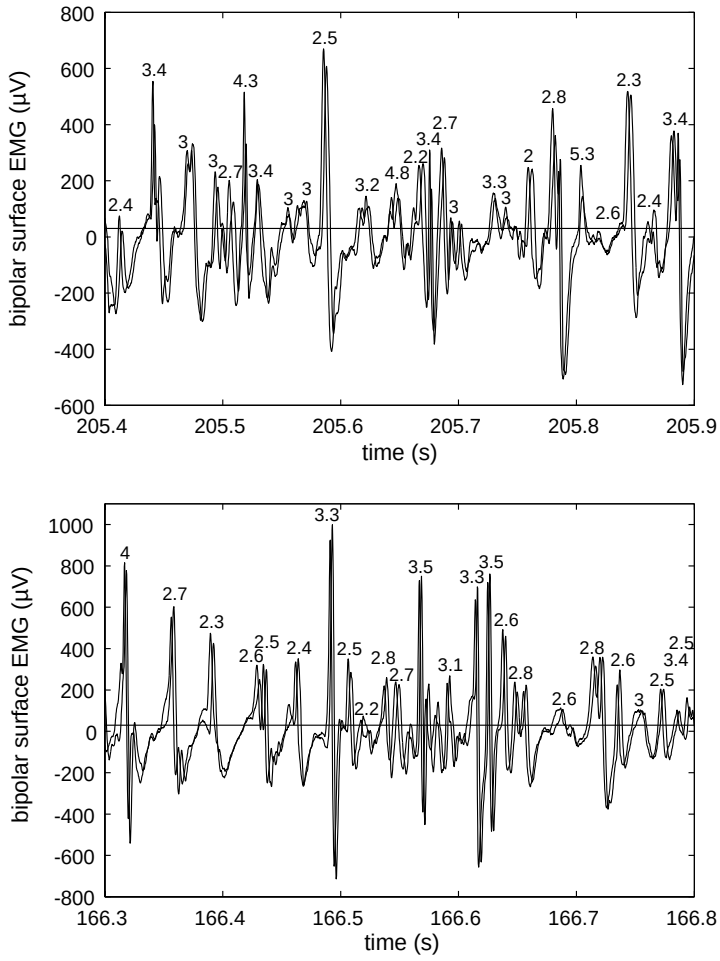

Figure 6.6A: surface EMG segment of 500 ms from subject 1, who performed at 30% MVC, taken 205 s after start of exercise (equal to segment 5 in figure 6.3A). PVs and the threshold for peak selection (horizontal line) are indicated. B: surface EMG segment of 500 ms from subject 5, who performed at 40% MVC, taken 166 s after start of exercise (equal to the segment 5 in figure 6.3B). Presentation is as in A.

Discontinuous recruitment

Although a straightforward explanation has been given here, the possibility of obtaining nearly distinct functional motor unit populations is a peculiar finding. Even if a fiber type dichotomy is often used in global discussions, histochemical and structural investigations often reveal more gradual transitions (e.g. Bottinelli & Reggiani, 2000). This cannot be ascribed to a more discrete division of fiber types especially in the TA, since also in this muscle a continuous distribution of motor unit properties was found (Van Cutsem et al. 1997). Therefore, the cause of the appearance of distinct motor unit populations has to be sought in the central nervous drive behavior, meaning a discontinuous recruitment of motor unit populations, which may be specific for this type of exercise and for the TA muscle (chapter 5).

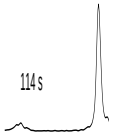

Bias and derecruitment

The PV method seems to be a powerful method to give insight into the composition of the MFCV, the latter being a mean value of the velocities of different action potentials in the surface EMG. However, with the present method we do not decompose the different action potentials into the contribution of specific motor units. Furthermore, the PV method is fire frequency biased: motor units with high firing rates will more often be detected than these with low firing rates. It is not easy to estimate which motor units are over-represented in the PV distribution: the threshold frequency of type II motor units is higher, but the firing rate of already recruited type I motor units may be increased (Erim et al. 1996).
A remarkable PV result is the decrease of the amount of detected peaks in the course of the exercise. This goes together with an emptier visual impression of the surface EMG signals. For the latter part of the exercise this is easiest to explain: synchronization of the motor units leads to occurrence of large very broadened action potentials and a decrease of the amount of peaks (Yao et al. 2000). For the intermediate part it might be related to a fatigue-induced decrease of firing rates for almost exhausted motor units (Bigland-Ritchie, 1981) (especially visible in subject 5) and probably a derecruitment of the first population of motor units.

Influences on amplitude and MFCV

The amplitude of the surface EMG signal is influenced by many factors. A first comment to make is about the basic underlying sources of the EMG signal, namely the transmembrane action potentials of the muscle fibers. The properties of these action potentials, mainly their conduction velocity and duration, are important factors influencing the surface EMG amplitude (Lateva, 1988; Stegeman & Linssen, 1992). This makes interpretation of surface EMG amplitudes solely in terms of motor unit recruitment and firing patterns rather risky under fatiguing circumstances. A constant or even decreasing amplitude accompanied with a decreasing MFCV (which happens often) can fully be ascribed to the influence of fatigue on the muscle fiber action potentials of already activated motor units. An amplitude increase accompanied with a constant MFCV (which happens sometimes) might be ascribable to recruitment of motor units with higher MFCV compensating the fatigued motor units with lowered velocities. An increase in amplitude with a decrease in MFCV (which happens towards the end of exercise) can be ascribed to synchronization of motor units (Yao et al. 2000).
But the surface EMG amplitude is also influenced by the motor unit firing frequencies; this can be seen nicely in subject #5 (figure 6.3B & 6.4B [6-126s]), where a decrease of peak density and not of peak amplitude is mainly responsible for the RMS decrease. Furthermore, the recruitment of a new motor unit with a large amplitude may increase the RMS substantially as can be seen in subject #1 at 30% MVC (figure 6.3A & 6.4A [205-255s]). As

was already indicated, the last part of these two exercises is characterized by a scattered distribution of peak amplitudes and velocities and irregularly occurring large broad peaks (figure 6.3A&B). The latter feature in particular points to an increased short-term synchronization of firings of different motor units. The irregular shapes of the peaks apparently lead to "unpredictable" peak amplitudes and velocities and thus, among others, to irregular amplitude values towards the end of exercise (figure 6.4A&B).

The transient variations of MFCV, which coincide with transient variations of amplitude (not always vice versa), can be ascribed to the temporal (de-)recruitment of large motor units with higher MFCV, possibly in connection with the influence of action potential velocity on motor unit potential amplitudes mentioned before.

Other factors that influence the MFCV are firing rate changes (Nishizono et al. 1989) and probably muscle swelling (Van der Hoeven et al. 1993). The decrease of peak density (firing rate) in subject #5 may also contribute to the decrease of MFCV during the first part of the exercise. Muscle swelling, because of water accumulation, seem to appear during the course of an isometric exercise at a low exertion level (Crenshaw et al. 1997) and will potentially increase MFCV. This will probably also affect MFCV in our subjects. However, it apparently does not compensate for the decrease of MFCV during large parts of the exercise for any of our subjects.

Cross talk

Cross talk is always difficult to exclude or to estimate. We measured at the distal side of the TA, where fibers are parallel to the skin surface, but where unfortunately, the cross sectional area of the TA is less. At this position along the TA, the extensors of the toes (m. extensor hallucis longus and m. extensor digitorum longus) located at the lateral side of the TA, together have about the same cross sectional area as the TA. To minimize the chance for cross talk, we placed the electrodes at the medial side of the TA (the most medial column of electrodes is placed along the tibia bone). Furthermore, we asked the subjects to concentrate on the contraction of the TA and to relax their toes as much as possible.

Absolute forces

In two of our subjects (#3 and #5) we repeated the exercise at the higher force level of 40% MVC to get comparable results as subjects #1, #2 and #4. It is noteworthy that for those subjects, at 40% MVC, the absolute forces are in the same range as the absolute forces of subjects #1 and #2 at their relative 30% MVC. Barnes (1980) showed that the intramuscular circulatory occlusion depends on absolute forces, regardless of maximum strength. Recruitment strategies of type I and type II motor units also appear to depend on absolute

forces. Unfortunately, subject #4, who showed the same pattern at 51 N (30% MVC), being close to half the absolute force of the others, breaks this hypothesized relationship.

Other muscles

Krogh-Lund & Jørgensen (1991, 1992 &1993) reported a leveling off of the decrease or an increase in MFCV simultaneously with an enlarged amplitude increase during a period of sustained exercises at 15, 25 and 30% MVC. They measured surface EMG from the m. triceps brachii (25% MVC), from the m. biceps brachii and from the m. brachioradialis (15% and 30% MVC). They ascribe their results to the recruitment of fresh large motor units increasing the amplitude and the MFCV and therefore compensating for the fatiguing of already recruited motor units, which tend to decrease the MFCV. Although in their data the same tendency was found as in our results, the illustration of the underlying processes appears much clearer from our data in the TA. Apart from a more detailed method of analysis, the specific muscle we studied may be a factor of importance. The mean percentage of type I fibers differs between the above muscles. It is typically 42% in the m. biceps brachii, 40% in the m. brachioradialis, 33% in the m. triceps brachii and it is much higher, namely 73%, in the TA (Johnson et al. 1973). The lower fraction of type I muscle fibers in the other muscles is likely to call for an earlier recruitment of type II motor units to maintain the desired force. This could be a possible explanation for the more gradual involvement of motor units with higher initial MFCV in the studies of Krogh-Lund & Jørgensen. The choice of the TA muscle was based on the clear-cut results obtained in metabolic variables studied by ^{31}P NMR spectroscopy (chapter 4 and 5).

Besides the percentage of type I fibers in a specific muscle, the occurrence of a clear alternating pattern of MFCV decrease and increase, as found in this study, depends on the chosen contraction level. At too low a level only type I motor units will be recruited, at too high a level motor units of both types will be already recruited in the beginning of the exercise. The extent to which a clear separation in time between the recruitment of type I and type II motor units respectively can be found in other muscles remains an interesting question.

Conclusions

We revealed a decrease, increase and subsequent decrease in MFCV during sustained isometric fatiguing contractions of the TA at 30-40% MVC. PV analysis shows two populations of PVs occurring simultaneously halfway through the exercise. It is most likely that the pattern of MFCV can be ascribed to the fatiguing of already recruited predominantly type I motor units, followed by the recruitment of fresh, predominantly type II, motor units, which similarly show signs of fatigue towards the end of the exercise.

References

Andreassen S & Arendt-Nielsen L. Muscle fiber conduction velocity in motor units of the human anterior tibial muscle: a new size-principle parameter. *J Physiol* 391: 561-571, 1987.

Arendt-Nielsen L & Mills KR. Muscle fiber conduction velocity, mean power frequency, mean EMG voltage and force during submaximal fatiguing contractions of human quadriceps. *Eur J Appl Physiol Occup Physiol* 58: 20-25, 1988.

Arendt-Nielsen L, Mills KR and Forster A. Changes in muscle fiber conduction velocity, mean power frequency, and mean EMG voltage during prolongend submaximal contractions. *Muscle Nerve* 12: 493-497, 1989.

Barnes WS. The relationship between maximum isometric strength and intramuscular circulatory occlusion. *Ergonomics* 23(4): 351-357, 1980.

Bigland-Ritchie B. EMG and fatigue of human voluntary and stimulated contractions. In: *Human muscle fatigue: physiological mechanisms*, edited by Edwards RHT. London: Ciba Foundation symposium 82, 1981, p. 130-156.

Blijham PJ, van Engelen BGM & Zwarts MJ. Correlation between muscle fiber conduction velocity and fiber diameter in vivo. *Clin Neurophysiol* 113: S39, 2002.

Blok JH, van Asselt S, van Dijk JP & Stegeman DF. On an optimal pasteless electrode to skin interface in surface EMG. In: *5th proceedings SENIAM*, edited by Hermens HJ & Freriks B. Enschede: RRD, 1998, p. 71 – 76.

Bottinelli R & Reggiani C. Human skeletal muscle fibres: molecular and functional diversity. *Prog Biophys Mol Biol* 73: 195-262, 2000.

Crenshaw AG, Karlsson S, Gerdle B & Friden J. Differential responses in intramuscular pressure and EMG fatigue indicators during low- vs.high-level isometric contractions to fatigue. *Acta Physiol Scand* 160: 353-361, 1997.

Erim Z, De Luca CJ, Mineo K & Aoki T. Rank-ordered regulation of motor units. *Muscle Nerve* 19: 563-573, 1996.

Fallentin N, Jorgensen K & Simonsen EB. Motor unit recruitment during prolonged isometric contractions. *Eur J Appl Physiol Occup Physiol* 67: 335-341, 1993.

Feiereisen P, Duchateau J & Hainaut K Motor unit recruitment order during voluntary and electrically induced contractions in the tibialis anterior. *Exp Brain Res* 114:117-123, 1997.

Gantchev N, Kossev A, Gydikov A & Gerasimenko Y. Relation between the motor units recruitment threshold and their potentials propagation velocity at isometric activity. *Electromyogr Clin Neurophysiol* 32: 221-228, 1992.

Henriksson-Larsen K. Distribution, number and size of different types of fibres in whole cross-sections of female m tibialis anterior. An enzyme histochemical study. *Acta Physiol Scand* 123: 229-235, 1985.

Henriksson-Larsen K, Friden J, Wretling ML. Distribution of fibre sizes in human skeletal muscle. An enzyme histochemical study in m tibialis anterior. *Acta Physiol Scand* 123: 171-177, 1985.

Henneman E. Recruitment of motor units: the size principle. In: *Motor Unit Types, Recruitment and Plasticity in Health and Disease*, edited by J. E. Desmedt. Basel: Karger, 1981, p. 26-60.

Hogrel JY, Duchene J & Marini JF. Variability of some sEMG parameter estimates with electrode location. *J Electromyogr Kinesiol* 8: 305-315, 1998.

Johnson MA, Polgar J, Weightman D & Appleton D. Data on the distribution of fiber types in thirty-six human muscles. An autopsy study. *J Neurol Sci* 18: 111-29, 1973.

Krogh-Lund C. Myo-electric fatigue and force failure from submaximal static elbow flexion sustained to exhaustion. *Eur J Appl Physiol Occup Physiol* 67: 389-401, 1993.

Krogh-Lund C & Jørgensen K. Changes in conduction velocity, median frequency, and root mean square-amplitude of the electromyogram during 25% maximal voluntary contraction of the triceps brachii muscle, to limit of endurance. *Eur J Appl Physiol Occup Physiol* 63: 60-69, 1991.

Krogh-Lund C & Jørgensen K. Modification of myo-electric power spectrum in fatigue from 15% maximal voluntary contraction of human elbow flexor muscles, to limit of endurance: reflection of conduction velocity variation and/or centrally mediated mechanisms? *Eur J Appl Physiol Occup Physiol* 64: 359-370, 1992.

Krogh-Lund C & Jørgensen K. Myo-electric fatigue manifestations revisited: power spectrum, conduction velocity, and amplitude of human elbow flexor muscles during isolated and repetitive endurance contractions at 30% maximal voluntary contraction. *Eur J Appl Physiol Occup Physiol* 66: 161-173, 1993.

Lange F, Van Weerden TW & Van Der Hoeven JH. A new surface electromyography analysis method to determine spread of muscle fiber conduction velocities. *J Appl Physiol* 93: 759-764, 2002.

Lateva ZC. Dependence of quantitative parameters of the extracellular potential power spectrum on propagation velocity, duration and asymmetry of action potentials. *Electromyogr Clin Neurophysiol* 28: 191-203, 1988.

Masuda K, Masuda T, Sadoyama T, Inaki M & Katsuta S. Changes in surface EMG parameters during static and dynamic fatiguing contractions. *J Electromyogr Kinesiol* 9: 39-46, 1999.

McGill KC & Dorfman LJ. High-resolution alignment of sampled waveforms. *IEEE Trans Biomed Eng* 31: 462-468, 1984.

Metting van Rijn AC, Peper A & Grimbergen CA. High-quality recording of bioelectric events. Part 1. Interference reduction, theory and practice. *Med Biol Eng Comput* 28: 389-397, 1990.

Nandedkar S & Stalberg E. Simulation of macro EMG motor unit potentials. *Electroencephalogr Clin Neurophysiol* 56: 52-62, 1983.

Nishizono H, Kurata H & Miyashita M. Muscle fiber conduction velocity related to stimulation rate. *Electroencephalogr Clin Neurophysiol* 72: 529-534, 1989.

Polgar J, Johnson MA, Weightman D & Appleton D. Data on fiber size in thirty-six human muscles. An autopsy study. *J Neurol Sci* 19: 307-318, 1973.

Stegeman DF & Linssen WH. Muscle fibre membrane electrophysiology and surface EMG: A simulation study. *J Electromyogr Kinesiol* 2, 130-140, 1992.

Van Cutsem M, Feiereisen P, Duchateau J & Hainaut K. Mechanical properties and behaviour of motor units in the tibialis anterior during voluntary contractions. *Can J Appl Physiol* 22: 585-597, 1997.

Van der Hoeven JH, van Weerden TW & Zwarts MJ. Long-lasting supernormal conduction velocity after sustained maximal isometric contraction in human muscle. *Muscle Nerve* 16: 312-320, 1993.

Yao W, Fuglevand RJ & Enoka RM. Motor-unit synchronization increases EMG amplitude and decreases force steadiness of simulated contractions. *J Neurophysiol* 83: 441-452, 2000.

Zwarts MJ & Arendt-Nielsen L. The influence of force and circulation on average muscle fibre conduction velocity during local muscle fatigue. *Eur J Appl Physiol* 58: 278-283, 1988.

Zwarts MJ, Van Weerden TW & Haenen HT. Relationship between average muscle fiber conduction velocity and EMG power spectra during isometric contraction, recovery and applied ischemia. *Eur J Appl Physiol Occup Physiol* 56: 212-216, 1987.

7

General discussion

Abstract

The preceding chapters (4-6) describe the study of the tibialis anterior muscle (TA) with two different methods during fatiguing submaximal isometric exercise. Phosphor nuclear magnetic resonance (^{31}P NMR) spectroscopy follows a part of the energy metabolism within the muscle fibers, surface electromyography (EMG) measures the electrical activity over the muscle fiber membranes. ^{31}P NMR spectroscopy demonstrates doubled inorganic phosphate (P_i) peaks, and thus two pH levels within the TA during a large part of the exercise. Acceleration of phosphocreatine (PCr) hydrolysis during the last part of the exercise was also seen. Surface EMG shows an increase in the mean muscle fiber conduction velocity (MFCV) following an initial decrease. Analysis of the velocities of motor unit action potentials shows that two populations of velocities occur simultaneously midway through the exercise. The orderly recruitment of motor units, with an increasing drive to the motor neurons, plays a central role in the interpretation of the results obtained with both methods. This chapter discusses whether the results and their interpretation may give rise to a uniform concept with respect to the underlying processes at a motor unit level.

Introduction

A spinal α-motoneuron, its peripheral motor axon and the muscle fibers innervated by the sprouts of that axon together form a so-called motor unit. Motor units are the functional building blocks of a muscle. Human motor units can roughly be subdivided in two types: type I, optimized for aerobic energy consumption and type II, optimized for anaerobic energy consumption. Type II motor units have more and thicker fibers, are stronger, but are also more easily fatigued than type I motor units (Polgar & Johnson, 1973; Essen et al. 1975; Enoka & Fuglevand, 2001). The so-called Henneman's size principle (Henneman, 1981) states that motor units are recruited with increasing (isometric) force in an orderly way according to their size. That indicates that the smaller type I motor units are recruited before the larger type II motor units. The same order of recruitment with central nervous drive can

be expected, but not proved, to be present in fatiguing submaximal isometric contractions (Krogh-Lund & Jørgensen 1991, 1992 & 1993; Fallentin et al. 1993; Krogh-Lund 1993). That is to say that when the first recruited motor units (predominantly type I) can no longer hold the required force, it can be assumed that fresh motor units (including type II) are recruited. The leading issues of this thesis are (i) the possibility to separate type I and type II motor unit recruitment and activity, (ii) the validity of the size principle for isometric submaximal fatiguing contractions and (iii) the question of how closely the results from the ^{31}P NMR experiments and the surface EMG measurements converge.

Background for this chapter

An introduction into ^{31}P NMR spectroscopy can be found in chapter 1 and chapter 2. The details concerning the ^{31}P NMR spectroscopy experiments and the results can be found in the chapters 4 and 5. An introduction in surface EMG can be found in the chapters 1 and 3. A detailed description of the surface EMG methods and results is given in chapter 6.

Discussion

The main body for this discussion consists of the results of chapter 4, 5 and 6 and their interpretation. We focus on some remaining, unanswered questions arising from these three chapters in the next seven subsections.

1. How acceptable is it to compare ^{31}P NMR spectroscopy and surface EMG results?

It should be noted that ^{31}P NMR spectroscopy and surface EMG provide different spatial views of the muscle. The ^{31}P NMR spectra as obtained with a surface coil arise from the whole TA, with dominance of the superficial layers, whereas surface EMG data are obtained from a small (and also superficial) area at the distal side of the TA. Moreover, the distribution of type I and type II fibers can be non-homogeneous as in animal TA (Wang & Kernell, 2001). Thus, a discrepancy may exist between the detected motor unit activity with surface EMG and the ^{31}P NMR spectra, based on these differences in detection volume. However, the ergometer, the position of the subjects, and the performed exercises are equal.

Of course, it would have been interesting to compare results from both techniques in one and the same subject, measured within a few days or weeks. Unfortunately, our measurements are separated by about two years and only subject #1 participated in both experiments. Many, mainly technical, difficulties prohibited an execution closer in time.

Beliveau et al. (1991, 1992), Vestergaard-Poulsen et al. (1992, 1994& 1995), Laurent et al. (1993), Bendahan et al. (1996) and Zange et al. (2003) showed the possibility of simultaneous measurements of ^{31}P NMR spectroscopy and surface EMG. They analyzed the amplitude and frequency content of the surface EMG signal. However, MFCV measurements were never done within the magnet as far as we know. The amplitude and the median frequency (a measure of the frequency content) of the surface EMG signal are both statistical variables. MFCV and PV are physiological variables and therefore easier to interpret than amplitude and median frequency. We preferred a detailed surface EMG experiment that yields direct physiological variables, more than a combined surface EMG – ^{31}P NMR spectroscopy experiment that only delivers statistical surface EMG variables. Obviously, the combination of a multi channel surface EMG experiment (suitable for MFCV and PV analysis) with ^{31}P NMR spectroscopy would increase the information content allowing a more detailed interpretation of our results, since it circumvents the large inter individual differences as they are discussed in the next section. However, such a combined experiment would also increase the technical difficulties. Considering all these aspects, a better comparison than we have made of the two types of experiments was not easy to realize.

2. How to explain large inter individual differences?

Large inter individual differences appear in the results of the ^{31}P NMR spectroscopy as well as in the surface EMG results, in terms of the duration of the exercises, the rates of PCr consumption, the pH values, the slopes and absolute values of MFCV and the mean surface EMG amplitude. Of course, there are also large anatomical and physiological variations between subjects: the composition of the muscle (the percentages of type I fibers versus type II fibers), the level and kind of training, age, gender and also motivation. We tried to enforce the subjects to go on until the bitter end, a state that is not precisely defined and certainly differs between subjects. In addition, the researcher influences the performance of the subjects as well, resulting in longer durations at 30% MVC than in a comparable study (Vestergaard-Poulsen, 1995). Johnson et al. (1973), Henriksson-Larsen et al. (1983) and Henriksson-Larsen (1985) show a range in the percentage of type II fibers of respectively 16–37% (95% confidence range, men), 2-52% (whole range, man), and 28-69% (whole range, women). In general, the amount and the size especially of type II fibers decrease with age (Lexell, 1995), although the level of activity also has some influence (Grimby, 1995). In general, endurance training enhances the capillary density and the mitochondrial activity, whereas strength or sprint training improves the glyco(geno)lytic capacity of the muscle. Both types of training enhance the regulation of K^+ and H^+ in the muscle (McKenna et al. 1996). As yet, there is no common opinion about gender differences in muscle performance

(i.e. Hunter & Enoka, 2001; Clark et al. 2003). One must conclude that despite all these largely diverging influences, similar patterns can clearly be recognized among all subjects, in both the spectroscopy and the EMG experiments.

3. When are type II motor units recruited initially?

In the ^{31}P NMR spectroscopy experiments, the recruitment and activity of type II motor units is recognized by their metabolic activity. Chapter 4 concludes that type II motor units are slightly metabolically active, early in the exercise. Halfway through the exercise, their metabolic activity increases remarkably and continues during the remaining part of the exercise. Chapter 5 confirms the conclusions. Distinguishing between different motor units types is more difficult in the surface EMG results. Chapter 6 (page 102) concludes that it is most likely that the first recruited motor unit population consists of type I motor units. The second population of motor units, appearing halfway through the exercise and causing an increase of MFCV, is expected to consist mainly of type II motor units. On the other hand, the increase of MFCV is not as high as might be expected by such a strict division (also chapter 6, page 102). This can be explained by: (i) the contribution of fatigued (and slower) motor units to the increased MFCV (as is confirmed by the PV distribution), (ii) a less strict division of motor unit types over both populations and/or (iii) the recruitment of only a part of the type II motor units in the second population. This means that a contribution of some type II motor units to the first population cannot be excluded. Therefore, the surface EMG results cannot answer the above question. In conclusion, the ^{31}P NMR spectroscopy results show the early recruitment of type II motor units an observation that is not confirmed, nor refuted by the surface EMG results.

4. When are extra motor units recruited?

A remarkable common result is the abrupt recruitment of extra motor units 'halfway through' the exercise. In chapter 5, the start of an accelerated decline of PCr indicates the recruitment of these extra motor units. The mean time of accelerated PCr decline is t_{PCr}= 63 ± 13% (mean ± SD) of the duration of the exercise. The accelerated decline of PCr is followed by a dramatic acceleration of the decline of the highest pH level, related to the loss of the aerobic glycolysis in the type I fibers. The mean time of accelerated pH decline is t_{pH}=77 ± 13% (mean ± SD) of the exercise duration. In chapter 6, the increase of MFCV, after an initial continuous decrease of this variable, points to the recruitment of fresh motor units. MFCV reaches a (local) maximum value at t_{emg}=76 ± 13% (mean ± SD) of the duration of the exercise. So, t_{emg} and t_{pH} are remarkably close, and t_{PCr} occurs the earliest. From this reasoning, the recruitment of extra type II motor units (t_{PCr}) starts before the type I motor units get into serious trouble (t_{pH}) (cut off from oxygen). When they get into problems at t_{pH},

more than a few fresh motor units are already simultaneously active (t_{emg}). These findings correspond to the results of Kent-Braun et al. (1993), who showed a similar delayed change in pH during progressive intermittent isometric exercise of the TA. An intermediate phase, in which P_i to PCr ratio increase accelerates, while pH remains constant, is followed by a last phase in which both P_i to PCr ratio and H^+ increase rapidly. They explain the intermediate phase by the recruitment of type II motor units and/or a deterioration of blood supply combined with sufficient recovery time in between the contractions.

5. Why does the recruitment of extra motor units occur so abruptly?

Several studies (i.e. Milner-Brown et al. 1973; Thomas et al. 1986; Feiereisen et al. 1997) use a gradual increase of the load to investigate the size principle and have reported a gradually increasing involvement of motor units. A remarkable result of our studies is the abrupt transitions in the ^{31}P NMR spectroscopy data, as well as in the surface EMG data. Of course, a sustained isometric contraction is a different exercise than a (isometric) ramp contraction. But why is there no step-by-step involvement of fresh motor units in the TA muscle? In chapter 6 (page 103) it is argued that the cause of the abrupt transitions cannot be found in a discontinuous distribution of motor unit properties, and therefore must be found in the organization of the central nervous drive to the muscle. But why should the central nervous system make such a discrete recruitment step halfway through the exercise? Chapters 4 and 5 (page 74-75 & 86-87) mention a deteriorated blood supply by an increase of intramuscular pressure at sustained isometric exercise at 30% MVC, favored by the confined anatomical position of the TA (chapter 5, page 86). This may be a cause of the abrupt recruitment of a new motor unit population. The deviating behavior in some subjects may help to understand the underlying mechanism. One subject shows a stable metabolic situation until the end of exercise, explained by the maintenance of microcirculation until the end of exercise and no extra recruitment of motor units (subject #3, chapter 5, page 88). Two other subjects show an exceedingly long period of irregular increase of MFCV after the initial decrease (subjects #3 and #5 at 30% MVC, chapter 6, page 95), whereas a more abrupt development of MFCV was seen in the same subjects performing at 40% MVC. This can be explained by a longer transition period of deterioration of the microcirculation, and thus longer (more gradual) period of recruitment of extra motor units. The development of the intramuscular pressure, and thus the degree of microcirculation, seems to play an important role in the (abrupt) recruitment of extra motor units.

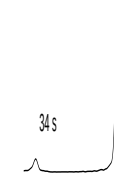

6. Is the size principle valid during fatiguing submaximal isometric contractions?

This may be considered as a central item of this thesis as a whole. Our results give converging evidence for the validity of the size principle for the recruitment of motor units during sustained submaximal isometric exercise of the TA. The contribution of type II motor units is rather small initially and rather substantial later in the exercise, as is made plausible by both methods. The decreasing amount of peaks in the surface EMG, may lead to the conclusion that fatigued motor units derecruit during the exercise (chapter 6, page 104). The disappearance of the first population of peak velocities (those with the lowest velocities) can hardly be explained entirely by a decrease in firing frequencies of the motor neurons. An extension of the present surface EMG analysis method by a decomposition of the different action potentials into the contribution of specific motor units would facilitate such an interpretation at a motor unit level (Beck et al. 2004a & 2004b). Of course, if the fatigued motor units derecruit during exercise, then the size principle, implicitly stating that the last recruited motor units are derecruited first, is not valid for the derecruiting process.

7. Can similar results be expected in other muscles?

As far as we know, results similar to ours, characterized by a sudden increase of the MFCV and an additional phase of accelerated PCr use in a fatiguing isometric contraction, have not been reported in the literature. Although pH heterogeneity is often reported, the combination with long lasting isometric exercise is rather scarce in ^{31}P NMR spectroscopy literature. Similarities with the results of PCr hydrolysis of Vestergaard-Poulsen et al. (1995) are discussed in chapter 5 (page 88). They also studied long-lasting isometric exercises of the TA. Unfortunately, pH values could not be compared, because they took the weighted mean of both pH levels if the P_i resonance split. Isometric exercises in combination with surface EMG are common practice. However, although statistical variables of the surface EMG signal (amplitude and frequency) are often reported, the study of a physiological variable like the MFCV is less frequently practiced. As discussed in chapter 6, the studies of Krugh-Lund & Jørgensen (1991, 1992, 1993) and Krogh-Lund (1993) show the development of the group mean MFCV during isometric exercises at 10, 15, 25, 30 and 40% MVC to the limit of endurance for either the m. biceps brachii, m. brachio radialis or m. triceps brachii. Their results certainly did make us curious about the development of individual MFCVs and PVs in these muscles.

To visualize both motor units types by ^{31}P NMR spectroscopy and two or more distinguishable motor unit populations by surface EMG, a clear division in pH levels (^{31}P NMR spectroscopy) and recruitment time (surface EMG) is necessary. In terms of the EMG

results, the early recruited motor unit population has to shift to lower conduction velocities before the next population appears. Measurements at a low contraction level (≤ 20% MVC) show only one pH level (unpublished). Measurements at a high contraction level (≥ 60% MVC) show two rapid decreasing pH levels, because of the ischemic condition of the muscle (chapter 4). At 30-40% MVC (the "optimal" percentage appears subject dependent, chapter 6) the two pH levels can be distinguished during exercise because both motor unit types are active during a large part of the exercise. Additionally, two motor units population can be distinguished by surface EMG due to the time delay between the recruitment of the two motor units populations. The confined location and the relatively high mean percentage of type I fibers of the TA may have influenced the nearly discrete recruitment pattern. Therefore, in other muscles, a more gradual involvement of fresh motor units may be expected. Hence, an alternating decrease and increase of MFCV may be expected, as is shown in some of the results of Krogh-Lund & Jørgensen (1991, 1992, 1993) and Krogh-Lund (1993). Our result may therefore be unique for the TA .

References

Beck RBJ, Houtman CJ, O'Malley MJ & Stegeman DF. A new technique to monitor the elektrical activity of a localized motor unit population from surface EMG. 2004a *Submitted*

Beck RBJ, O'Malley MJ, Stegeman DF, Houtman CJ, Nolan P, Connolly S & Zwarts MJ. Tracking motor unit action potentials in the tibialis anterior during fatigue. 2004b *Submitted*

Beliveau L, Helal JN, Gaillard E, Van Hoecke J, Atlan G, Bouissou P. EMG spectral shift- and 31P-NMR-determined intracellular pH in fatigued human biceps brachii muscle. *Neurology* 41: 1998-2001, 1991.

Beliveau L, Van Hoecke J, Garapon-Bar C, Gaillard E, Herry JP, Atlan G, Bouissou P. Myoelectrical and metabolic changes in muscle fatigue. *Int J Sports Med* 13: S153-155, 1992.

Bendahan D, Jammes Y, Salvan AM, Badier M, Confort-Gouny S, Guillot C, Cozzone PJ. Combined electromyography--31P-magnetic resonance spectroscopy study of human muscle fatigue during static contraction. *Muscle Nerve* 19: 715-721, 1996.

Clark BC, Manini TM, The DJ, Doldo NA & Ploutz-Snyder LL. Gender differences in skeletal muscle fatigability are related to contraction type and EMG spectral compression. *J Appl Physiol* 94: 2263-2272, 2003.

Enoka RM & Fuglevand AJ. Motor unit physiology: some unresolved issues. Muscle Nerve. 2001 Jan;24(1):4-17.

Essen B, Jansson E, Henriksson J, Taylor AW & Saltin B. Metabolic characteristics of fiber types in human skeletal muscle. *Acta Physiol Scand* 95: 153-165, 1975.

Fallentin N, Jorgensen K & Simonsen EB. Motor unit recruitment during prolonged isometric contractions. *Eur J Appl Physiol Occup Physiol* 67: 335-341, 1993.

Feiereisen P, Duchateau J & Hainaut K Motor unit recruitment order during voluntary and electrically induced contractions in the tibialis anterior. *Exp Brain Res* 114:117-123, 1997.

Grimby G. Muscle performance and structure in the elderly as studied cross-sectionally and longitudinally. *J Gerontol A Biol Sci Med Sci* 50:17-22, 1995.

Henneman E. Recruitment of motor units: the size principle. In: *Motor Unit Types, Recruitment and Plasticity in Health and Disease*, edited by J. E. Desmedt. Basel: Karger, 1981, p. 26-60.

Henriksson-Larsen K. Distribution, number and size of different types of fibres in whole cross-sections of female m tibialis anterior. An enzyme histochemical study. *Acta Physiol Scand* 123: 229-235, 1985.

Henriksson-Larsen KB, Lexell J & Sjostrom M. Distribution of different fibre types in human skeletal muscles. I. Method for the preparation and analysis of cross-sections of whole tibialis anterior. *Histochem J* 15:167-178, 1983.

Hunter SK & Enoka RM Sex differences in the fatigability of arm muscles depends on absolute force during isometric contractions. *J Appl Physiol* 91:2686-2694, 2001.

Johnson MA, Polgar J, Weightman D & Appleton D. Data on the distribution of fiber types in thirty-six human muscles. An autopsy study. *J Neurol Sci* 18: 111-29, 1973.

Kent-Braun JA, Miller RG & Weiner MW. Phases of metabolism during progressive exercise to fatigue in human skeletal muscle. *J Appl Physiol* 75: 573-580, 1993.

Krogh-Lund C. Myo-electric fatigue and force failure from submaximal static elbow flexion sustained to exhaustion. *Eur J Appl Physiol Occup Physiol* 67: 389-401, 1993.

Krogh-Lund C & Jørgensen K. Changes in conduction velocity, median frequency, and root mean square-amplitude of the electromyogram during 25% maximal voluntary contraction of the triceps brachii muscle, to limit of endurance. *Eur J Appl Physiol Occup Physiol* 63: 60-69, 1991.

Krogh-Lund C & Jørgensen K. Modification of myo-electric power spectrum in fatigue from 15% maximal voluntary contraction of human elbow flexor muscles, to limit of endurance: reflection of conduction velocity variation and/or centrally mediated mechanisms? *Eur J Appl Physiol Occup Physiol* 64: 359-370, 1992.

Krogh-Lund C & Jørgensen K. Myo-electric fatigue manifestations revisited: power spectrum, conduction velocity, and amplitude of human elbow flexor muscles during isolated and repetitive endurance contractions at 30% maximal voluntary contraction. *Eur J Appl Physiol Occup Physiol* 66: 161-173, 1993.

Laurent D, Portero P, Goubel F, Rossi A. Electromyogram spectrum changes during sustained contraction related to proton and diprotonated inorganic phosphate accumulation: a 31P nuclear magnetic resonance study on human calf muscles. *Eur J Appl Physiol Occup Physiol* 66: 263-268, 1993.

Lexell J. Human aging, muscle mass, and fiber type composition. *J Gerontol A Biol Sci Med Sci* 50:11-6, 1995.

McKenna MJ, Harmer AR, Fraser SF & Li JL. Effects of training on potassium, calcium and hydrogen ion regulation in skeletal muscle and blood during exercise. *Acta Physiol Scand* 156: 335-346, 1996.

Milner-Brown HS, Stein RB & Yemm R. The orderly recruitment of motor units during voluntary isometric contractions. *J Physiol Lond* 230: 359-370, 1973.

Polgar J, Johnson MA, Weightman D & Appleton D. Data on fiber size in thirty-six human muscles. An autopsy study. *J Neurol Sci* 19: 307-318, 1973.

Vestergaard-Poulsen P, Thomsen C, Sinkjaer T, Stubgaard M, Rosenfalck A, Henriksen O. Simultaneous electromyography and 31P nuclear magnetic resonance spectroscopy--with application to muscle fatigue. *Electroencephalogr Clin Neurophysiol* 85: 402-411, 1992.

Vestergaard-Poulsen P, Thomsen C, Sinkjaer T, Henriksen O. Simultaneous 31P NMR spectroscopy and EMG in exercising and recovering human skeletal muscle: technical aspects. *Magn Reson Med* 31: 93-102, 1994.

Vestergaard-Poulsen P, Thomsen C, Sinkjær T & Henriksen O. Simultaneous ^{31}P NMR spectroscopy and EMG in exercising and recovering human skeletal muscle: a correlation study. *J Appl Physiol* 79: 1469-1478, 1995.

Wang LC & Kernell D. Fibre type regionalisation in lower hindlimb muscles of rabbit, rat and mouse: a comparative study. *J Anat* 199: 631-643, 2001.

Zange J, Grehl T, Disselhorst-Klug C, Rau G, Muller K, Schroeder R, Tegenthoff M, Malin JP & Vorgerd M. Breakdown of adenine nucleotide pool in fatiguing skeletal muscle in McArdle's disease: a noninvasive ^{31}P-MRS and EMG study. *Muscle Nerve* 27: 728-736, 2003.

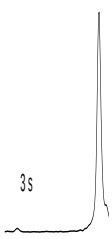

8

Summary

Introduction

The purpose of this thesis is to contribute to the knowledge of muscle physiology during *voluntary* exercise. We used surface EMG to study the electric activity of muscle fibers, and we used phosphor nuclear magnetic resonance (^{31}P NMR) spectroscopy to study aspects of the internal energy metabolism of the muscle fibers. The tibial anterior muscle was thought to best suit our experimental conditions, as was the protocol of sustained isometric exercise. The main issues dealt with in this thesis are: (i) the recognition of different types of motor units, and (ii) the order of activation of motor units.

Experimental setup

The subject lies backwards, with the left leg in a footplate as illustrated in figure 4.1 & 6.1 (page 61 & 93). The subject pulls against the fixated left foot. Visual feedback of the output force is provided for the subject. The subject is encouraged to hold on as long as possible.

Type I versus type II motor units

Human muscle fibers can roughly be divided into two types. Type I muscle fibers are better equipped for aerobic glycolysis (with oxygen) and more fatigue resistant than type II muscle fibers. Type II muscle fibers are specialized in anaerobic glycolysis (without oxygen). They also contain more and thicker muscle fibers than type I motor units. Action potentials travel along the outer muscle membrane with a certain velocity (about 4 m/s). This conduction velocity is related to the fiber diameter: the thicker the fiber, the higher its conduction velocity. The amplitudes of motor unit action potentials are among other things related to the amount of muscle fibers per motor unit. Thus, both the conduction velocity and the amplitude of the surface EMG signals can be different for both motor units types. If the production of protons by anaerobic glycolysis is higher than their removal via the vascular system, acidic build-up occurs. The preference for anaerobic glycolysis and their less

developed micro vascular system makes type II fibers more sensitive to acidification than type I fibers. Thus, the course of the pH level is expected to be different in both fiber types, as can be measured by ^{31}P NMR spectroscopy.

The size principle during isometric exercise

In isometric exercise, muscles do not largely change their length, in contrast to (cyclic) dynamic exercise, where muscle shortens and lengthens alternately. Carrying shopping bags requires isometric exercise of the arm muscles, walking and bicycling requires dynamic exercise of the leg muscles. The more force the muscle has to deliver, the more motor units have to be activated. During an isometric exercise with a gradually increasing effort, motor units are activated in order of size, starting with the smallest (i.e. the motor units with the thinnest motor neurons connected to the smallest number of muscle fibers). This is the so-called size principle. Thus, in gradually increasing isometric exercise, type I motor units are activated before the (larger) type II motor units.

Blood supply, pH level and conduction velocity

Dynamic exercise stimulates blood circulation in a working muscle. During sustained isometric exercises, however, blood supply may deteriorate during the course of the exercise. Water, produced by aerobic glycolysis, may accumulate within the muscle because of the static character of the exercise. This causes an increase of the intramuscular pressure. As the intramuscular pressure exceeds the blood pressure, the blood supply is blocked. A deterioration of the blood circulation will mostly effect type I fibers, because of their dependency on oxygen supply. Furthermore, the pH level within the muscle fibers will decrease as the removal of protons becomes obliterated. If an array of electrodes is placed on the skin, parallel to the muscle fibers, the propagation of the action potential along the outer muscle fiber membranes can be followed along the successive electrodes (figure 1.3, page 5). This conduction velocity of action potentials depends on the pH level, as well as the inorganic phosphate (P_i) concentration and the extracellular potassium (K^+) concentration. The higher the concentrations of P_i and extracellular K^+ and the lower the pH level, the more the conduction velocities of the fibers of active motor units slow down. The effect of isometric exercise on the conduction velocity and the pH level has been measured in this thesis, the underlying effect on blood supply can only be assumed.

Motor unit types and pH levels

In the ^{31}P NMR spectra, the pH is determined by the position of P_i resonance peak compared to the PCr resonance peak. If two pH compartments are present, than two P_i resonance peaks appear on different distances from the PCr resonance peak. Figures 4.2 &

4.3 (page 65 & 67) are examples of the measured splitting of P_i during exercise at respectively 60 and 30% of the maximal force. In chapter 4 we demonstrated that the left P_i resonance peak, belonging to the highest pH compartment, can be ascribed to type I muscle fibers. The right P_i resonance peak, belonging to the lowest pH compartment, is related to type II muscle fibers. Initially PCr is always used as the energy source for an activated muscle fiber. P_i is a product of phosphocreatine (PCr) conversion. Therefore, the development of the P_i resonance peaks tells us when each type of motor units is activated during exercise. In the first half of the exercise at 30% the maximal force, mainly type I motor units and a few type II motor units are active. The consumption of PCr (figure 5.3, page 83) shows an abrupt acceleration during the second half of the exercise. This coincides with an increase of the right P_i peak and is therefore ascribed to the activation of extra type II motor units.

Motor unit types and velocities

During activation, action potentials travel along the outer muscle fiber membrane. The propagation velocity can be calculated for single action potentials (peaks) or for a period of time, containing many action potentials (mean muscle fiber conduction velocity, MFCV). The latter operation is most common, and gives an average velocity of the activated motor units in that period. We measured the MFCV over periods of 2 s, and found a gradual decrease followed by a rather abrupt increase during 30-40% the maximal force (figure 6.2A-G, page 95). The gradual decrease of MFCV can be ascribed to the process of fatigue in the initial active motor units, for example by the above-mentioned accumulation of P_i or extracellular K^+. The next increase of MFCV can be explained by the activation of fresh motor units. These fresh motor units contain on average thicker fibers than the initially activated motor units, potentially explaining why the increase in MFCV exceeds the initial MFCV. Thus, the fraction of type II motor units is higher in the second population of motor units. In addition, the velocities of separate peaks in the surface EMG are calculated. Histograms of these peak velocities illustrate the underlying distribution of MFCV (figure 6.5, page 101). This means, a second population of motor units is activated, as the first population gets fatigued. Moreover, the second population contains more type II motor units than the first.

Converging evidence

Both experimental approaches indicate the activation of fresh mainly type II motor units in the second half of the exercise. The independent ^{31}P NMR spectroscopy and surface EMG results give additional information. A while after the onset of the activation of extra motor units, type I fibers show an accelerated acidification and thus more dependency on anaerobic glycolysis (for which they are less equipped). This is most likely caused by a

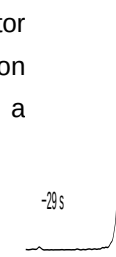

deteriorated blood supply. The histograms of peak velocities show the decrease in the number of detected peaks belonging to the first population (of initially activated motor units), while the number of detected peaks belonging to the second population increases (figure 6.5, page 101). Probably, the fatigued motor units are de-activated. Next, the peak velocities of the fresh activated motor units (belonging to the second population) decrease because these motor units also get fatigued.

Tibialis anterior muscle

The tibialis anterior muscle differs from other muscles in two respects. (i) It has a relatively high percentage of type I motor units, which may delay the activation of type II motor units. (ii) It is in an enclosed anatomical position, which may favor rather abrupt transitions in the microcirculation of blood. The level of activation appeared to be important. In the tibialis anterior 30-40% of the maximal isometric force seems to be a transition area. At lower force levels a small part of the motor unit population is activated initially and remains active until the end of the (aerobic) exercise. At greater force levels a large part of the motor unit population is activated initially and extra motor units are added rapidly during the short duration of the (anaerobic) exercise. The transition between aerobic and anaerobic conditions within the muscle in the course of the exercise makes our results interesting. The abruptness of this transition may be unique for the tibialis anterior muscle.

Conclusions

Two different motor unit types can be distinguished to contribute to the exercise by ^{31}P NMR spectroscopy thanks to their different pH levels. Moreover, the use of PCr indicates the initial activation of motor units. The analysis of peak conduction velocities in the surface EMG shows a nearly discrete activation pattern of motor unit populations during sustained isometric exercise at 30-40% MVC. The combination of surface EMG with ^{31}P NMR spectroscopy allows an interpretation of the surface EMG results in terms of type I and type II motor units. Therefore, we may conclude that (i) different types of motor units can be recognized, and (ii) in general the smaller type I motor units are active in the first and the larger type II motor units are active in the last part of the sustained isometric exercise at 30-40% MVC. Why such a discrete recruitment pattern was found is still an open and interesting question.

List of Publications

Articles

Houtman CJ, Heerschap A, Zwarts MJ & Stegeman DF. pH heterogeneity in tibial anterior muscle during isometric activity studied by ^{31}P-NMR spectroscopy. *J Appl Physiol* 91: 191-200, 2001.*

Houtman CJ, Heerschap A, Zwarts MJ & Stegeman DF. An additional phase in PCr use during sustained isometric exercise at 30% MVC in the tibialis anterior muscle. *NMR Biomed* 15: 270-277, 2002.*

Houtman CJ, Stegeman DF, Van Dijk JP & Zwarts MJ. Changes in muscle fiber conduction velocity indicate recruitment of distinct motor unit populations. *J Appl Physiol* 95: 1045-1054, 2003.*

Heerschap A, Houtman CJ, in 't Zandt HJ, van den Bergh AJ & Wieringa B. Introduction to in vivo 31P MR spectroscopy of (human) skeletal muscle. *Proc Nutr Soc* 58: 861-870, 1999.*

Beck RBJ, Houtman CJ, Malley MJO & Stegeman DF. A new technique to monitor the elektrical activity of a localized motor unit population from surface EMG. *Submitted*

Beck RBJ, Malley MJO, Stegeman DF, Houtman CJ, Nolan P, Connolly S & Zwarts MJ. Tracking motor unit action potentials in the tibialis anterior during fatigue. *Submitted*

Books chapter

Stegeman DF, Houtman CJ, Lapatki BG and Zwarts MJ. Multichannel surface EMG. In: *Clinical Neurophysiology of Disorders of Muscle and Neuromuscular Junction, Including Fatigue. Handbook of Clinical Neurophysiology, Vol. 2,* edited by Daube JR, Mauguière F (Ser. Eds.) and Stålberg E. (Vol. Ed.) Amsterdam: Elsevier Science B.V., 2003, p. 245-268, ISBN 0-444-50867-8.*

Abstracts and short papers

Houtman CJ, Heerschap A, van Engelen BGM, Wevers RA & Stegeman DF. NMR-spectroscopy in fatigue: two distinct pH levels in the tibialis anterior muscle. *In* 'ISEK 11th congress, Enschede, 1996', p. 182-183.

Houtman CJ, Heerschap A, Wevers RA & Stegeman DF. Patterns in aerobic and anaerobic meatbolism during isometric exercise in human tibialis anterior muscle. *In* 'ESMRMB 14th annual meeting, Brussels, 1997', p. 140.

Houtman CJ, Heerschap A, Wevers RA & Stegeman DF. NMR Spectroscopy in the study of muscle fatigue. *In* 'International conference on motion systems, Jena, 1997', p. 41-42.

Houtman CJ, Heerschap A, Zwarts MJ & Stegeman DF. PCr use and pH-heterogeneity in tibial anterior muscle during low level isometric activity studied by ^{31}P NMR spectroscopy. *In* 'PROCID symposium, Copenhagen, 1999', p. 180-181.

Houtman CJ, Stegeman DF, van Dijk H, Heerschap A & Zwarts MJ. Recruitment strategies of motor unit types in the tibial anterior muscle during fatigue studied with 31P NMR spectroscopy and surface EMG. *In* 'Motion Systems 2001, Jena, 2001', p. 159-164.

Houtman CJ, Heerschap A, Zwarts MJ & Stegeman DF. Additional phases in PCr use during a sustained isometric exercise of the tibial anterior muscle, studied by 31P NMRS. *In* 'ISMRM, 9th annual meeting, Glasgow, 2001'.

Blok J, Huiskamp GJ, Stegeman DF & Houtman CJ. An estimation procedure to determine motor unit structure from surface EMG data. Electroenceph Clin Neurophysiol 97, 166P, 1995.

Stegeman DF, Roeleveld K, Blok JH, Houtman CJ, Drost G & Zwarts MJ. Functional muscle imaging. *In* 'Abstracts 3. Arbeitstagung Motodiagnostik-Mototherapie, Jena, 1997'.

Stegeman DF & Houtman CJ. Changes of intracellular fibre action potentials and the surface EMG: a simulation study of fatigue. *In* '6th proceedings SENIAM, Enschede, 1998', p. 125-127.

* included in this thesis

Samenvatting

Introductie

Waardoor raken onze spieren vermoeid wanneer we ze langere tijd achtereen gebruiken? Wordt het voor de zenuwvezels, die de spieren aansturen steeds moeilijker boodschappen over te brengen? Is een verslechtering van de elektrische overdracht van de zenuwvezels naar de spiervezels de oorzaak? Is de voortgeleiding van de elektrische signalen over de spiervezels gemankeerd? Of raken vooral de energiebronnen uitgeput?

Er zijn al duizend en één experimenten gedaan en een aantal oorzaken zijn al uitgesloten. Toch weten we nog steeds niet precies hoe het zit. De ene proef laat zien dat de geleiding van elektrische signalen afneemt, de andere proef laat zien dat ionen ophopen of spiervezels verzuren. Er is veel kennis verkregen op basis van dierexperimenteel werk. Daarnaast is er veel onderzoek verricht aan mensen, waarbij de spier van buitenaf gestimuleerd werd (via elektrische schokjes). Maar uiteindelijk willen we weten wat er gebeurt tijdens normaal gebruik van spieren. Dit proefschrift wil een bijdrage leveren aan de kennis over spiervermoeidheid op basis van bewuste aanspanning van spieren. Een belangrijk begrip daarbij is ‘motorische eenheid’. Een motorische eenheid bestaat uit één motorische zenuwvezel plus een groot aantal spiervezels. Die ene zenuwvezel stuurt alle bijbehorende spiervezels tegelijk aan, zoals hieronder geïllustreerd. Belangrijke thema’s bij

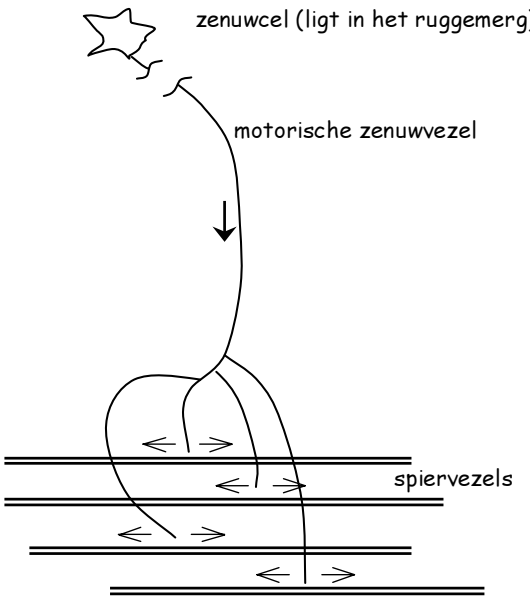

Een motorische eenheid bestaat uit één motorische zenuwvezel en vele daarbij horende spiervezels.

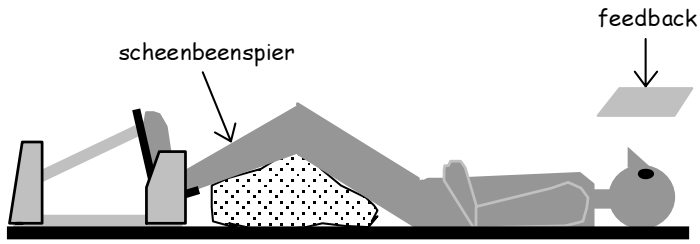

proefpersoon in meetopstelling

de interpretatie van onze resultaten zijn (i) het onderscheiden van twee verschillende typen motorische eenheden en (ii) de volgorde waarin motorische eenheden worden geactiveerd.

Uitwerking

We hebben er voor gekozen één spier uitvoerig te onderzoeken tijdens één soort oefening. De spier is de scheenbeenspier of de tibialis anterior spier. Deze spier voel je aanspannen als je je voorvoet heft. Om praktische redenen laten we de proefpersoon liggen met een licht gebogen linkerbeen ondersteund door kussens, zoals boven aan de pagina is geïllustreerd. De linkervoet plaatst de proefpersoon op een pedaal die onderdeel uitmaakt van een apparaat dat kracht meet. De voet wordt met brede banden aan het pedaal vastgebonden. Het pedaal zelf zit ook vast. Als de proefpersoon de voet heft (draaiend om de enkel), oefent zij* kracht uit zonder het pedaal noemenswaardig te verplaatsen. Dit heet een isometrische oefening. En daar wordt je wel degelijk moe van. We testen eerst wat de maximale kracht van de proefpersoon is. Na enige tijd rust begint de oefening: zolang mogelijk één en dezelfde kracht leveren, bijvoorbeeld 30% van de maximale kracht. Op een schermpje ziet de proefpersoon de kracht, zodat ze weet hoe hard of zacht zij haar voet op moet heffen. Een proefpersoon houdt dit gemiddeld 8 minuten vol. De langste tijd in onze experimenten was 11 minuten, de kortste 5. Tijdens de oefening meten we òf aan de energiehuishouding van de spier òf aan de elektrische signalen over de spiervezels.

Twee typen spiervezels

Er bestaan twee soorten spiervezels en dus twee soorten motorische eenheden. Langzame type I vezels met een voorkeur voor aërobe verbranding (dat wil zeggen met zuurstof) en snelle type II vezels met een voorkeur voor anaërobe verbranding (zonder zuurstof). Dankzij de betere doorbloeding en hun voorkeur voor aërobe verbranding raken type I vezels niet snel vermoeid. Doordat type II motorische eenheden gemiddeld bestaan uit meer en dikkere spiervezels dan type I motorische eenheden zijn ze sterker. Dankzij snel beschikbare (anaërobe) energiebronnen en hun grotere kracht kunnen type II motorische eenheden explosieve kracht leveren.
Om te weten komen welke motorische eenheid wanneer actief is tijdens de oefening, maken we gebruik van verschillen in energiehuishouding en anatomie. Ik noem twee voorbeelden.

1. Spiervezels verzuren door anaërobe verbranding met onvoldoende doorbloeding. Type II spiervezels met een voorkeur voor anaërobe verbranding, verzuren sneller dan type I spiervezels die een voorkeur voor aërobe verbranding hebben.

2. De geleiding van actiepotentialen gaat iets sneller over dikkere (type II) spiervezels dan over dunnere (type I) vezels.

Een actiepotentiaal is een elektrisch signaaltje (als dik pijltje weergegeven in de figuur op pagina 125) dat vanuit het ruggenmerg over de motorische zenuwvezel naar de spiervezels loopt. Vervolgens wordt het signaal overgedragen op alle spiervezels die bij deze ene zenuwvezel horen. De actiepotentialen (dunne pijltjes) lopen vanuit ongeveer het midden van een spiervezel naar de twee uiteinden die vastzitten aan een pees of peesblad. Actiepotentialen lopend over spiervezels zijn boodschappers die melden aan de vezels dat er werk aan de winkel is. Deze boodschapper zet processen in de spiervezel in gang, waardoor deze aanspant. Zolang de spiervezels aangespannen moeten blijven, blijven actiepotentialen dan ook zo'n 12 keer per seconde langskomen.

Hoe meet je de energiehuishouding van spiervezels?

De verzuring van de spier is aan de buitenkant te meten. Daarvoor gebruiken we een MRI scanner, een apparaat dat meestal voor de directe patiëntenzorg wordt gebruikt. MRI is inmiddels één van de meest gebruikte technieken om afbeeldingen te maken van het inwendige van de mens. MRI staat voor magnetische resonantie 'imaging', wat inhoudt dat je beelden maakt op basis van magnetische eigenschappen van water. Het apparaat meet per dwarsdoorsnede hoeveel water waar zit en vertaalt dit naar grijswaarden in een afbeelding.
In plaats van het meten van de hoeveelheid water, kan het apparaat andere stoffen in het

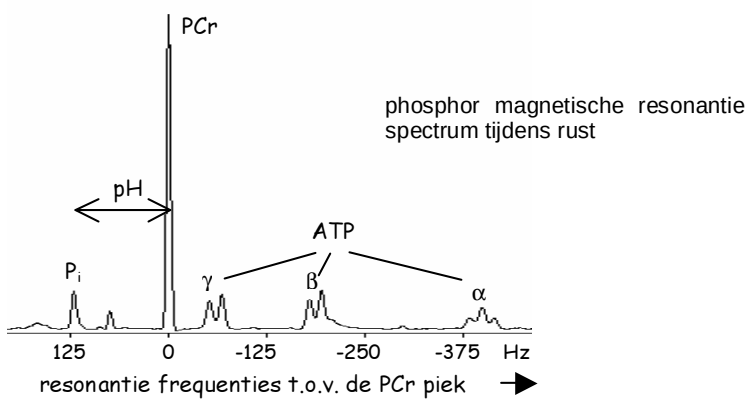

lichaam kwantificeren. Deze stoffen zijn in minder grote hoeveelheden aanwezig en hebben minder sterke magnetische eigenschappen dan water. Daarom maken we op basis van deze stoffen geen plaatjes (zoals bij water), maar zogenoemde spectra. Deze techniek wordt dan ook magnetische resonantie (MR) spectroscopie genoemd, wat inhoudt dat je spectra maakt op basis van de magnetische eigenschappen van bijv. fosfor (^{31}P). Een fosfor spectrum (zoals weergegeven op de vorige pagina) laat van de verschillende moleculen die fosfor bevatten zien hoeveel ervan aanwezig is. In een onvermoeide spier zit veel phosphocreatine (PCr) en weinig anorganisch fosfaat (P_i). In het spectrum is dit terug te vinden als een hoge piek voor phosphocreatine en een klein laag piekje voor anorganische fosfaat. Phosphocreatine is een snel beschikbare energiebron voor de spier. Tijdens oefening neemt de hoeveelheid phosphocreatine dan ook af. De hoeveelheid anorganisch fosfaat neemt juist toe, omdat dat vrijkomt als phosphocreatine verbrandt.
Er is nog iets opmerkelijks aan het fosfor spectrum: de anorganisch fosfaat piek kruipt dichter naar de phosphocreatine piek toe, gedurende de oefening. Dit komt omdat de zuurgraad van het spierweefsel de magnetische eigenschappen van anorganisch fosfaat licht verandert. Dus door een fosfor spectrum te meten, weet je ook wat de zuurgraad, ofwel de pH waarde, van het spierweefsel is. Deze pH waarde geeft een indruk van de mate van anaërobe verbranding en de mate van doorbloeding van de spier. Hoe beter de doorbloeding van het spierweefsel, hoe beter de zuurmakende protonen, die vrijkomen bij anaërobe verbranding, weggespoeld worden.

Hoe meet je de snelheid van actiepotentialen?

Langs spiervezels lopende elektrische signalen (actiepotentialen), zijn aan de buitenkant op de huid te meten. Dit type meting heet elektromyografie (EMG). ‘Myo’ betekent spier, ‘grafie’ betekent schrijfwijze. Op de huid worden elektroden geplaatst, in de lengterichting van de spiervezels. Een langskomend elektrisch signaal zal door de opeenvolgende elektroden met een klein tijdsverschil gemeten worden, zoals onderstaande figuur illustreert. Hoe trager de EMG signalen langskomen, hoe groter het tijdsverschil tussen de opeenvolgende

Twee oppervlakte EMG signalen tijdens flinke aanspanning. Het ene signaal (stippellijn) is net iets verschoven ten opzichte van het andere signaal (doorgetrokken lijn), want de ene elektrode registreert langlopende actie potentialen net iets eerder dan de andere (dichter bij de pees gesitueerde) elektrode.

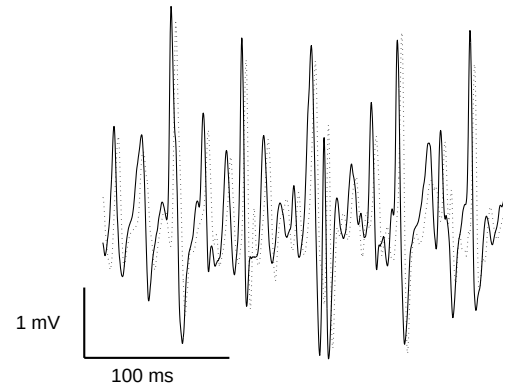

registraties. De zogenoemde geleidingsnelheid van het EMG signaal is de afstand tussen twee opeenvolgende elektroden gedeeld door het gemiddelde tijdsverschil tussen de EMG registraties van deze elektroden.

Hoe verloopt het energieverbruik?

Acht proefpersonen deden mee aan het fosfor MRS experiment. De resultaten laten zien dat phosphocreatine eerst heel snel en daarna minder snel afneemt tijdens de oefening. Een dergelijke afname van phosphocreatine viel te verwachten, omdat het vooral in het begin de belangrijkste energiebron van de spier is. Opvallend is de versnelde afname in het laatste deel van de oefening: de curve loopt weer steiler naar beneden. Het 'stripverhaal' in de rechter onderhoek van pagina 25–123 laat van één proefpersoon zien hoe phosphocreatine afneemt en anorganische fosfaat toeneemt tijdens oefening (pagina 117-45) en hoe phosphocreatine weer toeneemt en anorganisch fosfaat afneemt tijdens herstel (pagina 43-25).
In de spectra (bijvoorbeeld figuur 4.1B, pagina 61) is te zien dat anorganische fosfaat twee pieken heeft gedurende (een groot deel van de) oefening. Dat komt omdat type I spiervezels een andere zuurgraad hebben dan type II spiervezels. De linker piek, met de hoogste pH waarde (minst zuur), hoort bij de type I vezels, de rechter piek bij de type II vezels. De spectra laten zien dat type I spiervezels licht verzuurd en type II spiervezels sterk verzuurd raken tijdens de oefening. Opvallend is de versnelde afname van de zuurgraad (pH waarde) in de type I vezels tijdens het laatste deel van de oefening.

Welke geleidingssnelheden hebben we gevonden?

Vijf, op één na allemaal andere proefpersonen, deden mee aan het EMG experiment. De resultaten laten zien dat de geleidingssnelheid van het EMG signaal eerst afneemt, dan snel toeneemt en vervolgens weer afneemt. De curve op de omslag van dit proefschrift illustreert dit voor één proefpersoon. Het is bekend dat geleidingssnelheden afnemen tijdens een vermoeiende oefening. Opvallend is daarom vooral de snelle toename halverwege de oefening.

Conclusies

Met fosfor MR spectroscopie is het goed mogelijk de activiteit van type I en type II spiervezels te onderscheiden. De hoge pH waarde hoort immers bij type I, de lage bij type II spiervezels. Bovendien zegt de oppervlakte van de bijbehorende anorganisch fosfaat pieken iets over de hoeveelheid activiteit. Zo is te zien dat de activiteit van type II spiervezels sterk toeneemt in het laatste deel van de oefening: de rechter anorganisch fosfaat piek wordt snel groter.

Met EMG is het goed mogelijk de activering van afzonderlijke groepen motorische eenheden zichtbaar te maken. Aan het begin van de oefening wordt een groep motorische eenheden geactiveerd. Deze worden gedurende de oefening steeds vermoeider, zoals uit de afnemende geleidingssnelheid valt af te leiden. Dan wordt een volgende groep motorische eenheden ingezet, te herkennen aan een plotselinge toename van de geleidingssnelheid. Deze “frisse” motorische eenheden zijn nog onvermoeid en hebben bovendien iets hogere beginsnelheden dan de eerste groep. In de fosfor MR spectroscopie resultaten is de activiteit van deze frisse groep motorische eenheden te herkennen aan de versnelde afname van phosphocreatine. Om op gang te komen verbruiken de frisse motorische eenheden snel beschikbare energie in de vorm van phosphocreatine.
In de eerste helft van de oefening is de anorganische fosfaatpiek die hoort bij de type I vezels relatief groot, de anorganische fosfaat piek die hoort bij de type II vezels is juist erg klein. Daaruit concluderen we dat in de eerste helft van de oefening voornamelijk motorische eenheden van het type I actief zijn. Gedurende de tweede helft van de oefening neemt de anorganisch fosfaat piek behorende bij type II vezels sterk toe. Ook is de geleidingssnelheid van de tweede groep motorische eenheden bij aanvang wat hoger dan de beginsnelheden van de eerste groep. Uit beide gegevens concluderen we dat tijdens het laatste deel van de oefening voornamelijk motorische eenheden van het type II actief zijn.
Opvallend is het plotselinge karakter van een aantal veranderingen. We vermoeden dat deze veranderingen verband houden met een verslechterde doorbloeding van de spier. De inzet van type II motorische eenheden en de versnelde verzuring van de type I eenheden tijdens het laatste deel van de oefening wijzen in deze richting. De type II motorische eenheden functioneren immers beter bij gebrek aan zuurstof dan de type I eenheden. Bovendien zit de tibialis anterior spier in een opgesloten positie tussen (scheen)bot en membraanstructuren. Hierdoor kan de druk in de spier gemakkelijk oplopen.

Ten slotte: met dit onderzoek willen we een bijdrage leveren aan de kennis over normaal gebruik van spieren. De oefening die onze proefpersonen deden is niet zo gebruikelijk. Toch hebben we, door in detail te kijken naar één spier gedurende één soort oefening en de proefpersonen aan te moedigen zo lang mogelijk vol te houden, extra gegevens boven water gekregen over de inzet van motorische eenheden gedurende aanspanning van deze spier.

* er deden zowel vrouwen als mannen aan dit onderzoek mee, ten behoeve van de leesbaarheid is gekozen voor de ‘zij’ vorm.

Dankwoord

Mijn dank gaat als eerste uit naar mijn drie begeleiders die in de jaren dat ik aan dit onderzoek werkte alle drie tot hoogleraar werden benoemd. Bij wijze van uitzondering mocht het maximum aantal van twee promotores dan ook worden overschreden.

Ik bedank ….

Dick Stegeman, omdat jij in mij en mijn werk bleef geloven, juist ook in mindere tijden, is dit proefschrift er gekomen. Jouw bereidheid mogelijkheden te blijven zien, heeft mij goed gedaan. Je waardering voor mijn werkzaamheden buiten de universiteit eveneens.

Arend Heerschap, vanwege je niet aflatende enthousiasme voor je vak, NMR spectroscopie. Vooral de inhoudelijke discussies met jou wisten mij te motiveren. Het congres in Liverpool, net voor aanvang van mijn aanstelling, was een goed begin.

Machiel Zwarts, je inbreng vanuit een andere achtergrond was erg welkom. Met begeleiders uit drie disciplines (elektrotechniek, biochemie, klinische neurofysiologie) vormden we een waar multidisciplinair team.

Ron Wevers, dankjewel dat je samen met Dick en Arend bereid was mij aan te nemen als pas afgestudeerde natuurkundige en voor je betrokkenheid in het begin van dit project.

Hans van Dijk, dankjewel voor tien jaar voortreffelijke technische ondersteuning. En voor de zeer vele malen dat jij proefpersoon wilde zijn (zonder naaldjes). Het resultaat van een geslaagde meting prijkt op de voorkant van dit boek.

Erik van den Boogert en Erik van den Bergh, dank jullie wel voor de technische begeleiding van mijn NMR experimenten (hard- en software) en voor de geduldige uitleg van weer een foutmelding van het NMR apparaat, ook ‘s avonds en in het weekend (telefonisch).

Medewerkers van de Instrumentele Dienst Oost, ik vond het leuk in overleg met jullie hard- en software te ontwikkelen. Dank voor jullie inzet.

Karin Roeleveld, Joleen Blok, Robert Oostenveld, Gea Drost, Mireille van Beekvelt, Maartje Schillings en andere onderzoekers, het was prettig zoveel onderzoeker collegae te hebben. Zowel om mee te wandelen in de pauzes, als voor serieuzer overleg.

Dick Vingerhoets, gaandeweg verdwenen de naaldjes (stereoscopisch via een hoofd-telefoon) uit mijn onderzoek, en daarmee jouw supervisie daarop. Dankzij jou arriveerde mijn zeekano in Nijmegen en maakte ik kennis met de woelige wateren van de Waal.

Andrew Fuglevand, it was an adventure for me to travel to the US to visit you and to learn form you the technique of needle EMG with the thin microneurography needles. Thank you for your hospitality of staying at your house and showing me around, besides the scientifically coaching. An unforgettable impression.

Rebecca Beck, it is pleasure to see you continuing my EMG work. I liked our cooperation. And thank you for all the correction work you did in my English texts.

Elke Pastoors, dankjewel voor je snelle en professionele ondersteuning de keren dat ik een beroep op je deed.

May Eikholt en Netty Eikholt, wat heerlijk om met jullie een praatje te kunnen maken ter afwisseling van al het serieuze werk.

Alle laboranten klinische neurofysiologie (KNF), naast de gezelligheid in de koffiekamer, heb ik de prettige samenwerking gewaardeerd, de keren dat ik op jullie terrein vertoefde.

Alle proefpersonen - vrienden, collega's en kennissen - wil ik bedanken voor hun geduld en in mij gestelde vertrouwen. Mijn verhaal over de magnetronwerking van de oppervlakte spoel werkte daar niet altijd aan mee.

Curriculum Vitae

Caroline Houtman is geboren in Eindhoven op 16 september 1968. Tijdens haar lagere school tijd verhuisde het gezin naar Almelo, waar na de lagere school het Christelijk Lyceum werd doorlopen. Op zoek naar een β-opleiding kwam ze als 17-jarige in Groningen terecht voor een studie natuurkunde aan de Rijks Universiteit aldaar. Ze volgde bijvakken vrouwenstudies en milieukunde en nam deel aan afdelingsbestuur en faculteitsraad. In 1993 behaalde ze, als enige overgebleven vrouwelijke student uit haar jaar, haar diploma. In 1994 werd een onderzoeksbaan gevonden als Assistent In Opleiding (AIO) op de afdeling Klinische Neurofysiologie van het Universitair Medisch Centrum Nijmegen St Radboud. Het betrof een interdisciplinair onderzoek naar de oorzaken van spiervermoeidheid. Ze raakte actief betrokken bij de ontwikkeling van het interuniversitaire Instituut voor Klinische en Fundamentele Bewegingswetenschappen (IFKB) en blies het wekelijks wetenschappelijke overleg op de afdeling nieuw leven in. In 1998 verhuisde Caroline naar een oud pandje in het landelijk gelegen Zutphen. Naast haar werk op de universiteit werd ervaring opgedaan in het begeleiden van verstandelijk gehandicapten en in de biologisch-dynamische tuinbouw. Ook leerde ze zichzelf Noors. In 2001 vertrok zij naar Noorwegen om tijdelijk mee te draaien in een woonwerkgemeenschap voor verstandelijk gehandicapten. Van 2001 tot 2003 werkte ze als activiteiten begeleider op een kaarsenwerkplaats voor volwassen verstandelijk gehandicapten te Olst. In september 2003 werd ze gekozen in het afdelingsbestuur van Waterschap Rijn en IJssel. Voor u ligt het tastbare resultaat van haar wetenschappelijke werk.